Radioactive Contamination in Neutrino Experimental Physics: the Cases of NEXT and Super-Kamiokande Experiments

PhD dissertation by
Javier Pérez Pérez

under the supervision of
Luis A. Labarga Echeverría

2017

ABSTRACT

The current Standard Model (SM) of fundamental interactions has in its lightest particle, the neutrino, a key to open the door for a much profound understanding of the laws of the fundamental interactions. However, due to the low interaction cross section of the neutrinos, it is very hard to get information about them. Basic questions are the exact masses of the neutrinos and their hierarachy, the precise value of the mixing parameters and, in particular, the presence or not of a significant leptonic CP violation. Furthermore, there is overall the fundamental question of the nature of the neutrino particle: Majorana or Dirac, i.e., wether the neutrino is its own antiparticle or not. The scientific comunity is running numerous experiments to solve these questions, most of them in underground conditions to maximize the visibility of the neutrino signals.

This Thesis deals with NEXT, a 'double beta zero neutrino' ($2\beta0\nu$) experiment, and with Super-Kamiokande, a proton decay and neutrino detector.

NEXT (**N**eutrino **E**xperiment with a **X**enon **T**PC) is a $2\beta0\nu$ experiment designed to study if neutrino is a Majorana particle. These type of experiments is the only known way to solve this question. This decay is a special case of double beta decay, where the nuclei can't decay β but it's possible to decay twice. Because the the antineutrino is absorbed as a neutrino, all the energy of the reaction corresponding to the mass difference between parent and daughter nuclei is shared only between the two electrons. In the case of the ^{136}Xe isotope of NEXT, this energy is 2458 keV. Thus, NEXT searches for a narrow peak at this value in the two-electron total energy spectrum.

However, radioactive contaminations in the materials of the experiment can fake that signal and it is absolutely necessary to reduce and quantify the corresponding background from all the components of the detector down to tolerable values. Relevant for NEXT are the isotopes ^{208}Tl and ^{214}Bi, because photons emitted in their decays can have energies very close to the $2\beta0\nu$ signal.

Super-Kamiokande (**Super Kamioka N**ucleon **D**ecay **E**xperiment) is a water Cherenkov detector designed to search for proton decay and to detect neutrinos from cosmic and terrestrial sources. With 50 ktons of ultra pure water, the detector can observe clearly the cherenkov light produced by charged particles with enough energy; in particular those from the final state products of a neutrino interaction. However, it basically can not distinguish whether the interacting particle was a neutrino or an antineutrino. Along this direction comes the SuperK-Gd project (formerly called GADZOOKS!): an upgrade of the SK experiment to provide it with a very high efficiency neutron tagging capability. Neutron tagging opens Super-Kamiokande to a wealth of new measurements of important physics reactions and improves very much those already in its Scientific Program.

The idea is to dissolve in the Super-Kamiokande water a salt of Gadolinium ($Gd_2(SO_4)_3$) at a low concentration. Some of the isotopes of the Gd have a very large neutron capture cross section, emitting at capture a cascade of few photons with 8 MeV total energy that is measured by SK. As the Gd salt is uniformly distributed along the whole active volume of the detector, radioactive contaminations in the salt are an issue: the decay processes of unstable isotopes will induce low energy signals in SK that will fake those from neutron capture. Therefore, as in the case of NEXT, the presence of radioactive isotopes in the salt must be reduced to the minimum acceptable, and quantified precisely afterwards.

My contribution to both experiments is centered in the study of the radioactive contamination of the detectors, understanding how radioactive contaminations affects to our experiments, how decay chains evolve and how to reduce the impact of these backgrounds. Also, I have contributed with the selection of the materials, the preparation and measurement of the major part of the samples and, finally, with a complete mathematical analysis of the data taken and on deciding on the validity of the material for the experiment from the point of view of radioactivity background.

The text is organized as follows: Chapter 1 is an introduction to neutrino physics and the implications of its properties. This Chapter explains the actual status

of the open questions and experiments on this field and also presents both experiments where I am involved. Also, I introduce the usual presence of natural radioctivity contamination and the problems that we can find with this source of background.

Chapter 2 is an introduction to the physics of radioactivity. There, we discuss the most common types of nuclear decays, the decay chains and the emitted particles that can mimic our expected experimental signals.

Chapter 3 analyzes the impact of radioactivity contaminations in NEXT and SuperK-Gd and presents the rationale for the absolute necessity of a radiopurity campaign in order to reach the expected sensitivity of the detectors.

Chapter 4 presents the experimental techniques to measure this radioactivity and all the data analysis produres to obtain the value of the activity.

The discussion of the measurements results, their implications, etc. are in chapter 5 (for NEXT) and in chapter 6 (for Super-Kamiokande).

Finally, chapter 7 is for summarizing all these works and their conclusions.

The work of this Doctoral Thesis has been presented:

- NEXT collaboration (V. Álvarez et al.), *Radiopurity Control in the NEXT-100 double beta decay experiment: procedures and initial measurements*, JINST **8** (2013) T01002, [arXiv:1211.3961].
- S. Cebrian, J.Pérez, I. Bandac, L.Labarga et al., *Radiopurity assessments of the tracking readout for the NEXT double beta decay experiment*, JINST **10** (2015) P05006, [arXiv:1411.1433].
- S. Cebrian, J.Pérez, I. Bandac, L.Labarga et al., *Radiopurity assessment of the energy readout for the NEXT double beta decay experiment*, [arXiv:1706.06012v1] (submitted for publication to JINST)
- NEXT collaboration (J. Martín-Albo et al.), *Sensitivity of NEXT-100 to neutrinoless double beta decay*, [arXiv:1511.09246v1]

- Pérez J., *The NEXT-100 experiment for Neutrino-less Double Beta decay: Main features, Results from Prototypes and Radiopurity issues*, EPS-HEP 2013, $http : //pos.sissa.it/archive/conferences/180/528/EPS - HEP\%202013\_528.pdf$

- Pérez J., *The NEXT Radiopurity Campaign: Measurements and Results*, NEUTRINO 2014, $https : //indico.fnal.gov/getFile.py/access?contribId = 125\&sessionId = 30\&resId = 0\&materialId = poster\&confId = 8022$

All the work related to the Super-Kamiokande experiment has been documented by internal presentations; no publication yet.

RESUMEN

El Modelo Standard (SM por sus siglas en inglés) de interacciones fundamentales tiene en su partícula más ligera, el neutrino, la llave para abrir la puerta hacia una más profunda comprensión de las leyes de las interacciones fundamentales. Sin embargo, debido a su baja sección eficaz de interacción, es muy difícil obtener información sobre ellos. Los interrogantes fundamentales que se nos presentan son: el valor exacto de la masa y la jerarquía de los neutrinos, el valor de los parámetros de mezcla y, en particular, la posible presencia de significativa violación de la paridad CP en el sector leptónico. Además, tenemos la pregunta fundamental sobre la naturaleza del neutrino: Majorana o Fermi, o lo que es lo mismo, si el neutrino es su propia antipartícula o no. La comunidad científica está desarrollando numerosos experimentos para conseguir resolver estas cuestiones, estando la mayoría de ellos en laboratorios subterráneos para maximizar la visibilidad de las señales de los neutrinos.

Esta tesis está centrada en dos de estos experimentos, NEXT, un experimento de desintegración doble beta sin neutrinos, 'double beta zero neutrino' ($2\beta0\nu$); y también Super-Kamiokande, un detector de neutrinos y de decaimiento de protones.

NEXT (**N**eutrino **E**xperiment with a **X**enon **T**PC) es un experimento de $2\beta0\nu$ diseñado para estudiar si el neutrinos es una partícula de Majorana. Este tipo de experimentos es el único conocido que puede resolver esta pregunta. Este tipo de desintegración es un caso especial que se produce en núcleos que no pueden decaer vía β pero si son capaces de hacerlo dos veces simultáneamente. Debido a que los neutrinos se aniquilan mutuamente, toda la energÃa de la reacción (que se corresponde a la diferencia de masas entre el núcleo padre y el hijo) es emitida en los electrones. En el caso del isótopo empleado en NEXT, el ^{136}Xe, esta energía es de 2458 keV. Por lo tanto, NEXT busca en delgado pico con esa energía en el espectro de la energía total de los dos electrones emitidos.

Sin embargo, la contaminación radioactiva que podemos encontrar en los distintos materiales pueden darnos falsos eventos y eso hace que sea totalmente

necesario reducir y cuantificar el correspondiente fondo radioactivo de cada uno de los componentes del detector hasta unos valores aceptables. Los isótopos más influyentes para NEXT son ^{208}Tl y ^{214}Bi, los cuales emiten fotones al desintegrarse con unas energías mu cercanas a la señal de $2\beta0\nu$.

Super-Kamiokande (**Super Kamioka N**ucleon **D**ecay **E**xperiment) es un detector Cherenkov de agua diseñado para buscar la desintegración del protón y la detción de neutrinos producidos desde fuentes tanto cósmicas como terrestres. Con 50.000 toneladas de agua ultrapura, este detector puede observar con claridad la luz Cherenkov producida por partículas cargadas con suficiente energía; en particular, aquellas producidas después de la interacción con neutrinos. Sin embargo, es básicamente imposible saber si lo que se ha observado es un neutrino o un antineutrino. SuperK-Gd (previamente llamado GADZOOKS!) es una mejora del experimento SK en la cual adquiere la capacidad de detectar neutrones con alta eficiencia. Esta detección de neutrones conduce a Super-Kamiokande a un escenario lleno de nuevas e importantes medidas por hacer para la Física, mejorando también aquellas que ya estaban en su programa científico.

La idea consiste en disolver en muy baja concentración una sal de Gadolinio ($Gd_2(SO_4)_3$) en el agua de SuperKamiokande. Algunos de los isótopos del Gadolinio tienen una enorme sección eficaz de captura de neutrones térmicos, emitiendo después de la captura una cascada de fotones con una energía en total de unos 8 MeV, que serán medidos por el detector SK. Debido a que la sal va a estar distribuida uniformemente por toda el agua del detector, las contaminaciones radioactivas que encontremos en la misma son todo un problema: las desintegraciones que se puedan producir señales a baja energía que pueden comportarse de manera parecida a una captura de neutrones. Por lo tanto, como pasa en NEXT, la presencia de isótopos radioactivos debe verse reducida hasta llegar a unos mínimos aceptables, y además, cuantificando con precisión el valor de esta contaminación.

Mi contribución a ambos experimentos está centrada en el estudio de la contaminación radioactiva de ambos detectores; entendiendo cómo las contaminaciones radioactivas afectan a nuestros experimentos, cómo

evolucionan las cadenas radioactivas y cómo minimizar el impacto de estos fondos. Además, he contribuido con la selección de los materiales, la preparación y medida de la mayoría de las muestras y, finalmente, con un completo análisis matemático de los datos tomados y decidiendo sobre la idoneidad del material para el experimento desde el punto de vista del fondo radioactivo.

La tesis está organizada de la siguiente manera: el Capítulo 1 es una introducción a la Física de Neutrinos y las implicaciones de sus propiedades. Este capítulo explica el estado de las cuestiones abiertas aún sin resolver y los experimentos en este campo, además de presentar a ambos experimentos en los que estoy involucrado. Por último, introduce la contaminación radioactiva y los posibles problemas que podemos encontrar ocasionados por este fondo.

El Capítulo 2 es una introducción a la Física de la Radioactividad, donde discutimos las más habituales formas de desintegración, las cadenas de desintegración y las características de las partículas emitidas que pueden imitar a los verdaderos sucesos que esperamos ver en nuestros experimentos

El Capítulo 3 analiza el impacto de la contaminación radioactiva en NEXT y en Super-KGd y presenta las razones por las cuales una campaña de radiopureza es imprescindible si queremos alcanzar la sensibilidad necesaria en los detectores.

El Capítulo 4 presenta las técnicas experimentales para medir la radioactividad y todo el proceso de análisis de datos para obtener la actividad.

La discusión de los resultados de las medidas están en el Capítulo 5 (para el caso de NEXT) y en Capítulo 6 (para el caso de Super-Kamiokande)

Finalmente, el Capítulo 7 está dedicado a mostrar las conclusiones de este trabajo.

- NEXT collaboration (V. Álvarez et al.), *Radiopurity Control in the NEXT-100 double beta decay experiment: procedures and initial measurements*, JINST **8** (2013) T01002, [arXiv:1211.3961].

- S. Cebrian, J.Pérez, I. Bandac, L.Labarga et al., *Radiopurity assessments of the tracking readout for the NEXT double beta decay experiment*, JINST **10** (2015) P05006, [arXiv:1411.1433].

- S. Cebrian, J.Pérez, I. Bandac, L.Labarga et al., *Radiopurity assessment of the energy readout for the NEXT double beta decay experiment*, [arXiv:1706.06012v1] (submitted to publication to JINST)

- NEXT collaboration (J. Martín-Albo et al.), *Sensitivity of NEXT-100 to neutrinoless double beta decay*, [arXiv:1511.09246v1]

- Pérez J., *The NEXT-100 experiment for Neutrino-less Double Beta decay: Main features, Results from Prototypes and Radiopurity issues*, EPS-HEP 2013, $http://pos.sissa.it/archive/conferences/180/528/EPS-HEP\%202013\_528.pdf$

- Pérez J., *The NEXT Radiopurity Campaign: Measurements and Results*, NEUTRINO 2014, $https://indico.fnal.gov/getFile.py/access?contribId=125\&sessionId=30\&resId=0\&materialId=poster\&confId=8022$

La parte de trabajo hecha para Super-KGd ha sido presentada en charlas internas y no ha sido aún publicada.

AGRADECIMIENTOS

Bueno, pues al final hemos llegado al final de este camino. Ha sido largo y fructífero, pero no exento complicaciones. Es por ello que tengo que dedicar estas primeras páginas a toda la gente que ha estado ahí para acompañarme y apoyarme.

Obviamente, la primera persona a descatar es **Luis Labarga**, la persona que más ha puesto de su parte para que esta Tesis sea una realidad. Su apoyo, dirección y consejo han sido claves para que este proyecto salga adelante.

Junto a Luis y a mí, están los otros miembros de el equipo de Radiopureza de NEXT, **Susana** y **Iulian**. La verdad es que ha sido un equipo de trabajo de ensueño. Entre los cuatro, con muy buena voluntad y ganas, hemos sacado adelante gran parte del trabajo de radiopureza para este experimento.

Ya de vuelta al **IFIC**, hay mucha gente que han sido claves para esto. La gente del ZULO siempre han estado ahí y siempre ha sido un refugio para despejarse, tomarse un café, sacar una sonrisa. Vicente, Javi, Alberto, Sara, Marc, Ander... y los que ya han emprendido otros caminos. También en el piso de arriba hay mucha gente de la que acordarme, como Josh, Francesc, José Vicente, Pau, Neus, Paola, Andrew, Justo... y, claro, los de mi despacho: Carmen, José María, Alex, Miquel y Ryan. Bueno, y sin olvidarme de las personas con más galones: JJ, Michel, Curro, Raúl, Vicente H., Pepe y Nadia, la que fue mi guía en los primeros pasos de mi carrera investigadora. En el IFIC hay mucho talento pero mejores personas.

Por Torrent, sin tener tampoco mucha idea de neutrinos, ha habido mucha gente que me ha ayudado en este camino. La gente de **KEITA DAMIGOS**, mis amigos de toda la vida... esos que me vienen acompañando desde los tiempos del insti. José, Nacho, Luis, Enrique, Pedro, Martín, Vicente, Adrián y sus parejas. Cuando se acerca el sábado, ya se empiezan a ver por whastapp para hacer algo y al final siempre acabamos en el Paco's, con su mistela de despedida.

También en Torrent está mi parroquia, **San José de Torrent**. Remanso de paz y oasis, pero también lugar para encontrarme con muchos amigos: Adri, Neus, Mortes, Marta, Fran... muchos son. Muchos y de muy distintos grupos: todos los amigos de todas las edades de Juniors, los de Caminamos, los de Alpha, los de los Clavarios de la Fiesta de San José o el grupo de Confirmación para Adultos. Y no me quiero dejar a nuestro párroco, D. Javier Francés, todo un ejemplo de persona que ha contribuido mucho en mi vida personal y laboral durante el tiempo que lleva en Torrent.

¡Y la **Familia**! Importantísima en este camino. Padre, madre y hermanos. Remigio, Lucía, Jorge y Raúl. Gracias por vuestro apoyo y paciencia.

Bueno, a todos y los que seguro que me he dejado por el camino sin acordarme de ellos en estas líneas... **¡GRACIAS!**

Haber hecho algo por lo que
'tan solo' se percibe dinero es haber
sido un auténtico holgazán o peor aún.
Si un obrero no gana más que el sueldo
que le paga su patrón, le están engañando,
se está engañando a sí mismo.

Henry D. Thoreau

Contents

1

Introduction to the Neutrino Physics

Neutrinos, a desesperate solution for the beta decay problem, is nowadays one of the most important particles in Experimental Physics. It was in 1930 when Wolfgang Pauli postulated the neutrino (in that moment, he called it neutron), necessary to conserve energy, momentum and angular momentum in beta decay.

In that moment, he thought that it was better to postulate a ghost particle that to violate several conservation laws. And he was right.

This is a small part of his original letter, translated by Kurt Riesselmann[1]

Pauli letter to Gauverein meeting in Tübingen

Dear Radioactive Ladies and Gentlemen,

[...] the possibility that in the nuclei there could exist electrically neutral particles, which I will call neutrons, that have spin 1/2 and obey the exclusion principle and that further differ from light quanta in that they do not travel with the velocity of light. The mass of the neutrons should be of the same order of magnitude as the electron mass and in any event not larger than 0.01 proton mass. The continuous beta spectrum would then make sense with the assumption that in beta decay, in addition to the electron, a neutron is emitted such that the sum of the energies of neutron and electron is constant

Pauli was right in almost everything, but not in the mass of the neutrinos. Now we know that their masses are in the order than meV, several order of magnitude smaller than he expected.

Neutrinos are very **elusive particles** because they only interact via gravitational and weak forces. And therefore, the interaction cross section of these particles is very small. Thus, if you want to design a neutrino detector, it must be huge.

First Neutrino Observation

The first direct observation of neutrino interactions was in 1956, thanks to the **experiment of Cowan and Reines** [Reines and C. L. Cowan 1956]. In 1995, F. Reines was awarded with the Nobel Prize[2] *for pioneering experimental contributions to lepton physics*[3].

The experiment was placed close to Savannah River Plant, a nuclear facility in the United States in the state of South Carolina. Close to the nuclear reactor,

[1] *http : //microboone − docdb.fnal.gov/cgi − bin/RetrieveFile?docid = 953; filename = pauli%20letter1930.pdf*

[2] Both Physicists deserved the Nobel Prize, but unfortunately, C. Cowan died in 1974

[3] *http : //www.nobelprize.org/nobel_prizes/physics/laureates/1995/*

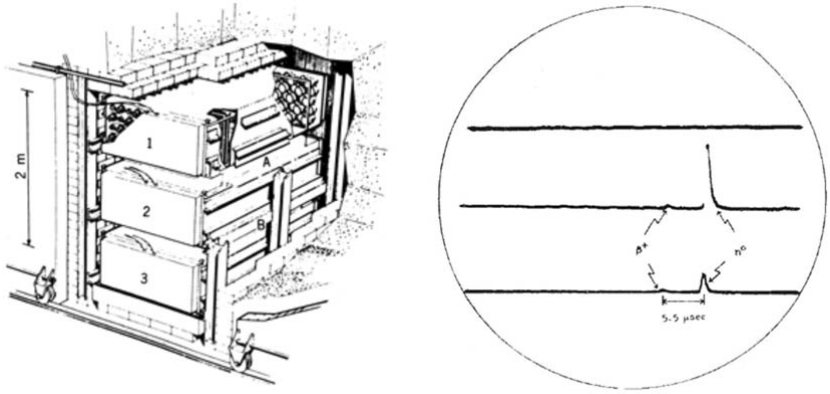

Figure 1.1: Conceptual design of the apparatus used by Cowan and Reines for their neutrino experiment; figure taken from NuMi-MINOS (left). Coincidence peaks from positron annihilation (right)

with a large flux of neutrinos, they wanted to observe an inverse beta decay interaction of some of those neutrinos with the detector. In Chapter 2 we can find a complete explanation of beta decay, but here, we are going to introduce inverse beta decay first:

$$\overline{\nu}_e + p \rightarrow n + e^+ \tag{1.1}$$

The detector consisted of a solution of $CdCl_2$ in water. This solution was sandwiched with liquid scintillators, were some PMTs detected the emitted light. The experimental idea was to detect both final-state particles.The positron will be annihilated with one environmental electron, prompting 511 KeV photons. The neutron will be captured by a ^{108}Cd nucleus, emitting a de-excitation delayed gamma.

$$n + {}^{108}Cd \rightarrow {}^{109m}Cd \rightarrow {}^{109}Cd + \gamma \tag{1.2}$$

In figure 1.1-right, taken from [Reines and C. L. Cowan 1956], we can observe both signals, the annhilation photon and the de-excitation photon, a $5.5\mu s$

delayed signal, that confirms the production of these two particles from the antineutrino interaction with one proton.

They observed about 3 neutrinos per hour, obtaining a neutrino interaction cross section very close to the theoretical predictions, about $6 \cdot 10^{-44} cm^2$. The neutrinos (in this case, antineutrinos) were discovered, thus starting a new era in High Energy Physics: Neutrino Experimental Physics.

Solar Neutrino Problem

The next step in the History of the Neutrino was the Neutrino Solar flux. The first observation of Neutrino Solar flux was made with **Homestake experiment** (also known like Davis experiment). This experiment, that was running from 1970 to 1994, was headed by Raymond Davis Jr. and John N. Bahcall. In 2002, R. Davis Jr. was awarded with the Nobel Prize for *for pioneering contributions to astrophysics, in particular for the detection of cosmic neutrinos*[4].

The detector, placed inside the Homestake Gold Mine (in Lead, South Dakota, USA), was a 380 cubic meter tank filled with perchloroethylene (very rich in chlorine), being able to count the argon atoms produced by the interaction of the neutrinos with chlorine atoms. The argon atom counting, done every few weeks, gave a three times lower value of the number of neutrino interactions than the theorical calculations, made mainly by John N. Bahcall, [Bahcall, Davis, and Wolfenstein 1988].

Other strong evidence was observed in Kamiokande-II in 1988, [Hirata et al. 1990], where the number of observed neutrinos coming from the solar direction was also smaller than the predictions. Additionally, to explore this question, some other experiments were built like GALLEX and SAGE.

the puzzle was solved by **SNO** experiment, [Ahmad et al. 2002], a neutrino detector filled with heavy water. This detector was sensitive to both neutral currents, a measurement of the total number of neutrino interactions; and sensitive to charged currents, a measurement of the total number of electron

[4] $http://www.nobelprize.org/nobel\_prizes/physics/laureates/2002/$

neutrino. The total number of observed were in a good agreement with J. Bahcall calculations, but electronic neutrinos were only 1/3 of the observed. They had oscillated.

It is important to remember that, nowadays, we know that there are three charged leptons with their associated neutrino. Then, we have three neutrino flavors with their own antiparticles: electron neutrinos ($\nu_e, \overline{\nu}_e$), muon neutrinos ($\nu_\mu, \overline{\nu}_\mu$) and tau neutrinos ($\nu_\tau, \overline{\nu}_\tau$). But it is important to remark that neutrinos don't have right-handed partners, as we illustrated in figure 1.2.

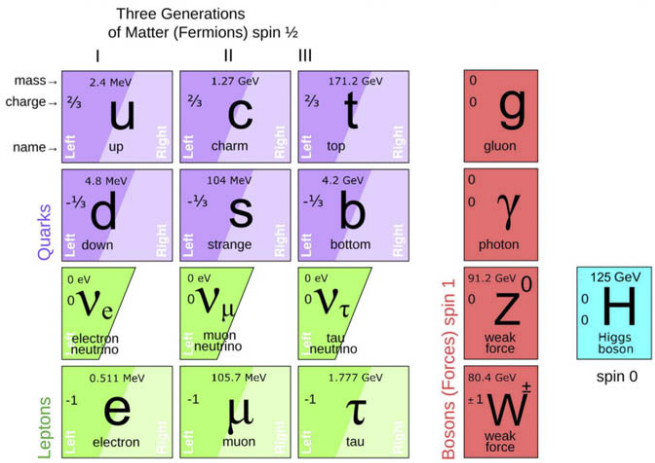

Figure 1.2: Particles considered in Standard Model. We can observe that neutrinos only have left-handed component

Neutrino Mass and Oscillations

Neutrino oscillations can be seen as the change of flavour of the neutrinos, because they are in a mixed state of three different eigenstates. The flavor oscillations can be expressed with the unitary rotation of the mass eigenstates:

$$|\nu_\alpha\rangle = \sum_i U^*_{\alpha i} |\nu_i\rangle \tag{1.3}$$

Where $\alpha = e, \mu, \tau$ and $i = 1, 2, 3$

When a neutrino is in propagation, the different masses of the eigenstates propagate in a different form and can produce changes in the neutrino flavor. This matrix, U^*, is the complex conjugated of U: the Pontecorvo-Maki-Nakagawa-Sakata matrix (PMNS or MNS). The PMNS matrix can be parameterized by the three Euler angles, $\theta_{12}, \theta_{23}, \theta_{13}$ and three phases, $\delta, \alpha_{21}, \alpha_{31}$.

$$U_{PMNS+M} = \begin{bmatrix} 1 & 0 & 0 \\ 0 & cos(\theta_{23}) & sin(\theta_{23}) \\ 0 & -sin(\theta_{23}) & cos(\theta_{23}) \end{bmatrix} \begin{bmatrix} cos(\theta_{13}) & 0 & sin(\theta_{13})e^{-i\delta_{CP}} \\ 0 & 1 & 0 \\ sin(\theta_{13})e^{-i\delta_{CP}} & 0 & cos(\theta_{13}) \end{bmatrix}$$

$$\begin{bmatrix} cos(\theta_{12}) & sin(\theta_{12}) & 0 \\ -sin(\theta_{12}) & cos(\theta_{12}) & 0 \\ 0 & 0 & 1 \end{bmatrix} \begin{bmatrix} 1 & 0 & 0 \\ 0 & e^{i\alpha_1} & 0 \\ 0 & 0 & e^{i\alpha_2} \end{bmatrix} \tag{1.4}$$

This matrix is product of three rotation matrices and also, the fourth matrix, has the Majorana extra phases but doesn't affect to neutrino oscillations, because these phases cancel out for any observable neutrino oscillations.

A good review of the current knowledge of those phases and angles can be found at [Gonzalez-Garcia, Maltoni, and Schwetz 2014].

Respecting the eigenstates mass values, the only quantities known are the so-called Solar Mass Splitting:

$$\Delta m^2_{sol} \equiv m_2^2 - m_1^2 = (7.45^{+0.19}_{-0.16}) \cdot 10^{-5} eV^2 \tag{1.5}$$

and the Atmospheric Mass Splitting

$$|\Delta m^2_{atm}| \equiv |m_3^2 - (m_1^2 + m_2^2)/2| = (2.421^{+0.022}_{-0.023}) \cdot 10^{-3} eV^2 \tag{1.6}$$

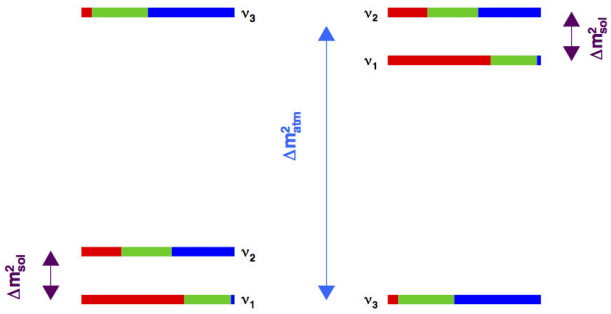

Figure 1.3: Summary of the knowledge about neutrino masses. In the left side, it is represented neutrino mass normal hierarchy. The other possibility, an inverted hierarchy is drawn in the right side

These two measurements are consistent with two different scenarios. In figure 1.3, we can observe in left side, the normal hierarchy and in the right side, the inverted hierarchy.

Majorana or Dirac neutrinos

Soon, in the neutrino's early years, when neutrino still was a theoretical particle, was postulated the double beta decay, where a nucleus cannot beta-decay once, but can twice. This decay was proposed by M. Goeppert-Mayer [Goeppert-Mayer 1935]

After this, it was proposed the theory of Majorana [Majorana 1937] and its application to beta decay [Racah 1937]

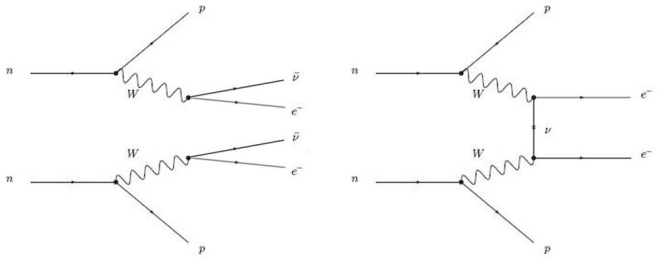

Figure 1.4: Feynmam diagram of the double beta decay. In the left side with neutrinos. In the right side, the theoretical decya without emission of neutrinos

There are two different explanations for neutrino behaviour: Dirac and Majorana. According to the Standard Model, all fermions are **Dirac particles**, i.e. particles that are distinguishable from their own antiparticles. On the contrary, **Majorana particles** are indistinguishable from their own antiparticle, making possible the mutual annhilition of two Majorana particles and may explain the smallness of the neutrino masses. Also, this decay violate lepton number conservation, and can be linked with the asymmetry between matter and antimatter in the Universe.

Therefore, if neutrinos are Majorana particles, it is possible to observe double beta processes where the neutrinos are not emitted and all the energy goes shared in the two emitted electrons.

$$ {}^{A}_{Z}X \rightarrow {}^{A}_{Z+2}Y + e^{-} + e^{-} \tag{1.7} $$

If NEXT observe unanbigously the ($2\beta 0\nu$) decay process, we can conclude that neutrinos are Majorana particles

Neutrino Sources

Because neutrinos are very elusive, they can travel very long distances in the Universe without interacting with anything and arrive to the Earth, and cross all of us with a extremely low interaction probability. Therefore, we are recieving a wide 'almost transparent' shower of neutrinos from very different sources. The kwon sources and their fluxes at the Earth are showed in figure 1.5, taken from [Spiering 2012].

The less energetic neutrinos come from the Cosmological Neutrino Background, the background after Big Bang with $T = 1.9K$. Next in enery are Solar neutrinos. Next are Supernova neutrinos; they are produced during the collapse of massive stars; Supernova 1987A is the only observed event. The Relic Supernova Neurtrino, also known as Diffuse Supernova Neutrino Background (DSNB), is the overall neutrino flux from all Supernova explosions during the history of our Universe. Atmospheric neutrinos are produced in the decay of π and K mesons,

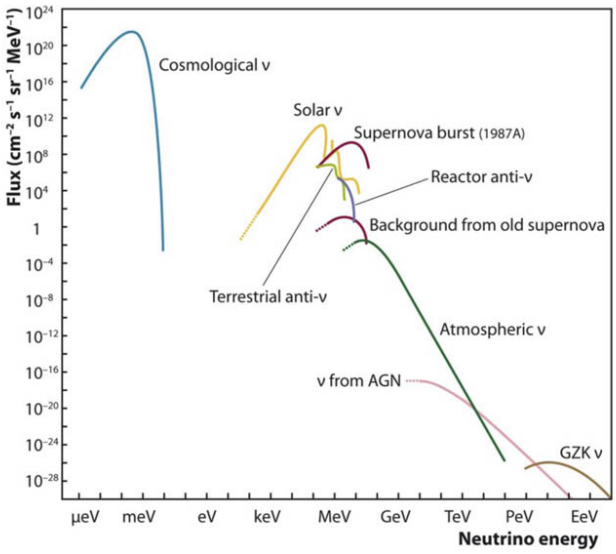

Figure 1.5: Representation of the most important neutrinos sources. Accelator neutrinos are not considered

produced by the interaction of heavy charged particles and nuclei from Cosmic Rays with the Atmosphere. Active Galaxy Nucleus (AGN) are a strong source of very high energy particles; they are placed in the center of active galaxies.

It is interesting to remark the terrestrial neutrinos, produced by the natural radioactivity: mainly the β decays of ^{40}K and the decay chains of ^{232}Th and ^{238}U. This neutrino flux is compossed by $\overline{\nu}_e$

Greisen-Zatsepin-Kuzmin (GZK) effect is a theoretical limit of the energy of the Cosmic Rays. Higher energy protons will interact with the Cosmic Microwave Background (CMB) producing π and the highest energy neutrinos predicted, after the π decay.

Man-made sources of neutrinos are mainly two: accelerators and reactors. These sources are very useful because they have well known propierties, like energy or travelled distance. Accelerators neutrinos are produced in the interaction of accelerated protons with a target, producing mesons and neutrinos in their decays. Reactor neutrinos are produced during the different reactions inside the

reactor, mainly the β decays of the fission fragments produced by the fission fuel (usually ^{235}U).

1.1 Experimental neutrino Physics; the physics cases of the experiments NEXT and SuperK-Gd

Around Neutrino Physics are built several experiments in different underground laboratories. Now, we are going to introduce the conceptual idea of this two experiments where I am involved: NEXT and SuperK-Gd.

SuperK-Gd is an upgrade of Super-Kamiokande, a neutrino detector. This new step will have gadolinium sulfate solved in the water to improve the capability to detect neutrinos.

NEXT is a Neutrino Physics detector, but not designed to observe neutrinos. This detector is designed to precisely measure the energy of the emitted electrons in double beta decay.

1.1.1 NEXT experiment

A electron produce a twisted track, producing new electrons during its path, and with a strong deposit of energy at the end. Later, a moderate electric field, enough to drift these electrons but not to produce new electrons, drifts them to the electroluminiscence region. Here, a strong electric field produce the emission of high energy photons.

NEXT detectors are asymmetric Time Projection Chambers (TPC) filled with high-pressure xenon gas, about 15 bar. The final detector, NEXT-100 will have 100 kg of enriched xenon, 90% of ^{136}Xe. These detectors has two different measurement planes: energy plane to perform a precise measure of the energy with a very good energy resolution, 0.5 - 1% at $Q_{\beta\beta}$ and tracking plane to reconstruct the track of the event and do background rejection.

NEXT Conceptual Idea: advantages

NEXT idea has several advantages over the other competitors. The advantages of using Xe are 2: a high $Q_{\beta\beta}$, it is a noble gas (the only noble gas with 2β-decay) and therefore features a low attachment, the high natural abundance of 136Xe isotope and it is easy to enrich. The advantages of using gas Xe are the good energy resolution $< 1\%$ and the possibility of tracking. In addition, combining tracking and radiopure selection of the components give us a very low background. Further, those properties make the NEXT concept scalable.

Light production

In the detector, the electrons from 2β-decay excite and ionize the Xenon gas, figure 1.6. The Xenon atoms de-excitate very rapidly (about 1 ns) emitting a rather small 172 nm light signal (S1), that is detected at the energy plane and serves as trigger. The ionization electrons are drifted by a weak electric field to the electroluminescent (EL) region. There, a larger electric field such to excite the xenon, but not enough to ionize it, accelerates electrons producing a big amount of 172 nm scintillation light (S2).

This light is wave-length-shifted (WLS) to the blue region by a *1,1,4,4-tetraphenyl-1,3-butadiene* (TPB), a wavelenght-shifter that increase the amount of light and converts the 175nm light to 440nm light. This blue light, can be easily detected with SiPM.

The energy plane will measure precisely the number of photons produced (Fig. 2, left).

Light detection: Energy plane

In the opposite of the EL region, it is the **Energy Plane**, designed to measure the energy of the event as precisely as we can. There, tens of radiopure-designed PMTs, Hamamatsu R11410-10, will precisely measure the energy of the event, with an energy resolution better than 1%. PMTs are the selected option

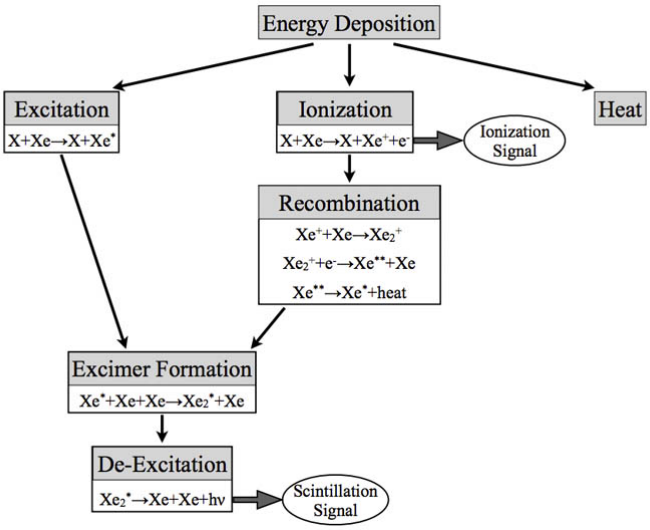

Figure 1.6: Schematic resume of how energy is deposited in Xenon. Both signal S1 and S2 are produced thanks to this process.

because of their low energy resolution, ideal to separate the signal from the close background peaks in the region of $2\beta0\nu$.

Light detection: Tracking plane

Close to the EL region, we have the tracking plane. There, TPB coated Si-Photomultipliers (SiPMs) reconstruct the two electrons tracks from the 2β-decay. They form a single twisted line with a strong energy deposition at both ends. This technique is crucial to reject background events.

Background control of the experiment

Similar to electron emission in double beta decay, gamma emitters can ionize some xenon atoms, producing a signal that can mimic the expected signal. The two main dangerous gamma emitters are ^{208}Tl with an gamma energy of 2615 keV and ^{214}Bi with a energy of 2448 keV, both values too close to the $Q_{\beta\beta}$ expected signal for the $2\beta0\nu$.

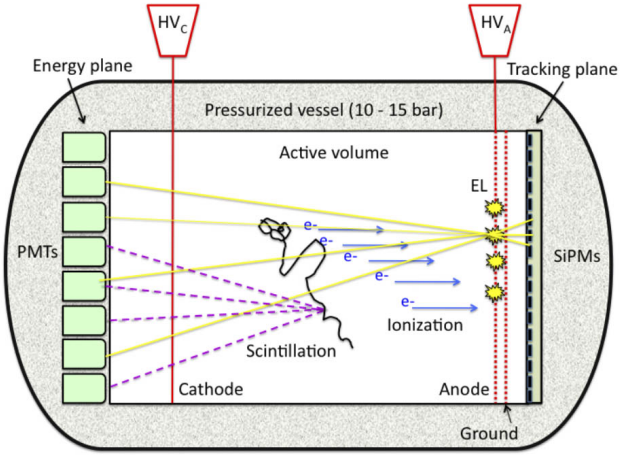

Figure 1.7: Schematic explanation of the light production in NEXT detector. We can observe S1, the drifting electrons and S2

To control the background of the experiment, there are two working groups that try to solve this problem: Radiopurity Group and Background Model Group.

Radiopurity Group, composed by Luis Labarga and me from Universidad de Madrid (UAM), by Susana Cebrián from Universidad of Zaragoza (UZ) and with the help of Iulian Bandac from Laboratorio Subterráneo de Canfranc (LSC) and several colleagues from Instituto de Física Corpuscular (IFIC) from Valencia; studies the effect of the radioactive contaminations in our low background detectors and also quantify these activities.

Background Model Group, composed mainly by several physicists from IFIC and from Universidad de Santiago de Compostela (USC), is working in MonteCarlo simulations to determine the acceptable upper limits of the background and also quantify the total effect of these background.

1.1.2 SuperKamiokande experiment

Super-Kamiokande (SK) is the most important detector for nucleon decay and neutrino physics. In this important collaboration, there are working about 150 people and 40 institutes from Japan, the United States, Korea, China, Poland, Spain, Canada, UK, Italy and France.

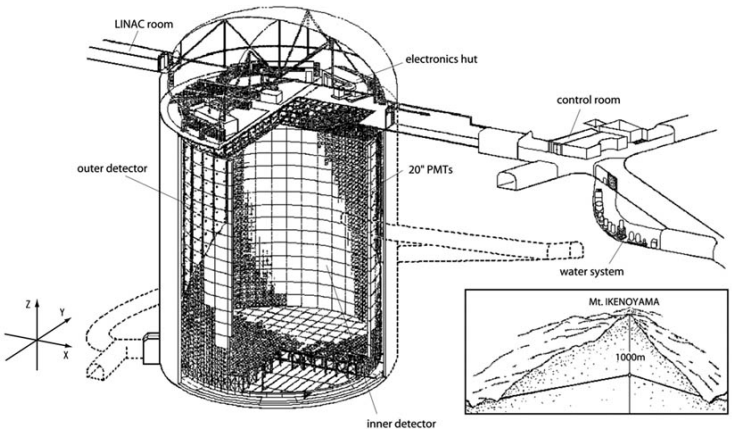

Figure 1.8: Schematic view of SuperKamiokande and the emplacement inside the Mt. Ikenoyama

History and milestones of the detectors

SuperKamiokande is the evolution of the detector **KamiokaNDE** (Kamioka Nucleon Decay Experiment). Kamiokande construction started in 1982 and finished in 1983. It was designed to observe the proton decay but it only could obtain a limit in this decay. Lately, the evolution Kammiokande-II, in 1985, made important neutrinos observations like the Solar Neutrinos, the Atmospheric Neutrinos, the Neutrinos from Supernova 1987A and the experiment KEK to Kamioka, K2K. But, no nucleon decay was observed. Thanks to its discoveries, in 2002, Masatoshi Koshiba was awarded with the Nobel Prize *for pioneering contributions to astrophysics, in particular for the detection of cosmic neutrinos*[5].

[5] *http : //www.nobelprize.org/nobel_prizes/physics/laureates/*2002/

The next upgrade of the detector was **Super-Kamiokande**. The SK detector is a cylindrical tank with 39.3 m in diameter and 41.4 m in height and filled with 50 kton of ultrapure water. This detector is located in the Kamioka mine (Gifu Prefecture, Japan) under Mountain Ikenoyama, with 1000 m of rock overburden (or 2700 m water equivalent), shielding the detector and reducing the cosmic ray muon background.

The detector is divided into two parts: the inner detector and the outer detector, Inside the **Inner Detector** have 32 kton of water. Inside, the cylindrical water tank has covered all its inner surface with 11148 PMTs, 20" model R3600. But, in any case, not all the water volumen is used for most of the physics measurements, it is usual to disregard the 2 m closer to the walls of the inner detector, that is about 22.5 kton. The **Outer Detector**, also covered with 1885 PMTs, 8", is another water Cherenkov detector that acts like a veto for Cosmic Rays events.

The SK experiment started in April 1996 and shut down for maintenance in July 2001. The first phase of the experiment is called SK-I. During refilling after maintenance, an accident occurred in November 2001, in which more than half of the PMTs were destroyed due to the implosion of a PMT. After the accident, the SK detector was rebuilt with half of the original PMT density in the inner detector. A Fibre-reinforced plastic (FRP) cover was used in each PMT to prevent chain reaction implosions. The operation was resumed in October, 2002, phase called SK-II. In October 2005, the experiment was completely rebuilt and resumed data taking with the all of PMTs in July 2006, this phase is SK-III. Finally, in September 2008 starts the current phase, SK-IV, with upgraded new version of the front-end electronics.

SK is a very successful collaboration: it has discovered atmospheric neutrino oscillations, it was key in the solution of the solar neutrino problem and it is measuring precisely an important fraction of the elements of the leptonic mixing matrix. With K2K collaboration, it was the first time that was observed neutrino oscillations in a long baseline experiment. With T2K collaboration, has provided evidence of a non-vanishing value for θ_{13}, exploring the idea of CP violation in

the lepton sector. In 2015, Dr. Takaaki Kajita was awarded with the Nobel Prize *or the discovery of neutrino oscillations, which shows that neutrinos have mass*[6].

Super-Kamiokande, a water Cherekov detector

All of these Kamioka detectors are a Cherenkov light detector. This phenomena was firstly postulated by Oliver Heaviside [Heaviside 2008] and observed by Pavel A. Cherenkov [Cherenkov 1937]. Cherenkov, I. Frank and I. Tamm were awarded by the Nobel Prize in 1958 *for the discovery and the interpretation of the Cherenkov effect*[7].

Cherenkov light is an emitted light from charged particle moving through a dielectric medium with a speed higher than the light in this medium. This light has a cylindrical symmetry in the direction of the relativistic particle, with an angle of emission that follow this equation:

$$cos(\theta) = \frac{1}{n \cdot \beta} = \frac{1}{n}\sqrt{1 - \frac{m}{|\overrightarrow{p}|}} \tag{1.8}$$

Where n is the refraction index in this medium, m is the mass of the particle, $\overrightarrow{p}$ is the momentum of the particle and β is the quotient between the speed of the particle and of speed of light in vacuum.

In our case, in ultra-pure water detector, the speed of light is about $0.75c$, the speed of the ionizating particles are very close to c and $n = 1.33$. Therefore, it is easy to observe high energy particle with a speed close to the light. Then, according to these values, the typical Cherenkov angle is:

$$cos(\theta) = \frac{1}{n \cdot \beta} \longrightarrow \theta = cos^{-1}\left(\frac{1}{1.33}\right) = 41.2^{\circ} \tag{1.9}$$

[6] $http://www.nobelprize.org/nobel\_prizes/physics/laureates/2015/$
[7] $http://www.nobelprize.org/nobel\_prizes/physics/laureates/1958/$

This emitted visible emitted light, follows a spectra peaked at 375 nm, blue light, shown at figure 1.9, left. At the right side, we can observe the spectrum of Quantum Efficiency (QE) of the PMTs used in SK.

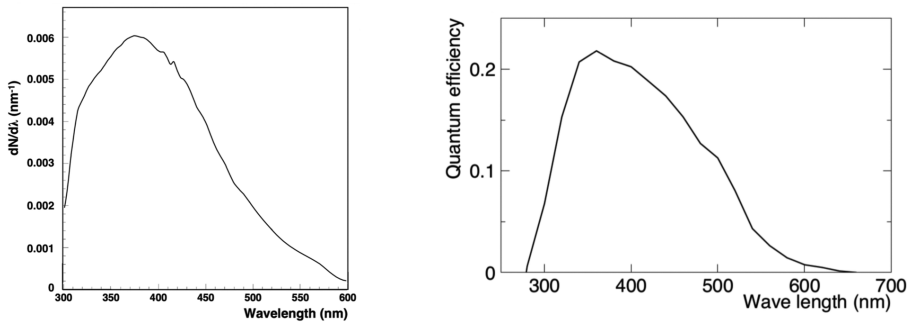

Figure 1.9: Inthe left box, we can observe the wavelength spectrum of the Cherenkov light produced in water. In the right box, the quantum efficiency of PMTs used in SuperK

Quantum efficiency is the conversion factor of photons to electrons, usually called photoelectrons. These PMTs were chosen to maximize the detected signal of each event.

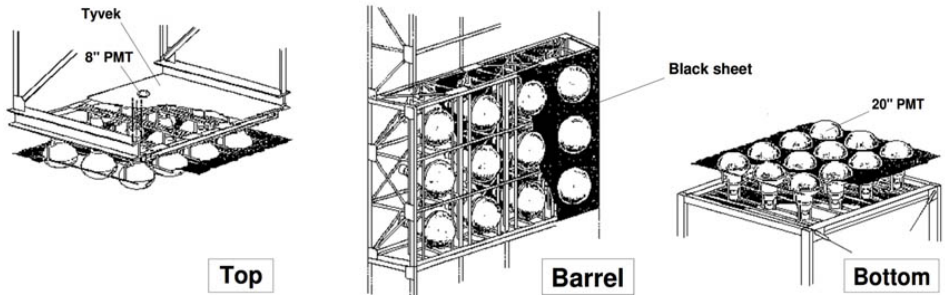

Figure 1.10: Three different supporting structures for the PMTs in SuperK detector

The next two future steps are **Hyper-Kamiokande** and **SuperK-Gd**. Hyper-Kamiokande is a new and larger version of the water Cherenkov detectors in Kamioka, that is scheduled for 2020. SuperK-Gd, where a UAM Physicists Group, composed by Luis Labarga, Pablo Fernández and me, takes part on this Collaboration, is an upgrade of Super-Kamiokande detector. In this new version, we will solve a gadolinium salt to capable to distinguish between neutrinos and antineutrinos. It will be explained widely in Chapter 3.

1.2 Radioactive contamination in materials

In neutrino experiments, where the number of events are very small, we have to select the materials with high precision to control every possible source of background.

We have to consider that materials are not completely pure. Not only one element compose a material. That means that we will find out several impurities and we have to evaluate them in terms of their radioactivity. For a more complete explanation on this field, I recommend to read this reference paper in the field, [Heusser 1995].

1.2.1 Origin of the radioisotopes

First of all, we are going to identify the different sources of radioisotopes. This information is useful to understand the activity of some radioisotopes and to know why some samples have this radiosotope in its composition.

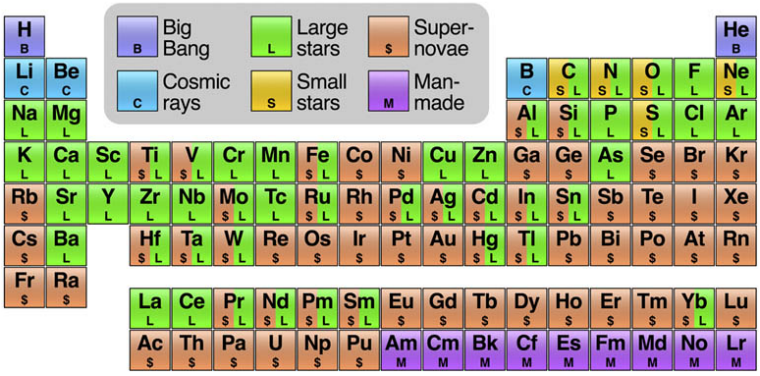

Figure 1.11: Periodic table where are indicated the origin of all the elements. Picture taken from wikipedia.

- **Primordial radionuclides**: these radionuclides were created before the formation of the Earth. In the nucleosynthesis process, there are three different sources: Big Bang, Stellar nucleosynthesis and Supernova explosions.

In Big Bang where created hydrogen, helium and some traces of lithium. In stellar nucleosynthesis were produced some other small nuclei like carbon, nitrogen and oxygen. Finally, in Supernova explosions, we will find a broader number of new nuclei, some of them radiosotopes. But, most of them have decayed due to its short half-life in comparison with the moment when they were created.

At the present time, we only can observe those isotopes with half-lifes in the order of hundreds of millions of years, like ^{40}K, ^{238}U, ^{232}Th and ^{235}U. Additionaly, we can observe several secondary radionuclides, that are the succession of decays of the unstable daughters of these primordial radionuclides, known as **Decay Chains**. We will take deeply about this in section 2.2.

The 32 Primordial radionuclides are: ^{40}K, ^{48}Ca, ^{50}V, ^{76}Ge, ^{82}Se, ^{87}Rb, ^{96}Zr, ^{100}Mo, ^{113}Cd, ^{115}In, ^{116}Cd, ^{128}Te, ^{130}Te, ^{130}Ba, ^{136}Xe, ^{138}La, ^{144}Nd, ^{147}Sm, ^{148}Sm, ^{150}Nd, ^{151}Eu, ^{152}Gd, ^{174}Hf, ^{176}Lu, ^{180}W, ^{186}Os, ^{187}Re, ^{190}Pt, ^{209}Bi, ^{232}Th, ^{235}U and ^{238}U.

- **Cosmogenic radionuclides**: cosmic rays are a high-energy shower of charged particles mainly originated outside our Solar System. 90% of these particles are protons, 9% are alpha particles and the other particles are positive-charged nuclei, electrons and a small fraction of these are antimatter particles.

  Cosmic rays can produce new nuclides directly by spallation[8] or can undergo various transformations with the upper part of our atmosphere, creating some particles that will produce the new nuclides.

  The most used cosmogenic radionuclides are ^{3}H, ^{10}Be, ^{14}C, ^{21}Ne, ^{26}Al, and ^{36}Cl; usually for dating geologic materials or rocks. For example, ^{14}C is the most famous cosmogenic radionuclide used in dating methods. Cosmogenic production of ^{14}C and its decay rate, gives a constant ratio

[8] Cosmic Spallation is a process where a high energy cosmic rays collide with a nucleus expulsing a high number of the nucleons

between ^{14}C and ^{12}C. When a sample is isolated from new cosmogenic ^{14}C, the measure of this ratio gives the age of this sample.

But, in our case, the exposure of the detectors components to the high energy particles shower can produce a wide presence of not welcome radiosiotopes. Specifically, in [L. Baudis et al. 2015], they have studied the cosmogenics activation of two very important elements for NEXT: xenon and copper. In Xenon, has been observed these isotopes: ^{7}Be, ^{85}Sr, ^{88}Zr, $^{91*}Nb$, ^{99}Rh, ^{101}Rh, $^{110*}Ag$, ^{113}Sn, ^{125}Sb, $^{121*}Te$, $^{123*}Te$, ^{126}I, ^{131}I, ^{127}Xe, $^{129*}Xe$, $^{131*}Xe$, ^{133}Xe, and ^{132}Cs. In copper, has been observed: ^{46}Sc, ^{48}V, ^{54}Mn, ^{59}Fe, ^{56}Co, ^{57}Co, ^{58}Co and ^{60}Co.

- **Anthropogenic radionuclides**: in Twentieth century, we started to understand and control the power of the atomic nucleus. This knowledge allows us to create new radiosotopes. For example, most of the radionuclides for medical purposes are produced in nuclear plants like Petten nuclear reactor (Netherlands) or Chalk River Laboratories (Canada), but also it can be produced in cyclotrons. With this techniques, they create short-lived radioisotopes for therapies. But anycase, this sources are well controlled and they are not an usual source of radioimpurities.

  The main sources of radioimpurities of anthropogenic radionuclides are nuclear weapons, nuclear power plants and uranium minning. The most recent and strong contributions to the contaminations of anthropogenic raadionuclides where the two most important nuclear power plants accidents: Chernobyl (1986) and Fukushima (2011).

  These two accidents and the nuclear weapons testing thrown to the atmosphere various radionuclides (some of them short half-lifes), but the most important are ^{90}Sr and ^{137}Cs.

1.2.2 Sources of radioactive

Now, after showing the origin of the radioisotopes, we can present where we can find them in a experiment, also presenting how to protect the experiment from these sources of background.

Environmental Radioactivity

The most significant radiosotopes in the Earth Crust are Decay Chains of ^{238}U and ^{232}Th and ^{40}K. The typical activity of ^{40}K is about hundreds of Bq/kg. In the case of these two Decay Chains the activities are about tenths of Bq/kg

Usually, these chains are not in equilibrium in surface samples, because they suffer some migrations due to physical or chemical processes.

This is one of the reason why all the low activity experiments as also an external shielding to avoid this source of background.

Radon in the air

One of these elements that breaks the equilibrium of the decay chains is Radon, present in the three decay series. This element can emanate from the material due to the recoil of the alpha particle emission or also due to the diffusion from the material. Typically, the concentration in air is about $40 Bq/m^3$.

These radon atoms are particularly dangerous, because the can enter inside the detector but also can be found attached to the surface of the materials of the detectors. The most important isotope is ^{222}Rn, with a half-life about 4 days, that can decay to ^{214}Bi, a very important and dangerous source of background.

Then, one of the best solutions is to have a gas system to reduce the presence of this isotope in the air.

Cosmic Rays background

Cosmic rays in the upper part of the atmosphere are an indirect source of background, because can produce several particles. Primary cosmic rays, mainly protons and alpha particles, produce different interections with the upper part of the atmosphere. Therefore, can be produced the secondary Cosmic Rays, that are (ordered by intensity at sea level): muons, neutrons, electrons, protons and pions.

Cosmic Rays background can be divided into two different forms: the secondaries Cosmic Rays and the the activation of the materials, explained previously.

Then, it is necessary to place the detectors inside a underground laboratory, to shield with the mountain the flux of secondary Cosmic Rays, mainly neutrons and mouns.

Radioactivity from Detector and Shielding

To reduce these previous sources of background, we have to shield the detector from them. Therefore, we will find the two last possible sources of background: the shielding and the detector itself.

The shielding are usually two elements: lead and copper. Lead is cheaper and is used for the external part of the shielding, because unfortunately it has also some radioactive contaminations. Then, the internal part of the shielding is made by copper. This metal, thanks to its high redox potential, can be easily separated from K, U and Th, producing a very low bakground material with also a strong capability to reduce external backgrounds.

Finally, to build a successful low background detector, it is mandatory to carry out a **Radiopurity Campaign**. It consist of a deep study of the behaviour of the radioactivity in materials, a coordinate work with the engineers to design the detectors and a precise selection of the materials to build a detector capable to fullfill the background requeriments that we have.

2

Introduction to radioactivity physics

An atomic nucleus is a small region (of the order of the fentometers) where it is located the most massive part of the atom. In this region we can find the nucleons (protons and neutrons) that compose the nucleus and some exchanging particles to keep the nucleus together.

Radioactivity is a transition process where the state of a atomic nuclei changes emitting some particles. **Spontaneous Radioactivity** is a exothermic proccess where the nucleus emits particles, losing energy, trying to reach a more stable configuration.

Radioactivity was discovered by Henri Becquerel[1] in 1896, thanks to the observation of radiation from uranium that interacts with photographic paper. After discarting other hypotheses, he concluded that uranium emits rays by itself.

Following this work, Pierre and Marie Curie discovered that thorium is also a radioactive element. They also discovered polonium and radium trying to isolate the sources of these rays.

In 1903, Henri Becquerel won the Nobel Prize, shared with Pierre and Marie Curie *in recognition of the extraordinary services he has rendered by his discovery of spontaneous radioactivity*[2].

To finish this short historical review, in 1899, Ernest Rutherford discovered that a magnetic field can interact with this radioactive emissions, binding them into two different directions. The positive particles were **Alpha Rays** and the negative were **Beta Rays**. In 1900, Paul Villard discovered a different type of radiation from radium, not affected by magnetic fields and named by Rutherford with **Gamma Rays**. This classification also follows their power to penetrate materials, where the less penetrating radiation are Alpha Rays. This three type of emissions are the most common radioactive emission produced in a nuclear decay.

To continue this chapter, we are going to present some usual concepts related with radioactivity.

First of all, in a nuclear desintegration, we define as the **parent nucleus** that one before the nuclear decay and we also define as the **daughter nucleus** the new nucleus after the decay, that also might produce the emission of particles and energy. Each radioactive isotope can also be called **radioisotope**, **radionuclide** or only **nuclide**.

[1] It is necessary to use the name to name this Physicist, because his family had a long tradition in science: grandfather (Antoine César Becquerel), father (Alexandre-Edmond Becquerel) and son (Jean Becquerel)

[2] *http://www.nobelprize.org/nobel_prizes/physics/laureates/1903/*

Other important parameter in nuclear decays is the Q-value. It is defined like the released energy during a desintegration.

$$Q = (m_{initial} - m_{final})c^2 \tag{2.1}$$

This energy will be shared by the emitted particles.

To quantifity the radioactivity, The International System of Units (in French, Système international d'unités, SI) define the derivated unit known as **Becquerel, Bq**. One becquerel is the activity of one radioactive sample with one desintegration per second. An older radioactivity unit used to meausure radioactivity is the **Curie** (Ci), that is the activity of one gram of ^{226}Ra (1 Ci = 37 GBq).

Radioactivity is a quantum process and we cannot predict when an atom will decay. But, in our work in radiopurity, we are only considering very massive samples, where we can define several constants and laws to study this process. One of this macroscopic constants to study radioactivity is the **mean lifetime** τ (usually call lifetime). It is also related with the decay constant, λ:

$$\lambda = \frac{1}{\tau} \tag{2.2}$$

The third usual constant to quantify the decay rate is the half-life, $t_{1/2}$ that is the time required for a decaying sample to reduce its quantity by a half of its initial value. The relation with the other constants is as follows:

$$t_{1/2} = \frac{ln(2)}{\lambda} = ln(2) \cdot \tau \tag{2.3}$$

Since every nucleus has an intrinsic probability to decay, we can affirm that the number of decays depend on the number of atoms we have, N. Then, we can write:

$$\frac{dN}{dt} = constant \cdot N \tag{2.4}$$

And by solving this equation, we can find the most important equation for nuclear decays, where the constants reflect the initial conditions.

$$N = N_0 \cdot e^{-\lambda t} \tag{2.5}$$

The last parameter (but not the least... maybe is the most useful) to consider is **Activity**. This is the rate of decays of a radioactive sample:

$$A = -\frac{dN}{dt} = \lambda \cdot N \tag{2.6}$$

The activity depends on two factors: the number of atoms and the half-life of these atoms. When you observe a sample during periods in the order of magnitude of its half-life, you can observe changes in the number of atoms and also in its activity.

We can also define the **specific activity** that is the activity divided per mass unit. The specific activity is the unit used for the measurements we have taken in several laboratories, but usually we only call it as activity.

Finally, we have the **Decay Scheme** diagram, figure 2.1, where are arranged certically the energy level of the parents and daughters nuclei. For a spontaneous decay, the energy levels of the daughters nuclei must be below the parent energy level.

With horizontal lines, we represent the energy levels of the parent nucleus and the different possible energy states of the daughter nuclei. For spontaneous decays, you have to reach to a lower energy level. Vertical arrows present the

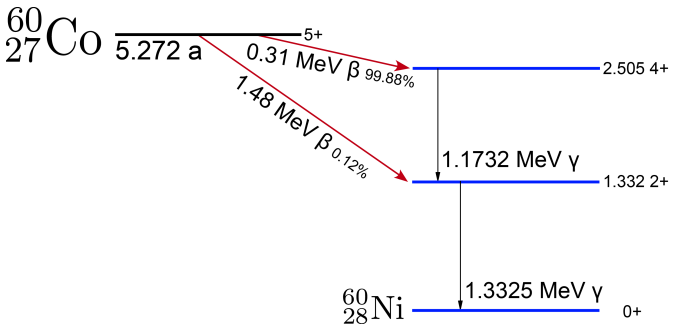

Figure 2.1: Decay scheme of 60Co

gamma photons emitted to reduce the energy of the nucleus, in the way for a more stable state.

Diagonal arrows indicate the type of decay and the branching ratio of this decay: the probability to undergo this decay branch. In the example in Figure 2.1, ^{60}Co decays beta with 0.31 MeV (prob 99.88 %) and emiting two photons with 1.17 MeV and 1.33 MeV. But it can also beta decay with 1.48 MeV (prob 0.12 %) emiting only one photon with 1.33 MeV.

In the right side of the diagram we have the J^P of this state, where J is the value of the nulcear angular momentum and P is the value of the parity.

The probability of each decay are ruled for several factors. In alpha decay, for instance, a change in the nuclear angular momentum between the parent and the daughter nuclei implies a more complicated way to escape for the alpha particle, significantly decreasing the probability of this decay branch.

Sometimes, after a decay, the nuclei remain excited. Thus, to reach the ground state, the nucleus emits **Gamma Rays** carrying out the excess of energy. These transitions between ground and excited states are commonly very fast (lower than picoseconds). But, there also exist some long-lived excited states called **Nuclear Isomers**. A Nuclear Isomer is a metastable[3] state of the nuclei, because its decay time is several orders of magnitude bigger than the usual decay time, typically about $1\mu s$. The most usually observed case in our work is $^{234*}Pa$.

[3]The usual notation for a metastable nuclei is * or ^{m} after the mass number

For a more complete information in this field, I recommend to read *Radioactivity Radionuclides Radiation* [Magill and Galy 2005], *Radiation Detection And Measurement* [Knoll 2000], *Techniques for Nuclear and Particle Physics Experiments: A How-to Approach* [Leo 2012], *Introductory Nuclear Physics* [Krane 1987], *An Introduction to Nuclear Physics* [Cottingham and Greenwood 2001] and also with the lessons of Prof. H. C. Verma (Department of Physics, IIT Kanpur) in the youtube channel of National Programme on Technology Enhanced Learning (NPTEL) from India.

One last comment, this work in centered in radiopurity and in radioactive decays in very low background detectors. Then we will not consider the induced radioactivity like, for example, the one produced by neutrons (the most usual purpose is the induced nuclear fission) or the one produced induced by laser, used to increase the probability for a nuclear decay.

2.1 Type of nuclei radioactivity decays

Radioactive decays have a wide range of different decays. These are the most common observed nuclear decays:

- Hadronic decays: a hadron is a particle composed by quarks, for example neutrons, protons, pions, etc. In these decays, the emission of hadrons is the way used to release energy. The most usual is **alpha decay** (with the emission of an alpha particle composed by 2 protons and 2 neutrons), but we also can find proton emission, neutron emission, double proton emission and cluster decay (emission of a specific type of smaller nucleus bigger than an alpha particle).

  Fission is also a hadronic decay, where a very massive nucleus stochastically splits into two new nuclei (sometimes can be 3 daughter nuclei) with the emission of several neutrons and high energy photons.

- Leptonic decays: this decay emits leptons but always following lepton number conservation. The most common leptonic decay, called **beta decay**, emits an electron and an electron antineutrino. We can also find

positron emission, electron capture, bound state beta decay, double beta decay, double electron capture, electron capture with positron emission and double positron emission.

In any case, we are going to consider only those that are important in radioactive contamination in our experiments, mainly because of their frequency.

Alpha Decay

Alpha decay is a process where one nucleus decays emiting an alpha particle. In 1909, Becquerel and Royds discovered that an alpha particle is an Hellium[4] nucleus. This emission reduces the number of protons by 2 and the number of nucleons by 4. Soon after this decay, the nucleus and the alpha particle reach a neutral configuration with the emission/capture of electrons

$$ {}^{A}_{Z}X \rightarrow {}^{A-4}_{Z-2}Y + {}^{4}_{2}\alpha \tag{2.7} $$

In terms of energy, we can write the equation considering the binding energy of the electrons negligible in comparison with the masses.

$$ Q_\alpha \approx (M_{parent} - M_{daughter} - M_{He})c^2 \tag{2.8} $$

Typically, we can observe that for atomic number $A \gtrsim 150$, Q is positive. That means that this decay can be produced spontaneously.

Then, using the conservation of the linear momentun, we can conclude that the emitted particle and the recoiling nucleus are in the same line but with opposite direction. And, also according to conservation of the energy, we can calculate the kinetic energy of the emitted alpha particle and the small recoil in the nucleus

[4]Despite Hellium is the second most common element in the Universe and is produced in stars by Nuclear Fusion, in the Earth is not so common and mainly produced by alpha decay.

produced with this decay. But, in any case, the alpha particle transport most of the kinetic energy of this decay.

$$K_\alpha \simeq Q(1 - \frac{4}{A}) \tag{2.9}$$

This kinetic energy of the alpha particle, that is the magnitude we are going to observe with our detector (because the nucleus is not usually free), is strongly depended with A; where for a very massive nuclei all the kinetic energy is mainly for the emitted particle.

A very good approach for alpha decays can be obtained with the Geiger-Nuttall law [Geiger and Nuttall 1911], which relates the decay constant with the number of protons of the nucleus and the energy of the released alpha. It is important to know that this law works properly in nucleus with even number of protons and even number of neutrons, as we can see in Figure 2.2. In other configurations (odd-even, even-odd and odd-odd) is not as precise as it is in that configuration. The law is as follows:

$$ln(\lambda) = -a_1 \frac{Z}{\sqrt{E}} + a_2 \tag{2.10}$$

After alpha emission discovering, there was a twofold unsolved question about alpha decay: how an alpha particle can scape from the nucleus with a Coulumb potencial barrier several times bigger than the kinetic energy of the particle and why this decay follows equation 2.10.

In 1928, George Gamow [Gamow 1928] found an explanation for these two problems. According to Gamow's description, the emission of a particle with less energy than the Coulomb potencial barrier was described by a simple toy-model that was one of the first applications of quantum tunneling predictions. The approximation starts with previously-formed alpha particle inside the nucleus with an energy between 4 and 10 MeV, and also with the nuclear Coulomb potential barrier about 20-30 MeV. Then, the alpha particle inside the nucleus tries to escape from the nucleus according to the probability predicted

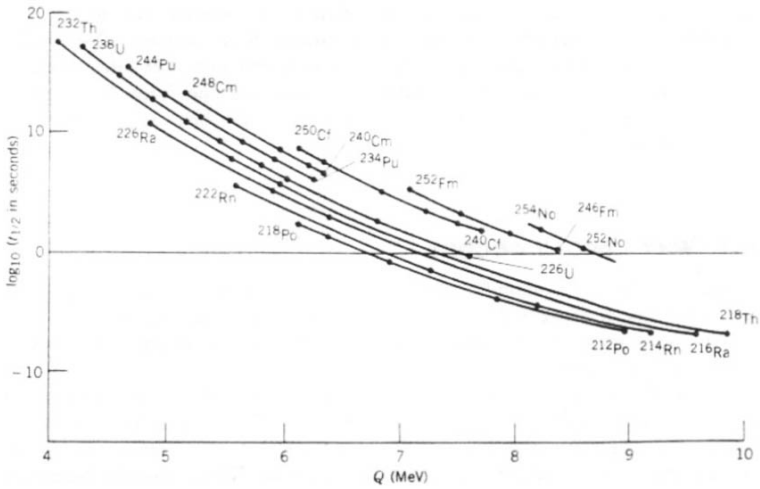

Figure 2.2: Representation of evenZ evenN nuclei, picture taken from Introductory Nuclear Physics (Kenneth S. Krane), chapter 8.

by quantum tunneling theory. With this simple hypothesis and with some calculations, Gamow also obtained this formula and the explanation of how an alpha particle can escape from a nucleus.

As a source of radioactive background, alpha decay is not dangerous for our experiments because an alpha particle can be easily recognized in our detectors. But, an alpha particle can also produce an (α, n) reaction and also the unstable daughters can emit gamma rays.

After an alpha decay, it is important to consider the emission of gamma rays from excited daughters. We will talk about this in 2.1

We also have to consider another type of background from Alpha Decay, the **Induced Neutrons** after an Alpha decay. (α, n) **reaction** is the process where a nucleus capture an alpha particle and undergo the emission of a neutron. Now, the alpha particle follows the reverse process: it has to cross the Coulomb potential barrier to enter inside the nucleus and also has to prompt a neutron.

Depending of the Q of the reaction, the energy threshold can be:

Element (Natural Isotopic Composition)	Neutron Yield per 10^6 Alphas of Energy 4.7 MeV (^{234}U)	Neutron Yield per 10^6 Alphas of Energy 5.2 MeV (av. Pu)	References	Av. Neutron Energy (MeV) for 5.2 MeV Alphas (Ref. 29)
Li	0.16 ± 0.04	1.13 ± 0.25	30	0.3
Be	44 ± 4	65 ± 5	31	4.2
B	12.4 ± 0.6	17.5 ± 0.4	29, 30, 33	2.9
C	0.051 ± 0.002	0.078 ± 0.004	29, 30, 31	4.4
O	0.040 ± 0.001	0.059 ± 0.002	29, 30, 31	1.9
F	3.1 ± 0.3	5.9 ± 0.6	29, 30, 33	1.2
Na	0.5 ± 0.5	1.1 ± 0.5	32	
Mg	0.42 ± 0.03	0.89 ± 0.02	29, 30, 31	2.7
Al	0.13 ± 0.01	0.41 ± 0.01	29, 30, 31	1.0
Si	0.028 ± 0.002	0.076 ± 0.003	29, 30, 31	1.2
Cl	0.01 ± 0.01	0.07 ± 0.04	32	

Figure 2.3: In this table, taken from Passive Nondestructive Assay of Nuclear Materials, were measured several neutron production rate from some low A isotopes

- for negative values of Q

$$E_{Threshold} = -Q(1 + \frac{A}{4}) \tag{2.11}$$

- for positive values of Q

$$E_{Threshold} = 0 \tag{2.12}$$

With these two conditions, we can estimate that most of these reactions will take place in light (low number of nucleons) nuclei.

In NEXT, where most of the elements are very heavy, this reaction is not a problem. But, in SuperK-Gd we mainly will have water with Gadolinium sulfate, then it is possible that oxygen can capture some of these alpha particles

We can observe in figure 2.3 that it is possible to produce a neutron background from (α, n) reactions with oxygen present inside the water tank. Alpha particles lose energy in very short distances, but Gadolinium salt is disolved in the water and alpha-emitter impurities in the salt can produce this reaction.

This can be a very dangerous source of background in SuperK-Gd, because the contamination with ^{238}U, ^{232}Th and ^{235}U chain produces a neutron background that can mimic the expected signal.

Beta Decay

Beta Decay is a weak-interaction decay of a nucleon with the emission of a lepton and an antilepton. At the first observations of beta decays only an emitted electron with a non-discreet energy spectrum was detected. This is the most significant difference with alpha decay: the energy spectra of the detected emitted particle is not constant. It follows a distribution of energy with the mean value approximately 1/3 of the maximun value.

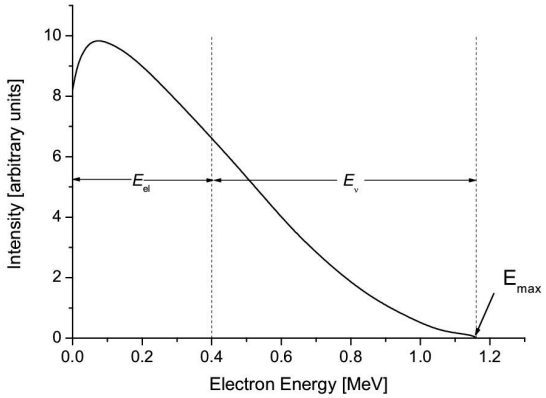

Figure 2.4: Schematic view of the energy distribution of an beta decay

Wolfgang Pauli in 1930[5] found an explanation to this decay: there are emitted two particles but the second **was** undetectable and has neither mass nor charge, the neutrino. I used 'was' because that was the first definition. Now we know that neutrino can be detected and that it has mass since oscillations have been observed.

[5]This famous letter is known by how it starts: *Dear Radioactive Ladies and Gentlemen...*

The first complete explanation of this spectra was given by Enrico Fermi in 1934 [Fermi 1974], using time dependent Perturbation Theory and the Fermi's Golden Rule:

$$\lambda = \frac{2\pi}{\hbar} \mid H_{if} \mid^2 \frac{dn}{dE_f} \tag{2.13}$$

Where λ is the transition rate, H_{if} is the interaction Hamoltonian (that depends of the inicial and final states) and dn/dE_f is the density of states at final energy.

Inside beta decay category, we can consider three different types of reactions that involves this decay[6]

$$n \rightarrow p + e^- + \overline{\nu} \tag{2.14}$$

In this case, an electron, e^-, and a antineutrino, $\overline{\nu}$ are emitted. This is due to the lepton number conservation, which implies that the sum of leptons and antileptons must be constant. The observation of the ($2\beta 0\nu$) will imply the violation of the conservation of the lepton number measured.

The three most common beta decays reactions are:

β^- decay

$$^A_Z X \rightarrow ^A_{Z+1} Y + e^- + \overline{\nu} \tag{2.15}$$

β^+ decay

$$^A_Z X \rightarrow ^A_{Z-1} Y + e^+ + \nu \tag{2.16}$$

[6] A free neutron has a half-life about 10 minutes, but when the neutron is bounded in a nucleus there are different forces and processes that modifies that half-life.

Electron Capture

$$ {}^{A}_{Z}X + e \rightarrow {}^{A}_{Z-1}Y^{*} + \nu \tag{2.17} $$

Now, we will talk about the most usually observed decay in world of radiopurity, β^{-}. It is produced to balance the number of neutrons and protons and also can be described as a neutron decay.

The decay energy of β^{-} can be approximated to:

$$ Q_{\beta^{-}} \cong (M_{parent} - M_{daughter})c^{2} \tag{2.18} $$

The energy spectrum is wider than alpha decay, with energies between some tenths of keV and 4 MeV. Additionally, after this emission, the nucleus usually remains excited and have to emit gamma photons or inner bounded electrons to release this energy.

Regarding health risks, high energy beta particles can be dangerous because of its penetration capability, bigger than alpha particles.

Spontaneous Fission

In a very massive nucleus (in the order of 240 nucleons or more), it is possible to have an uncommon decay type known as **nuclear fission**[7]. In this case, the nuclei splits into two lighter nucleus emitting several photons and neutrons with energies around 1 MeV per particle. This process is much more energetic than the other usual decays like beta and alpha decays.

We can distingish between two different types of Nuclear Fission: 'Induced Fission' and 'Spontaneous Fission' (SF), depending of the need of a external particle to excite the nucleus or not.

[7] In ${}^{8}Be$ we have alpha decay that splits the nucleus into two identical components: the daughter nucleus and the emitted alpha particle. It can be consider like the less massive nucleus that decays into Spontaneous Fission

Induced Fission is the first Nuclear Fission reaction observed, where a neutron absorbed by a nucleus causes this decay. This decay, observed by Otto Hahn and Fritz Strassmann [Hahn and Strassmann 1939] bombarding uranium with slow neutrons, was the openning of a door to a new high energy proccesses. In uranium, the isotope ^{235}U has several orders of magnitude bigger thermal neutron capture cross section, that makes this one the perfect candidate for a nuclear chain reaction. This energetic process was used firstly to produce nuclear bombs and it is commonly used to obtain energy in a nuclear plant [8].

Later, **Spontaneous Fission** was discovered by Flerov (Flyorov) and Petrjak (Petrzhak) [Petrzhak and Flerov 1940] showing their work in this short paper:

Fission of Uranium

With 15 plates ionization chambers adjusted for detection of uranium fission products we observed 6 pulses per hour which we ascribe to spontaneous fission of uranium. A series of control experiments seem to exclude other possible explanations. Energy of pulses and absorption properties coincide with fission products of uranium bombarded by neutrons. No pulses were found with UX and Th. Mean lifetime of uranium follows ten to sixteen or seventeen years

Some years later, they write a new paper with more complete information about their discovery [Petrzhak and Flerov 1941].

This process follows a stochastic law, producing hundreds of different daughters nuclei and with a wide multiplicity of number and energies of the photons and the neutrons emitted.

For a more complete review of this process, I recommend to read 'Passive Nondestructive Assay of Nuclear Materials', [Relly et al. 1991]

Inside the nucleus, there is a competition between two forces that retain the nucleus together: the short range nuclear force and the electrostacic repulsion.

[8] To control this reaction, you have to reduce the number of neutrons with a material that absorbs and control this number. An usual element used is Gadolinium, that thanks to its big thermal neutron capture cross section, controls this reaction.

With a very low probability, the nucleons can reach a configuration with two droplets (similar to a peanut) that finally will separate into two new nuclei with usually between 100 and 140 nucleons per daughter nuclei. During this process, some neutrons and photons are prompted. But, the daughter nuclei most of the times are in a unstable state. Then, within miliseconds or seconds, they decay again emitting electrons, neutrons or gamma particles.

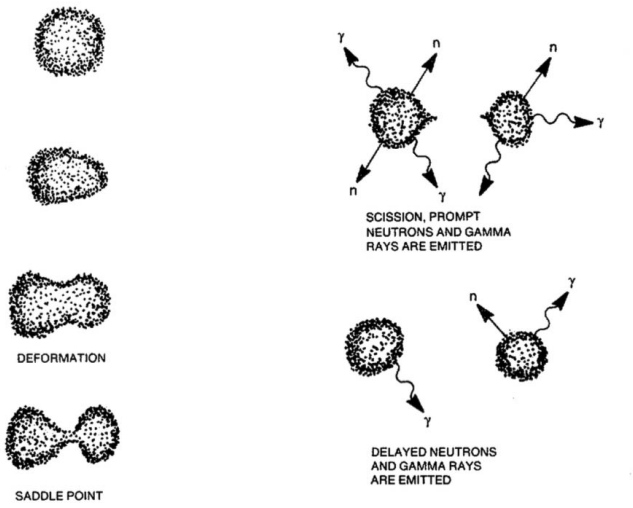

Figure 2.5: Schematic view of the Spontaneous Fission.

In this type of decay is impossible to know the daughters that will be produced. It is possible to obtain more than 100 different daughters, with several quantities of photons and neutrons emitted. We only can talk about the distribution and the mean value of the photons and neutrons emitted.

Before discussing the emitted photons and neutrons, we are going to show the important correlation between the total energy of the photons, $E_{\gamma Total}$, and the number of emitted neutrons $n_{neutron}$[9]

$$E_{\gamma Total} = \varphi(Z, A) \cdot n_{neutron} + 4.0 \tag{2.19}$$

[9]To name the number of neutrons, is usually used ν, but we prefer to use $n_{neutron}$ in order to avoid confusions with neutrinos

where $\varphi(Z, A)$ is a function that depends on Z and A and its value is close to 1 [Valentine 2001].

It is very hard to find information about photons and neutrons emitted in Spontaneus Fission. Our principal source of Spontaneous Fission background is ^{238}U and we try to present information about this isotope. But, if it is not possible, we will present information about other isotopes, where we expect similar behaviour.

Photons in Spontaneus Fission

The emission of photons is very strong in number and in energy compared with the most common decays [Valentine 2001]. The mean energy emitted per decay is about 1 MeV per emitted photon. Total gamma energy emitted is about 6 MeV. This energy must be shared with the emitted photons.

About the **energy of the emitted gammas**, its mean value of this follows an empirical equation, obtained by fitting data from ^{235}U, ^{239}Pu and ^{252}Cf decays:

$$< E_\gamma >= -1.33 + 119.6\frac{Z^{1/3}}{A} \tag{2.20}$$

The energy distribution of these photons is shown in figure 2.6-left, [Sobel et al. 1973]. It follows an exponential law.

Concerning the **number of emitted gammas**, it is about 6 photons per fission. The average number can be approximated with this equation:

$$< n_\gamma >= \frac{E_{total}}{< E_\gamma >} \tag{2.21}$$

A typical distribution of the number of photons is shown in figure 2.6, -right. This distribution, from ^{252}Cf, it is fitted to a double Poisson function, and also to a negative binomial distribution, depending of the autors.

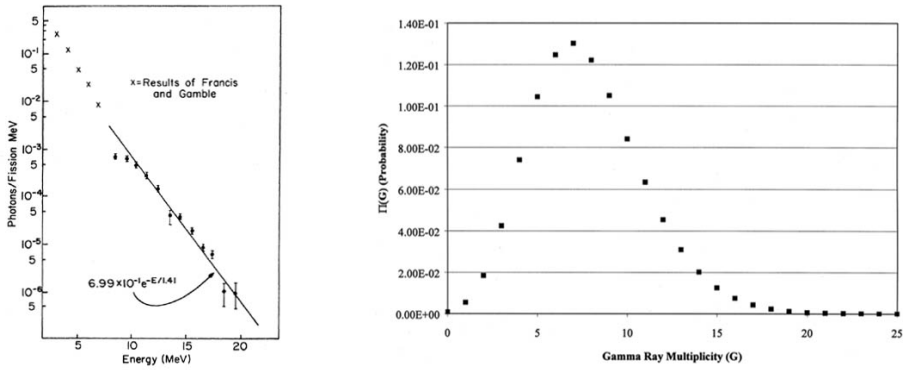

Figure 2.6: Left, energy distribution of the emitted photons in SF in ^{238}U. Right, distribution of number of emitted photons (in this case, in ^{252}Cf).

Neutrons in Spontaneus Fission

In SF, several neutrons are emitted together with the photons. The **mean neutron energy** of these emitted neutrons is about 2 MeV, and follows Maxwellian distribution. See Figure 2.7 for the case of ^{252}Cf.

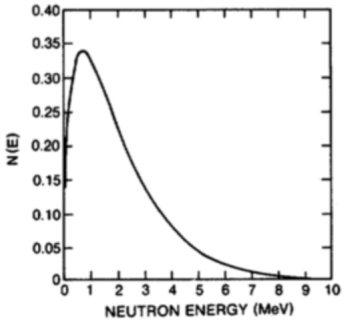

Figure 2.7: Energy distribution of the emitted neutrons in Spontaneus Fission. The isotope of this distribuiton is ^{252}Cf

We know that the mean total energy emitted with photons is about 6 MeV; then, and according with equation 2.19, the mean number of emitted neutrons is about 2 per decay.

This table shows the probability of the number of emitted neutrons per decay.

isotope	ν=0	1	2	3	4	5	6	7	8	9
^{238}U [8]	.0481677	.2485215	.4253044	.2284094	.0423438	.0072533	0	0	0	0
^{236}Pu [9]	.0802878	.2126177	.3773740	.2345049	.0750387	.0201770	0	0	0	0
^{238}Pu [9]	.0562929	.2106764	.3797428	.2224395	.1046818	.0261665	0	0	0	0
^{240}Pu [8]	.0631852	.2319644	.3333230	.2528207	.0986461	.0180199	.0020406	0	0	0
^{242}Pu [8]	.0679423	.2293159	.3341228	.2475507	.0996922	.0182398	.0031364	0	0	0
^{242}Cm [8]	.0212550	.1467407	.3267531	.3268277	.1375090	.0373815	.0025912	.0007551	.0001867	0
^{244}Cm [8]	.0150050	.1161725	.2998427	.3331614	.1837748	.0429780	.0087914	.0002744	0	0
^{246}Cm [10]	.0152182	.0762769	.2627039	.3449236	.2180653	.0755895	.0072227	0	0	0
^{248}Cm [10]	.0067352	.0596495	.2205536	.3509030	.2543767	.0893555	.0167386	.0016888	0	0
^{246}Cf [11]	.0005084	.1135987	.2345989	.2742853	.2208697	.1259660	.0301731	0	0	0
^{250}Cf [12]	.0038191	.0365432	.1673371	.2945302	.2982732	.1451396	.0472215	.0040174	.0031188	0
^{252}Cf [14]	.00211	.02467	.12290	.27144	.30763	.18770	.06770	.01406	.00167	.0001
^{252}Cf [15]	.00209	.02621	.12620	.27520	.30180	.18460	.06680	.01500	.00210	0
^{254}Cf [12]	.0001979	.0190236	.1126406	.2638883	.3183439	.1941768	.0745282	.0150039	.0021968	0
^{257}Fm [12]	.0205736	.0520335	.1172580	.1997003	.2627898	.2007776	.1061661	.0333033	.0073979	0
^{252}No [13]	.0569148	.0576845	.0924873	.1437439	.1832482	.1831510	.1455905	.0962973	.0382048	.0026776

Figure 2.8: Spontaneous Fission neutron multiplicity of several isotopes.

Double Beta Decay

Double Beta Decay might also be a source of background in our experiments. Among the usual elements that we consider in our background, the only one that can undergo double beta decay is Uranium.

Double Beta decay in Uranium was observed by Turkevich [Turkevich 1991] and it is one of the lowest energy double beta decay, with a $Q_{\beta\beta} = 1.1 MeV$.

In addition, the rate of double beta decay in Uranium is about 6 order of magnitude slower than spontaneous fission, which itself is about 6 order of magnitude slower than alpha decay.

Therefore, because of its long half-life and its very low $Q_{\beta\beta}$, very far away from our ROI we will not consider this as a background source

Photon emissions after the decay processes

After a nuclear decay the daughter nucleus can be in an excited state. To reach the ground state, it has to emit this energy by gamma emission or by internal conversion. These emissions are mostly produced after a beta decay, for example the most important photons for our experiments are emitted after a beta decay.

Typically, Gamma emission is very fast, about $10^{-14}s$; however in some cases, the nucleus can remain excited more time.

We have also to consider that not all the excitation energy is released by the gamma particle. There is also a small nuclear recoil, very small, in the order of a few of eV.

Internal conversion is the electromagnetic process where the nucleus prompts a tighly bound electron with the excess of energy from its excited state. After this, some electrons fall into lower energy levels with the emission of X-Rays or electrons (also called Auger electrons) or both. These emissions are not important for us as a background source because their energies are always below 1 MeV.

These discreet energy photons **can be easily detected by gamma ray detectors** and used to quantify the amount of these isotope present in our samples, because each decay as a characteristic energy. This is our usual technique to quantify the amount of radioactive contaminations.

These emissions obey two rules: conservation of angular momentum and parity. Conservation of angular momentum follows this equation

$$\overrightarrow{J_i} = \overrightarrow{J_f} + \overrightarrow{L} \tag{2.22}$$

Where J_i is the parent angular momentum, J_f is the daughter angular momentum and L is the angular momentum of the emitted photon. Then, the angular momentum can be:

$$|J_i - J_f| \leq L \leq J_i + J_f \tag{2.23}$$

If there isn't any possible value for L in the photon, this energy only can be released through internal conversion, transfering it to a nearby strong bounded electron.

Even though photons could be emitted, internal conversion also competes for the emission. We can define conversion coefficient wich is the ratio between the probability of internal conversion and probability of gamma decay.

Respecting parity, we can classify into two differen type of decays:

Electric transitions

$$\pi^f = \pi^i \cdot (-1)^L \tag{2.24}$$

Magnetic transitions

$$\pi^f = \pi^i \cdot (-1)^{L+1} \tag{2.25}$$

The most favored are low L transitions and electric transitions, then sometimes there are almost forbidden decays. Because of these rules, you can explain the existance of the nuclear isomers: excited nuclei with a highly forbidden decay probability.

2.2 Decay chains

A parent nucleus decays to its daughter nucleus emitting particles. After the decay, there are three different options for the daughter:

- Unstable state: the new nucleus is still not stable; it will decay again trying to reach a stable state.
- Metastable state: the nucleus is in a long-time excited state. It needs more time to emit a gamma particle. After the emission, the nucleus can be stable or unstable. It is not a decay because the nucleus remains the same.
- Stable state: after the decay, this new nucleus will remain in this state (as far as we know) and the decay chain is finished.

A **Decay Chain** is a process of several decays between unstable and metastable states until it is arrived to a stable nucleus; the end of the chain. In this process, we can observe alpha decays, beta decays and gamma emissions to stabilize the energy of the nucleus [10].

The most commonly observed decay series are the four **transuranic decay series**, where the first isotope is a heavy element with a very long half-life (those radioisotopes have an age similar to the Earth age). In our description, we are only going to consider the natural isotopes for these chains. For example, Thorium series starts with ^{232}Th naturally but it could also start with ^{252}Cf, an artifical element.

There are also natural decay chains produced by cosmic radiation, **cosmogenic decay chains**, that are shorter than transuranic ones. For example, ^{28}Mg, produced by cosmogenic spallation of ^{36}Ar, undergoes beta decay to ^{28}Al and ^{28}Si, a stable isotope. Other cosmogenic decay chains are ^{32}Si, ^{36}Cl and ^{39}Cl.

We could also consider the **artificial decay chains**, that requires accelerators, nuclear plants o nuclear bombs to create the isotope. For example, one of the radiosotopes that can be produced as daughter nucleus in a nuclear fission, ^{144}Ba, beta decays several times to ^{144}La, ^{144}Ce, ^{144}Pr and finally to ^{144}Nd, a very stable alpha decay radioisotope with a half-life of $2.29 \cdot 10^{15}$ years. The last isotope of this chain is ^{140}Ce, that is stable.

The four transuranic decays chains are:

4n Thorium series: this chain starts with ^{232}Th and includes, alphabetically, the following elements: actinium, astatine, bismuth, francium, lead, polonium, protactinium, radium, radon, thallium, and thorium. The total energy released in this chain is 42.6 MeV.

4n+1 Neptunium series: this chain is a bit special because it doesn't have any isotope with its half-life large enough to be actually observed. It has not been detected in any of our measurements.

[10] Stricly, we can consider other very low probability paths in this chains, with β^+, 2β, cluster decays, etc. However, they are negligible for our experiments.

4n+2 Uranium series: this chain starts with ^{238}U and includes astatine, bismuth, lead, polonium, protactinium, radium, radon, thallium, and thorium. The total energy released is 51.7 MeV

4n+3 Actinium series: this is the only observable odd chain. It starts with ^{235}U and includes actinium, astatine, bismuth, francium, lead, polonium, protactinium, radium, radon, thallium, and thorium. The total energy released is 46.4 MeV

We can see a schematic description of the Decay Chains in figures 2.9, 2.10 and 2.11. The black arrows represent the alpha decays of the isotopes and the blue ones represent the beta decays. In the arrows it is also indicated the half-lifes of these decays. And, in the case of two posible branches, the probability of each branch.

We can observe 4 **different colours for the isotopes**: green is for those isotopes that decay fast, yellow for intermediate time, red for long half-life and white for the stable isotopes, the end of the chains. This colour will determine how this chain will evolve if the equilibrium is broken.

In some decays, we can observe **grey boxes** that include the value of the energy of some gamma particles emitted in the decays. The detection of these gammas is our way to quantify the amount of that particular radioisotope in the sample.

Semitransparent radioisotopes and arrows are low probability decay paths, important to understand the decay chains but not important for radiopurity purposes.

Finally in some of the heaviers nuclides, we can find a number with SF, that indicates the probability to undergo a decay with **Spontaneous Fission**.

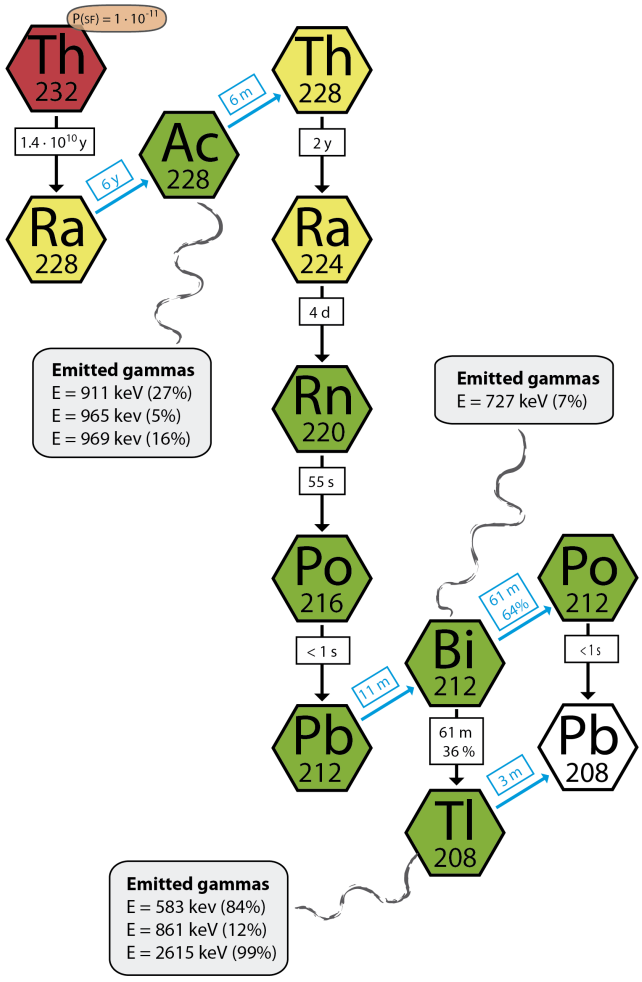

Figure 2.9: ^{232}Th Decay Chain.

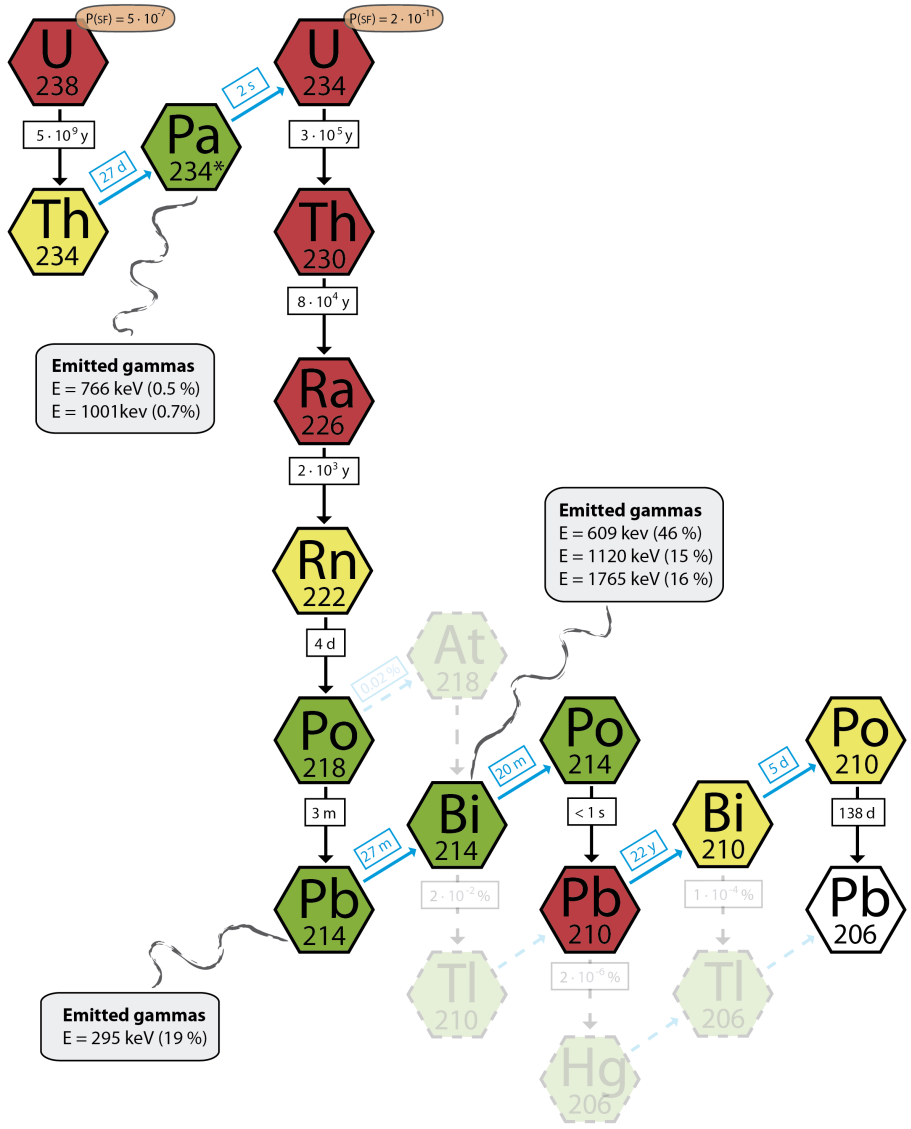

Figure 2.10: ^{238}U Decay Chain.

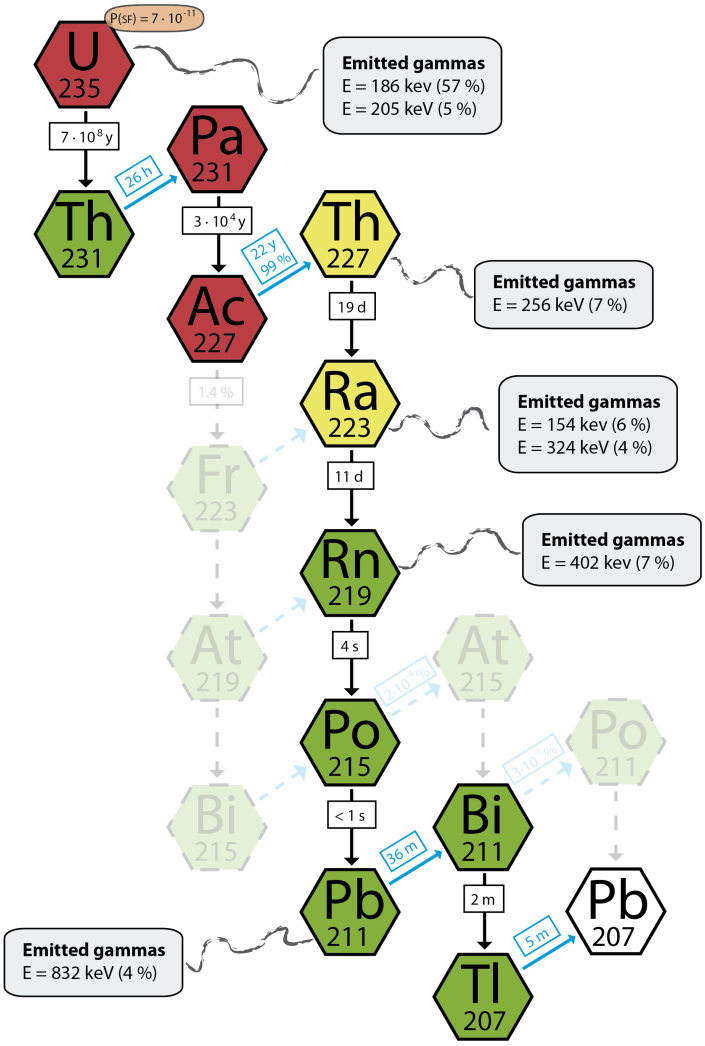

Figure 2.11: ^{235}U Decay Chain.

2.2.1 Radon Emanation in Decay Chains

During the decay processes within the chains, we find three different isotopes of radon: ^{220}Rn in the ^{232}Th chain, with a half-life of 55 seconds; ^{219}Rn in the ^{235}U chain, with a half-life of 4 seconds; and ^{222}Rn in the ^{238}U chain, with a half-life of 4 days.

Radon is a noble gas and can scape outside the material; mainly by diffussion but can also be produced by the nuclear recoil from the alpha decay. These radon isotopes will decay and decay, emitting particles and photons away from the material where the initial radon was originated.

The most important radon radisotope that we have to consider is ^{222}Rn because of its relatively long half-life of $\sim$ 4 days. Environmental radon in the air of the laboratory and from contaminations in the surface of the different exposed materials are important sources of background, for instance the photons emitted by the daughter ^{214}Bi.

Then, the problem of a high concentration of radon in air is a important problem for the underground laboratories, all of them surrounded by tons of rocks and concrete. Because of this, they have to measure the concentration and install systems to reduce the amount of radon in the air inside the laboratory.

Additionaly, in HPGe detectors and to reduce the presence of radon near by the detector, we create a nitrogen atmosphere inside a methacrylate box to avoid airborne radon intrusion. This prodecure will reduce the amount of background of the detector.

In the NEXT itself, we are following three different strategies to reduce this background:

- Heating the detector: with heating, the kinetic energy of the particle is increased. Then, the emanattion time is lower than in normal conditions. Therefore, we heat the detector for several days to reduce the number of attached atoms in the surface of our materials.

- Radon emanation measurements: we also are carrying out several measurements to quantify the amount of emanatted radon from some of our materials. We have choosen the most massive and internal materials for these first measurements.
- Getters: in the gas system of NEXT, we have placed getters to reduce the impurities of the gas. Theses getters can remove several types of gases that are mixed with the xenon, including the emanatted radon.

Secular Equilibrium

A decay chain is in **equilibrium** when the activities of all the isotopes are the same. It is needed a few of half-life of the isotopes to reach this equilibrium.

Equilibrium doesn't mean same number of atoms of the different isotopes of the chains, but same activity. When a chain is in equilibrium, the number of atoms produced by the decay of the parents is the same that the number of decays of the daughter; both have the same activity.

It often happens that radioactive contaminations are in non-equilibrated chains, with different activities in some of the isotopes of the chain. This is due to the different chemical and physical behavior of the chain elements during any industrial production process underwent by the sample, that can change the relative amount of the elements in the chain, thus breaking its equilibrium. Therefore, we have to study how this new scenario evolves.

Time evolution of Decay Chains

When equilibrium is broken, the following are the equations that define how a chain evolves in time. The idea is simple, one builds a system of differential decay equations each including in each term the number of atoms coming from its parent and the number of atoms that decay.

$$\begin{aligned}
\frac{dN_1}{dt} &= -\lambda_1 N_1 \\
\frac{dN_2}{dt} &= \lambda_1 N_1 - \lambda_2 N_2 \\
\frac{dN_3}{dt} &= \lambda_2 N_2 - \lambda_3 N_3 \\
&\vdots \\
\frac{dN_i}{dt} &= \lambda_{i-1} N_{i-1} - \lambda_i N_i \\
&\vdots \\
\frac{dN_j}{dt} &= \lambda_{j-1} N_{j-1}
\end{aligned} \tag{2.26}$$

The general solution for these equations were found by Harry Bateman [Bateman 1910] in the first years of the past century:

$$N_n(t) = \sum_{i=1}^{n} \left(N_i(0) \cdot \prod_{j=i}^{n-1} \lambda_j \cdot \sum_{j=i}^{n} \left(\frac{e^{-\lambda_j t}}{\prod_{p=i, p\neq j}^{n} (\lambda_p - \lambda_j)} \right) \right) \tag{2.27}$$

Where for each radioisotope 'i', $N_i(0)$ is the initial number of atoms, $N_i(t)$ is the number of atoms after a time t and λ_i is its decay constant.

In figures 2.9, 2.10 and 2.11 we can observe the different colours of the radioisotopes. Depending of the state of equilibrium with the neighbour isotopes, we can consider three scenarios related with the time evolution of the decay chains:

- Green radiosotope: (half-lifes about some minutes or lower). These half-lifes are so short that we cannot observe any changes in their activities during the measurements. They reach the equilibrium with their neighbours very fast.
- Yellow radiosotope: (half-lifes between some minutes and few years). Within those half-lifes times, we can observe how the activities evolve during the measurement (for the shorter half-lifed isotopes of the interval)

or how it has changed when the measurement is repeated some time later (for the longer ones). One typical example of this is the decay of the trapped radon in the measurements with High Purity Germanium detectors.

- Red radiosotope (half-lifes of about tens of years or longer). These radiosotopes have a very long half-life: it means that we need very long time intervals to observe changes in the activity. Depending of the half-lifes of all the radiosotopes involved, we can observe small evolution in the activity of these isotopes or, in the case of the longer ones, we can observe partial equilibrum between red-coloured radiosotopes.

  In this case, we can define sub-chains (part of the chains) that will be in local equilibrium in our time scales.

2.2.2 Most important gamma lines in the decay chains

To quantify the activity of a sample, we use germanium detector that count the numbers of detected photons. In the decay chains there are a wide variety of emitted photons. For instance, in the Thorium series there are about 100 photons with intensity over 0.1%. Next, we discuss a criteria to select which photons are the best for quantify the activity:

- Photon energy: there are two factors that limit the energy interval: the background of the detector and the photon detection efficiency. Usually, the background of the detector is bigger at low energies, more or less below 200 keV. The second factor is the photon detection efficiency, that typically follows a distribution with the maximun about 150 keV and decreases while the energy increases. A complete description of germanium detectors can be found in Chapter 4.1

  Therefore, the recommended interval is between 200 keV and 1500 keV; however there are also some interesting photons outside this interval.

- Intensity: not all the transitions have the same probability, with some photons having greater probability to be emitted. Low probability photons

has low activity that cannot be distinguished from the background except some of them with high energy that have basically no background.

We can find some very intense and interesting photons with low energy (about 200 keV and below). And, in the Actinium series, we also can use for our analysis some high energy photons, for instance the 2614.5 kev from ^{208}Tl.

- Non-overlaping photons: to simplify the analysis, we prefer to avoid photons with almost the same energy as it is almost imposible to quantify the contribution of each one. In anycase, if the diference of intensity of the photons is very big, we can ignore the small one.

- To cover all the parts of the chain: because of the usual non-equilibrium of the decay chains in our samples, we have to choose photons in all the parts of the chains. In Uranium series, to quantify the upper part of the chain, we only can use a very low intensity photon (0.6%) from $^{234*}Pa$.

Acording to the criteria, we can find in figures 2.9, 2.10 and 2.11, the most recommended photons for the analysis.

Also, to minimize the uncertainty of the measurement we try to measure several gamma lines of each part of the chain. Then, is possible that some activities are quantified with the combined analysis of two or three photons.

Isotope	Decay Chain	Energy (keV)	Intensity	Possible Interferences Isotope (keV, Intensity)
^{228}Ac	^{232}Th	911.2	0.266	
		964.8	0.051	^{214}Bi (964.1/0.004)
		969.0	0.162	
^{208}Tl	^{232}Th	583.2	0.304	^{214}Pb (580.2/0.004), ^{228}Ac (583.4/0.001)
		860.6	0.045	
		2614.5	0.356	
^{238}U	^{238}U	1001.0	0.006	
		766.4	0.002	^{214}Bi (768.4/0.049)
^{214}Pb	^{238}U	295.2	0.192	
^{214}Bi	^{238}U	609.3	0.461	
		1120.3	0.150	
^{235}U	^{235}U	185.7	0.572	^{226}Ra (186.1/0.035)
		205.3	0.050	^{228}Ac (204.0/0.001)
^{219}Rn	^{235}U	401.7	0.066	
^{211}Pb	^{235}U	831.8	0.038	^{228}Ac (830.5/0.006)

Table 2.1: Table of the most used emitted photons from Decay Chains

It is important to remark that the most important gamma photon of ^{235}U, (185.7 keV and 0.572 of intensity) has very close one photon from ^{226}Ra (186.1 kev and 0.035 of intensity).

Therefore, if a sample had big contribution of the lower part of the ^{238}U, it can mimic the peak of ^{235}U. In the case that we only can estimate an upper limit for ^{235}U activity, we can suppose that all the counts measured arround 186 keV come from ^{235}U. With this hypothesis, we would find a wrong value of the activity, but if we treat it as an upper limit.

It sure will be lower that the one obtained with 205.3 keV gamma photon.

2.3 Other radioctive isotopes

There are other sources of radioactive background in our experiments. There are individual radionuclides that are a background source and a dangerous source of events. Some of them are primordial radionuclides (^{40}K, ^{176}Lu, ^{138}La), cosmogenic radionuclides (^{60}Co, ^{56}Co, ^{58}Co and ^{54}Mn) and there are also anthropogenic radionuclides (^{134}Cs and ^{137}Cs)

We are only going to remark the most important gamma lines emitted per each radiosotope, i.e. those ones used in our analysis to estimate their activities.

- ^{40}K: This is one of the three most common sources of natural radiactivity in the Earth crust, with ^{238}U and ^{232}Th. This isotope is present in potasium with a 0.0117% of atoms. This isotope undergo beta decay (with 10.7% of probability) emitting a gamma photon of 1460.8 keV. The half-life is $1.248 \cdot 10^9$ years.

  It is a very common isotope that usually can be found in plastic and in many organic materials. This isotope is widely present in our lifes (and bodies) since potasium is a mineral needed for the human body.

  In terms of radioactive background, its activity is a background signal in the region of the $2\beta2\nu$ signal.

- ^{60}Co, ^{56}Co, ^{58}Co : the most important radiosotope of cobalt is ^{60}Co. This isotope undergo beta decay emitting two photons with 1173.2 keV (with 99.85% of probability) and 1332.5 keV (with 99.98% of probability). The half-life is 5.27 years

  Also can be observed peaks from ^{56}Co ($T_{1/2} = 77.27d$, γ emissions at 846.77 keV and 1238.28 keV) and specially ^{58}Co ($T_{1/2} = 70.86d$, γ emission at 810.78 keV). Typically, the half-lives of these two isotopes are of the order of the live time in the screening measurement and usually they are not observed.

  They are typical cosmogenic products of copper. They are produced at the exposure of the material to cosmic nucleons.

^{60}Co is commonly observed in metals and electronic components. Also it is often used as callibration sources.

- ^{134}Cs and ^{137}Cs. They are produced after nuclear fission processes; nowadays, the Fukushima accident is the major source of these isotopes. ^{137}Cs undergoes beta decay to $^{137*}Ba$ (with 94.6% of probability) that emits a photon with 661.7 keV. ^{134}Cs undergo beta decay emitting two gamma photons with 604.7 keV (with 97.62% of probability) and 795.9 keV (with 85.46% of probability)

  We have found some samples contaminated with these isotopes after the Fukushima accident, for example some resistors from Japan Fenichem Company, Inc; a chemistry and electronic japanese company. Also, in some samples of Gadolinium salt treated as well in Japan.

- ^{176}Lu, ^{138}La: we only have found these two isotopes in rare earth samples, the gadolinium samples for Super-Kamiokande. The very similar chemical behaviour of the rare-earths make very complicated the total separation among them.

  ^{176}Lu undergoes beta decay emitting two gamma photons with 201.8 keV (with 77.97% of probability) and 306.8 keV (with 93.6% probability)

  ^{138}La undergo β^- (with 34.4% probability) emitting one gamma of 788.7 keV; but also can undergo β^+ (65.6% probability) emitting one gamma of 1435.8 keV.

  In terms of background, they are dangerous because both of them are β^- emitters with energies about 1 MeV.

- ^{54}Mn: This radionuclide is an usual product from the cosmogenical activation of the copper, like the cobalt radionuclides. ^{54}Mn undergoes electron capture emitting one photon of 834.8 keV (99.98% probability)

Isotope	Energy (keV)	Intensity	Possible Interferences Isotope (keV, Intensity)
^{40}K	1460.8	0.107	^{228}Ac (1459.1/0.008)
^{60}Co	1173.2	0.999	
	1332.5	1.000	
^{134}Cs	604.7	0.976	
	795.8	0.855	^{228}Ac (795.9/0.043)
^{137}Cs	661.6	0.805	
^{176}Lu	201.8	0.840	^{228}Ac (199.5/0.003), ^{228}Ac (204.0/0.001)
	306.9	0.930	
^{138}La	788.7	0.335	^{214}Pb (785.9/0.011), ^{214}Bi (786.1/0.003)
	1435.8	0.663	

Table 2.2: Most relevant emitted photons from the most common radiosotopes.

It is important to remark that for samples with a very big amount of ^{228}Ac, the gamma line with 1459.1 keV can easily mimic the ^{40}K peak. Therefore, to estimate the activity of ^{40}K, first is necessary to know the activity of ^{228}Ac and use this information to estimate the number of counts that can came from this radioisotope. Subtracting this value and the contribution of the background, we can obtain the activity of ^{40}K radioisotope.

3

Experimental techniques in NEXT and SuperK-Gd; the impact of radioactivity on them

3.1 NEXT

NEXT-100 detector is a 100 kg xenon gas TPC scheduled to be at LSC in 2018. Its demostrator is detector NEW (NEXT-WHITE)[1], a detector that is a 1:2 scale (1:10 in mass) the design using the same materials and photosensors that NEXT-100.

[1]The name honours the memory of the late Professor James White, guide and mentor of NEXT project

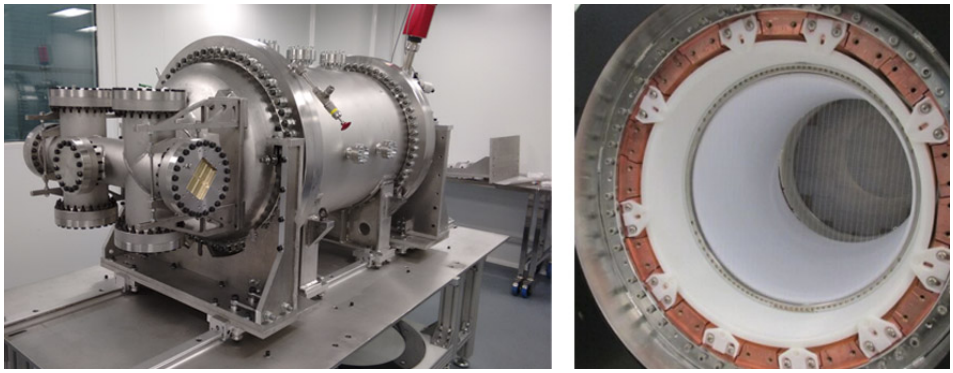

Figure 3.1: Left side, the detector outside the castle, in a clean room for the instalation of the Tracking Plane. Right side, Internal view of the detector

3.1.1 NEW Detector

NEW is a TPC with an active xenon mass of about 10 kg at 15 bar. Right now, it is taking data at Laboratorio Subterráneo de Canfranc (LSC). A complete information about this detector can be found in *The NEW detector: construction, commissioning and first results*, a poster of M. Nebot-Guinot in the NEUTRINO 2016, [Nebot-Guinot 2016].

Right now, the detector is in Run II, with several callibration sources: Krypton, Cobalt and ^{22}N. First results are shown in Figure 3.2.

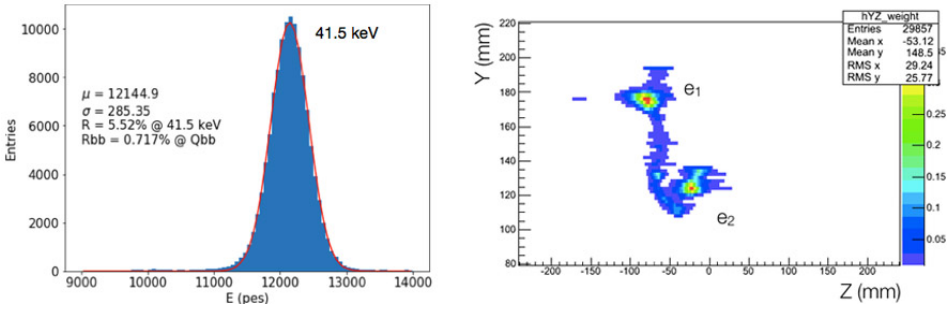

Figure 3.2: Left side, a krypton peak. Right side, an electron-positron track from cobalt source

Vessel

The pressure vessel is made of titanium-steel alloy with a wall thickness of 12 mm, designed to work to a maximun pressure of 15 bar. The total mass is $\sim 700kg$. All the different internal layers of the detector can be seen in Figure 3.1, in the right figure. They are the Inner Copper Shielding, the Field Cage and the Light Tube.

The first layer is the Inner Copper Shielding, a thick copper background protection with 6 cm in the barrel and 12 in the endcaps. Both endcaps are designed to place sensors, one for the Energy Plane with PMTs and the other with SiPMs for the Tracking Plane.

The second layer is the Field Cage. The best solution found for an uniform electric field was to use several copper rings placed in the High Density Polyethylene of the Field Cage and also connected to a resistor chain. In the uppper part of the detector are the High Voltage feedthroughs. These High voltage feedthroughs have been designed to operate the cathode at up to 50 kV and the grid at up to 20 kV.

The last layer of the detector is the Light Tube, where the Teflon were coated with Tetraphenyl butadiene (TPB), a wavelength shifter (WLS) that converts VUV light to blue. This is necessary to make the SiPMs capable to see the emitted light.

The totas mass of the detector with all the layers is $\sim 1900kg$.

Energy Plane

The Energy Plane is the plane designed to measure the energy of the events with high precision. This plane has 12 PMTs (64 in the case of NEXT-100), model Hamamatsu R11410-10, coupled with an optical gel to sapphire windows coated with TPB. These PMTs use a divider circuit with several components selected to increase their radiopurity as much as possible.

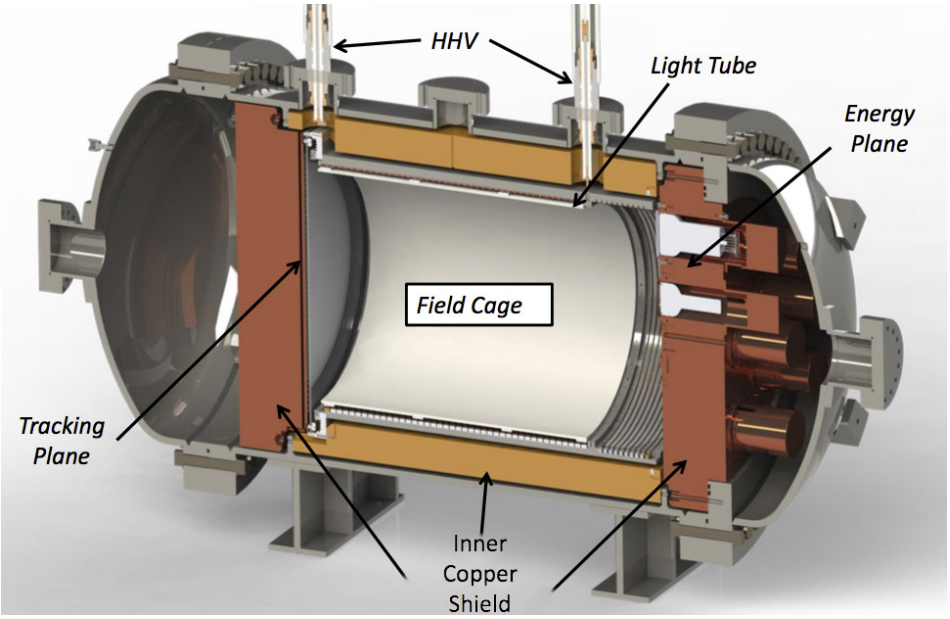

Figure 3.3: Draw of the detector NEW with the most important parts.

The 12cm thick copper plate holds all the PMTs and also is an excellent shielding for the detector.

Tracking Plane

The NEW tracking plane, placed in the other copper plate, is made of 28 Kapton DICE-Boards (KDB), printed circuit boards (PCB) that satisfy radiopurity requeriments. Each KDB will have 64 SiPMS; 1792 SiPMS for al the detector. For NEXT-100 will be used 111 KDB with 7104 SiPMS.

First option for these tracking where S10362-11- 050P/NG from Hamamatu, but finally we found a more radiopure option, SensL SiPMs $1x1mm^2$. These photosensors provide a dense array of 1 cm pitch for topological reconstruction of the track of the event produced inside the chamber.

A reflective teflon mask is fitted on each KDB to increase the luminosity.

Lead Castle

The wall rocks of the LSC are a important source of gamma photons from the Nuclear Decay Chains. To shield them, we have build a Lead Castle with 20-cm thick lead shield. The structure is made by Carbon Steel with the inner parts of 316 Ti. More than 400 lead bricks ($200x100x50mm^3$) have been used in this castle. Several samples of Lead have been screened in HPGe detectors to find the best option for this shielding.

We have estimate that this castle can attenuate the gamma flux from the rock walls of the laboratory in 4 orders of magnitude.

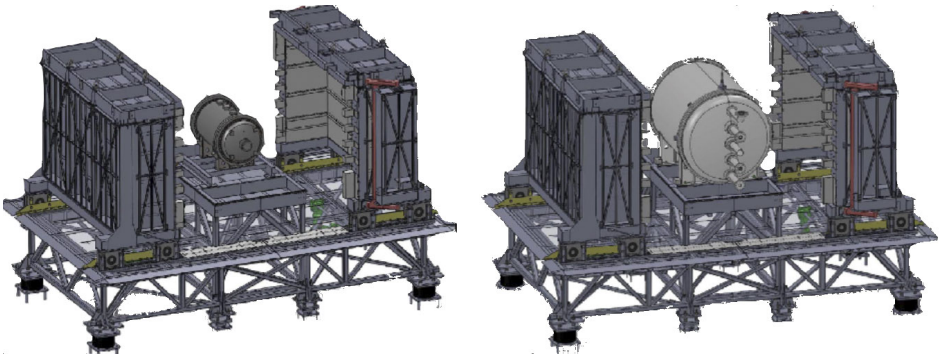

Figure 3.4: Left side, the detector outside the castle, in a clean room for the instalation of the Tracking Plane. Right side, Internal view of the detector

Gas System

In a TCP with ultra low background, the control of the level of purity of the gas is a must.

A complete gas system has been developed to make vacuum inside the detector, fill the detector with high pressure Xenon, the recirculation of the Xenon through the purification getters (using two cold getters and with one hot), cryo-recover the enriched Xe and also in a emergency to recover the enriched Xe.

Slow Control

To control all these systems, we have developed a complete Slow Control to monitorize all the status of the most important elements of the detectors. Four computers, using Labview programs, show the information and allow to control the High Voltage of the Cathode and the Gate, the Voltage of all the photosensors, the temperature of different components of the system, the status of the Gas System and some other features.

In any case, weekly shifts are done to be close to the detector and act as fast as possible in case of emergency.

3.1.2 Impact of radioactivity

Natural radioactivity in detector materials and surroundings is, as in most other $2\beta0\nu$ decay experiments, the main source of background in NEXT. Other possible sources of background like airbone radon, neutrino and neutrons are under control and their contributions are negligible compared with natural radioactivity.

For NEXT, the expected $2\beta0\nu$ peak of ^{136}Xe ($Q_{\beta\beta} = 2458.1 \pm 0.3keV$) [M. Redshaw and Myers 2007] and [P. M. Cowan and Barber 2010] lies in between the photo-peaks of the high-energy gammas emitted after the β decays of ^{214}Bi and ^{208}Tl, intermediate products of the uranium and thorium series, respectively:

In the lower part of the ^{238}U, we will find out ^{214}Bi. After its decay, the daughter isotope, ^{214}Po, emits a number of de-excitation gammas with energies around and above the Q value of ^{136}Xe. The gamma line at 2447 keV (1.57% intensity) is very close to $Q_{\beta\beta}$, and its photoelectric peak would overlap the signal peak even for energy resolutions as good as 0.5% FWHM. All the other gamma lines emitted after the decay of ^{214}Bi have very low intensity (at least two orders of magnitude lower than the 2447 keV line), and hence their contribution to the background rate can be neglected.

In the lower part of the ^{232}Th, we will find out ^{208}Tl. After its decay, the daughter isotope, ^{208}Pb, emits a de-excitation photon of 2615keV with an intensity of 99.75%. Electron tracks from its photo-peak can lose energy via bremsstrahlung and fall in the region of interest (ROI) around $Q_{\beta\beta}$ defined by the energy resolution of the detector. Additionally, even though the Compton edge of the 2.6 MeV gamma is at 2382 keV, well below $Q_{\beta\beta}$, the Compton-scattered photon can generate other electron tracks close enough to the initial Compton electron to be reconstructed as a single track with energy around $Q_{\beta\beta}$.

3.1.3 The NEXT background model

NEXUS is a Geant4-based detector simulation developed by the NEXT Collaboration. More information about it can be found in *The NEXT experiment for neutrinoless double beta decay searches*, PhD thesis of J. Martín-Albo [Justo Martín-Albo 2015], and also in [J. Martín-Albo et al. 2016] and [Lopez-March 2016].

NEXUS has been used to estimate the $2\beta0\nu$ signal and background detection efficiencies using Monte Carlo (MC) simulations.

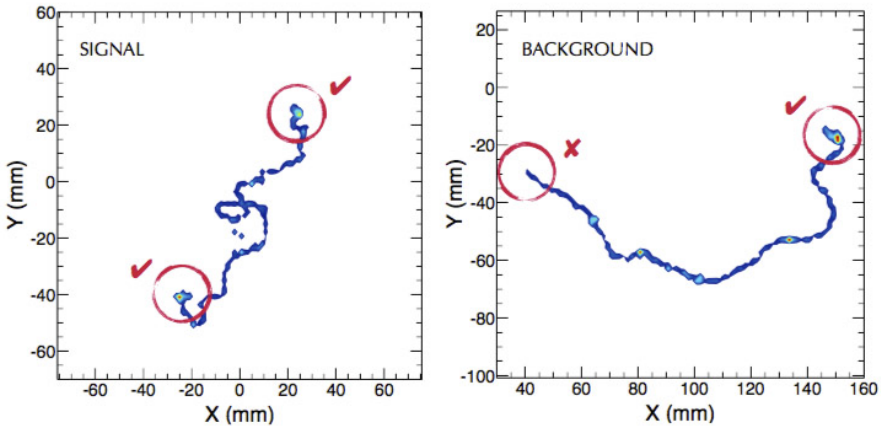

Figure 3.5: Left side, a signal event. Right side, a background event

A $2\beta0\nu$ candidate event requires that:

- only one track is reconstructed fully contained within the fiducial volume of the detector (defined by excluding a region of 2 cm around the boundaries of the active volume. The definition of a fiducial volume has two purposes: it rejects all charged backgrounds entering the detector and it discards those events in which the tracked particles may have left the active volume, depositing part of their energy in passive materials.
- the reconstructed track features a blob at both ends. As can be seen in figure 3.5, two blobs are produced by two electrons but only one means that there is only one particle.
- the energy of the event is within the region of interest (ROI) 2.448 < E < 2.477 MeV.

This selection gives an efficiency of 28% for $2\beta0\nu$ signal events. But, the good point is that backgrounds from ^{208}Tl and ^{214}Bi are suppressed by more than 6 orders of magnitude and the background from $2\beta2\nu$ decays is completely negligible.

The Background rejection rates are obtained dividing the initial activities of ^{208}Tl and ^{214}Bi by the corresponding background rejection factors (defined as the inverse of the background acceptance resulting from the $2\beta0\nu$-decay event selection described in the previous section).

Is important to remark that the knowledge of some activities is quite uncertain, given that for many background sources we only have at present a limit to their activity. The NEW data will make possible the validation of the NEXT-100 background model, currently based on detailed Monte Carlo detector simulation and radiopurity measurements that predict the background rate for NEXT-100.

3.2 SuperK-Gd

Super-Kamionade is the evolved version of KamiokaNDE (Kamioka Nucleon Decay Experiment). In Chapter 1 are explained several of the milestones and prizes from Super-Kamiokande detector. This section is destinated to explain the next upgrade of the detector, SuperK-Gd.

The SuperK-Gd project is the upgrade of the Super-Kamiokande detector in order to enable it to efficiently detect thermal neutrons, dissolving $Gd_2(SO_4)_3$ into SK at a concentration of 0.2%. Once the neutrons (produced for instance by the interaction of an antineutrino) are thermalised, they are captured by Gadolinium, emitting a delayed 8 MeV photons cascade from its de-excitation. The detection of this cascade in coincidence with a neutrino event produces a double event detector, opening new goals for the experiment.

For a more complete explanation about SuperK-Gd project, one can read 'Neutrino Physics in Present and Future Kamioka Water-Cherenkov Detectors with Neutron Tagging', PhD Thesis written by P. Fernández from UAM, [Fernández 2016]

3.2.1 Neutrino-Neutron Physics

First of all, we are going to introduce the tyical interactions of neutrinos and antineutrinos with nucleons:

$$\nu_\alpha + n \rightarrow lepton_\alpha + p \tag{3.1}$$

$$\overline{\nu_\alpha} + p \rightarrow \overline{lepton_\alpha} + n \tag{3.2}$$

Considering **low energy** events, $\leq 100MeV$, only $\overline{\nu_e}$ can produce a charged lepton, the positron, therefore a neutron. This free neutron is a very important source of information. With neutron tagging, we have a very useful way of discerning antineutrinos from neutrinos.

Considering **high energy** events, the process is more complex and harder to explain, with several neutron production mechanisms and with a bigger neutron emission multiplicity. These reactions can be classified into three categories: elastic and quasi-elastic scattering, resonant and coherent meson production and deep inelastic scattering.

It is important to remark that not all the physics goals of the detector will be directly improved with the addition of a neutron tagger. For example, in proton decay no neutron must be present in this decay, and Gd adding only brings sort of veto requirement thus reducing the background.

3.2.2 Gadolinium as a Neutron Capturer

The best choice for neutron capture was Gadolinium, a rare earth with the largest neutron capture cross section, mainly the odd isotopes. Other good point of Gd is that these odd isotopes are present in Gd with about $\sim$ 30% of the total abundance (see Table 3.1).

Gadolinum Isotope	Natural Abundance (%)	Neutron Capture Cross Section (barn)	De-excitation energy (MeV)
^{152}Gd	0.20	1050	6.25
^{154}Gd	2.18	85.0	6.44
^{155}Gd	14.80	60700	8.54
^{156}Gd	20.47	1.71	6.36
^{157}Gd	15.65	254000	7.94
^{158}Gd	24.84	2.01	5.94
^{160}Gd	21.86	0.765	5.64

Table 3.1: Gadolinium isotopes with the most important characteristic for neutron tagging. The high Neutron Capture Cross Section and the high Energy released are superb.

Therefore, we can estimate that the neutron capture will be made mainly by ^{155}Gd and ^{157}Gd and the emitted energy will be about 8 MeV.

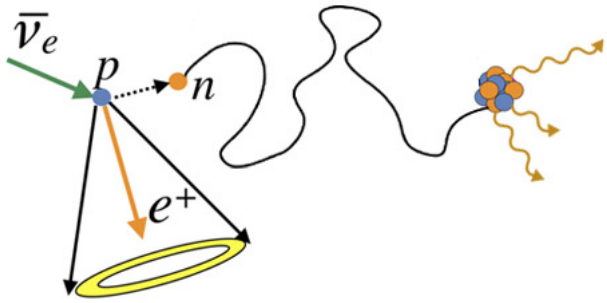

Figure 3.6: Neutron capture process by a Gd atom.

The Neutron Capture process, a double event process with a delayed coincidence, in time but also in space, (shown in figure 3.6) is as follow:

- Neutrino interaction and creation of a neutron, as usually is produced in previous versions of Kamiokande detectors.
- Neutron is thermalised in the water and captured by a Gd atom, traveling typically about 2 meters. The time of this thermalisation is $\sim 10\mu s$.
- Once thermalised the neutron, a Gadolinium atom will capture it. Finally, the de-excitation with the emission of photons is produced. This process is $\sim 20\mu s$.

Once chosen Gd as the neutron capturer, it is necessary to decide how to dissolve this element, because it a metal and is not soluble. Therefore, Gadolinium salts were best solution, thanks to its solubility.

Two different candidates were the most promissing options: a binary salt, $GdCl_3$, and ternary salt, $Gd_2(SO_4)_3$. Both salts were interesting candidates, but $GdCl_3$ presented light absortion close to Cherenkov light peak ($\sim 350nm$) and some undesired corrosion effects.

The main characteristics of the chosen salt $Gd_2(SO_4)_3$ are: no observed corrosion effects in the water tank, excellent solubility in water, small light attenuation and an excellent uniformity of the solution.

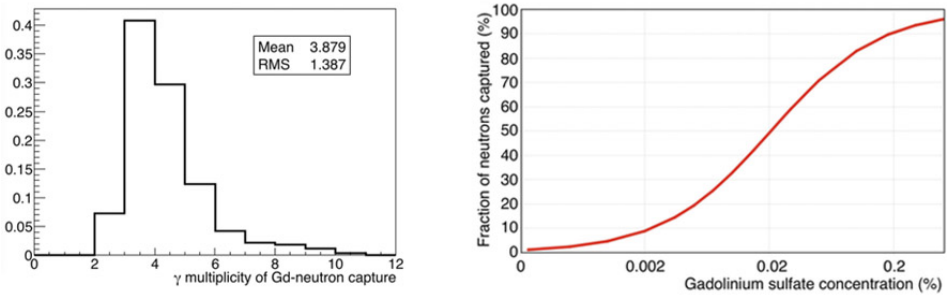

Figure 3.7: Left side, photon multiplicity emitted after the de-excitation of the Gadolinium. Right side, Fraction of neutrons captured by Gd vs concentration of Gd in thw water.

The final decision is to use 100 Tons of $Gd_2(SO_4)_3$, 0.2% of concentration. With this concentration, the capability of the detector to measure emitted neutrons is $\sim$ 80%.

3.2.3 EGADS R&D

EGADS (**E**valuating **G**adolinium's **A**ction on **D**etector **S**ystems) is the name of a Research and Development program to test a water Cherenkov detector with Gadolinium as a neutron tagger.

The EGADS detector, placed in a new cavern done for this detector, is scale 1:250 similar to Super-Kamiokande. The EGADS water tank contains 200 ton of ultrapure water, with 5.417 m in diameter and 4.949 m in height. Inside this water tank, there are 240 photomultipliers, which 227 of them are similar to those in the SK detector, 151 PMTs without any cover, 16 PMTs with an FRP housing and the 60 remaining PMTs with FRP and acrylic cover.

As in every ultra low background detector, during its construction and operation, cleanliness is a must and all the team were properly equipped, all the parts were cleanned with alcohol or pure water and continuous flux of air inside the detector were used to avoid the presence of dust.

Once dissolved Gd, a Water Purification System is responsible to keep the excellent conditions of the water. This system mainly consist of three stages:

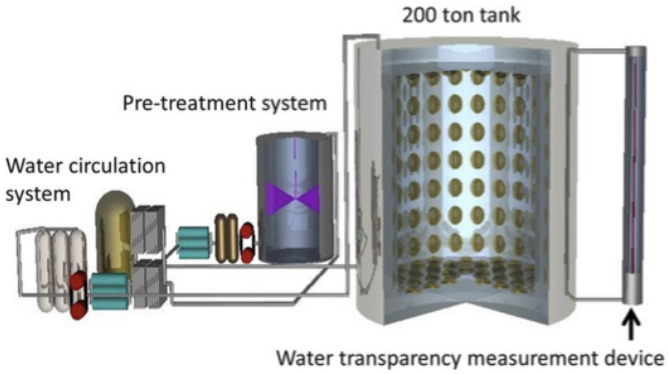

Figure 3.8: Most important parts of the EGADS water tank

first, several microfilters to remove the largest particles of dust; second, an UV to kill the possible bacterias and the third is a special resin, AJ4400, designed to remove Uranium, in order to improve radiopurity of the solution.

Thanks to this system, the solution propierties fulfill our requeriments: the luminosity of the water is very similar to Super-Kamiokande (only with pure water) and Gd concentration has a very good uniformity in all the parts of the detector.

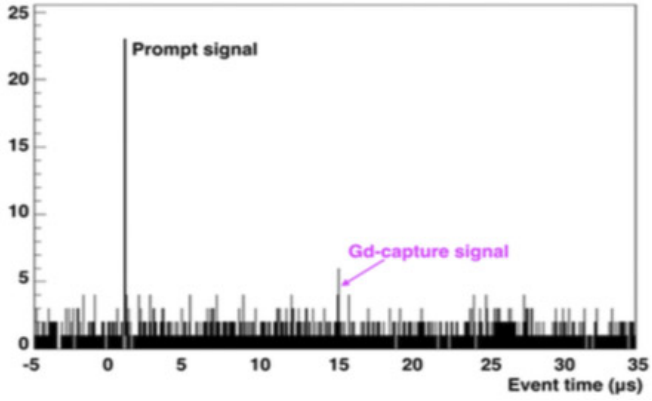

Figure 3.9: Example of the double signal produced by the neutrino and the neutron.

Finally, after a fruitfull period, this technology has been probed and the SuperK-Gd were approved:

'On June 27, 2015, the Super-Kamiokande collaboration approved the SK-Gd project which will enhance neutrino detectability by dissolving gadolinium in the Super-K water[...]'

3.2.4 Impact of radioactivity in SuperK-Gd

In previous version of the detector, only ultra pure water were present inside the water tank. But, with the addition of $Gd_2(SO_4)_3$, some impurities can produce some dangerous backgrounds in the fiducial volume. We have to quantify and minimize these backgrounds. Thus, it is possible to saturate the detector in cases of large radioactive contamination. Radiopurity of the chosen Gd sample is a must to have a powerful detector. The different materials used for the detector and the walls are less important because it is more complicate for them to contribute to the background entering in the fiducial volume.

Mainly, there are three sources of background: Spontaneous Fission, (α, n) reactions and High Energy Beta Decays. All these decays as been explained in detail in Subsection 2.1.

Spontaneous Fission

In our case, we have two different sources of SF backgrounds: from U and from Th. Because the probability of this decay is 4 order of magnitude lower in ^{232}Th than ^{238}U, we only are going to consider this uranium isotope.

Uranium has three different observed decay modes: alpha decay, Spontaneous Fission and double beta decay. Other decay type, Cluster Decay[2] emitting a ^{14}C nuclei is energetically possible but not observed. The first of these modes can be a possible source of background.

The Spontaneous Fission is deeply explained previosuly, but is useful to remember that the mean gamma energy emitted is about 6 MeV, where the energy is shared by the emitted photons with about 1 MeV per each one. In

[2]Cluster Decay is a nuclear decay where an atomic nucleus emits a small cluster of neutrons and protons, bigger than an alpha particle, but smaller than an usual binary fission fragment

the case of the neutrons, the mean energy is between 1 and 2 MeV per neutron, with a mean number of emitted neutrons ~ 2 per decay.

The problem of SF is that the photon and a neutron produced after these decays, have a very similar signature in the detector that the inverse β antineutrino reaction, producing a irreducible background in the detector.

alpha, n

After an α decay, can be produced a secondary decay, the (α, n) reaction. This alpha particle can be captured by some elements in the fiducial volume. The best candidates for these reactions are two oxygen isotopes: ^{17}O and ^{18}O.

$$^{18}O + \alpha \rightarrow^{22*} Ne \rightarrow^{20} Ne + 2n \tag{3.3}$$

We can observe that in this case, the multiplicity of neutrons is 2. These background, in coincidence with some other neutrino events, can fake the expected signals.

High Energy Beta Decays

After a beta decay, there are two emitted particles, the electron and the de-excitation photon. The most dangerous isotopes are those with higher energies, like ^{208}Tl ($Q_\beta = 5.00MeV$), ^{212}Bi ($Q_\beta = 2.25MeV$) and ^{214}Bi ($Q_\beta = 3.27MeV$), that can fake the signal of a low energy neutrino or the neutron capture event if it coincides with a solar neutrino candidate.

3.2.5 Impact of radioactivity in SuperK-Gd

With all these information and with the expected values of the events we want to observe, we have these radiopurity requeriments for SuperK-Gd.

Decay Chain	Sub Chain	SRN (mBq/kg)	Solar ν (mBq/kg)
^{238}U	^{238}U	< 5	-
	^{226}Ra	-	< 0.5
^{232}Th	^{228}Ra	-	< 0.05
	^{228}Th	-	< 0.05
^{235}U	^{235}U	-	< 3
	$^{227}Ac/^{227}Th$	-	< 3

Table 3.2: physics-based requirements for radioactive impurities in the $Gd_2(SO_4)_3$ salt. Where no number is given (-), the corresponding requirement is less restrictive than that for the other physics analysis

In these case, is important to remark that these levels are easy to obtain with our usual measuring procedures, except for the ^{232}Th, where the restrictive limits of < 0.05 make harder the possibility to achieve these goals.

4

The characterization of radioactivity contamination in materials: experimental techniques

The precise estimation of the activity of the materials for very low background experiments requires a deep understanding of the high precision detectors employed to quantify these contaminations.

The most used technique is High Purity Germanium detectors, HPGe, but sometimes were used Mass Spectrometers. Both types of detectors and the study of the signal obtained are explained in this Chapter.

4.1 High Purity Germanium detector (HPGe)

For gamma spectroscopy, typically were used Iodide-based detectors. But, nowadays, semiconductors detectors have take their place. First, silicon-based detectors but, finally, germanium detectors became the most used in gamma spectroscopy.

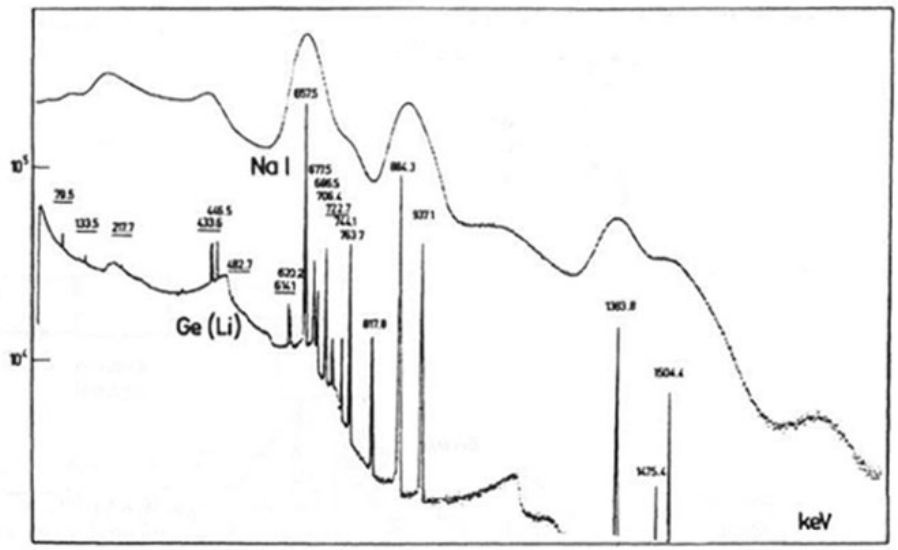

Figure 4.1: Comparison between a sodium iodide scintillator and a Ge(Li) detector, where it is easy to observe the better pulse height and energy resolution in germanium detectors. The gamma source was $^{108*}Ag$ and $^{110*}Ag$. The original picture was taken and adapted from Radiation Detection and Measurement, Glenn F. Knoll

Germanium detectors have bigger photoelectric cross section than silicon detectors, thanks to their bigger atomic number. Ionizing radiation produces in germanium electron-hole pairs, where the number of pairs are proportional to the energy of the incident radiation. The most important advantage with other detectors is that the energy to create a pair electron-hole is lower that in other detector, for example, paired ions in gas detectors. Therefore, the effect of the statistical fluctuation is less important and the energy resolution is actually the best for this measurement. This excellent energy resolution allows these detectors to precisely observe closer peaks than others detectors, improving the measurement techniques.

Ge(Li) detectors, where lithium drifting process is produced, were the first type of germanium detectors. Lately, in the mid 1970s were developed the **High Purity Germanium** (also called Intrinsic Germanium). These detectors have impurities lower than $10^{10} atoms/cm^3$ thanks to the improvement of the production techniques of production.

The interval of working energies for silicon detectors depends of several factors, mainly the composition of the detector and the size. With these characteristics, HPGe covers energies from a few of keV to several MeV, detecting almost all gamma rays produced in nuclear decays. Also, they can observe several atomic x-rays events with energies around 100 kev. For radiopurity studies, energies above 2700 keV are not necessary.

To improve the signal-noise ratio, it is necessary to operate in underground conditions and also to place the detector inside shielding castle. This castle has usually two parts: the outer part, made of Pb and the inner part, made by Cu. A complete explanation of shielding can be found in [Heusser 1995].

But, the main disadvantage of germanium detectors is that germanium has a small band gap (0.7 eV) and they need to be operated at low temperature. Usually they are cooled liquid nitrogen to 77K, kept in a dewar in thermal contact with the detector. The emanating gaseous nitrogen from this dewar, also is employed to create a nitrogen atmosphere inside the shielding to reduce the presence of radon. Luckily, HPGe detectors can be in room temperature between uses. Then, HPGe are replacing Ge(Li) because the need to be always at low temperatures.

But, despite the worst energy resolution, Iodide detectors are still important like a relative reference for detector efficiency. Then, the efficiency is still often quoted in relative terms to a standard 3" x 3" of NaI(Tl). For HPGe's installed at LSC, this efficiency is about 100%.

4.1.1 Gamma-ray interaction with matter

To understand the behavior of the gamma ray with the detector and also the shielding is necessary to know how gamma rays interact with the matter. When a collimated source of monoenergetic photons cross a material, the intensity varies as follows:

$$I = I_0 \cdot e^{-\mu x} \tag{4.1}$$

where μ is the absorption coefficient (also known like attenuation coefficient) of the material, I and I_0 are the initial and final intensity of the beam, and x is the thickness of the material

Absorption coefficient of the material is dependent of the energy of the incident photons and strongly dependent with the atomic mass. This coefficient can be defined like the sum of the three most important different interactions that can happen:

$$\mu = \tau(photoelectric) + \sigma(Compton) + \kappa(pair) \tag{4.2}$$

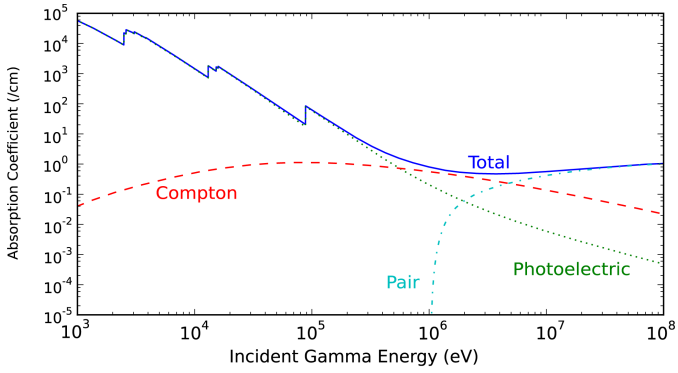

Figure 4.2: Total absorption coefficient of Lead (including three absorption processes) versus energy of the photons.

Where $\tau(photoelectric)$ is Photoelectric Effect coefficient, $\sigma(Compton)$ is Compton Scattering coefficient and $\kappa(pair)$ is Pair Production coefficient. The three different processes of attenuation ionize the material following this laws:

- Photoelectric effect: in this process, the photon vanishes transferring the main part of its energy to an electron and unbounding it from the nucleus. Very small part of the energy is transferred to the nucleus as a recoil. It follows the Einstein equation for photoelectric effect:

$$E_e = h\nu - E_b \tag{4.3}$$

  Where E_e is the energy of the unbounded electron, $h\nu$ is the energy of the electron and E_b is the bounding energy of the electron. It is important to remark that to cover the vacancy of the electron can be used a free electron from the medium a can be produced a rearrangement of the electrons of the atoms, with the emission of x-rays or Auger electrons. This x-rays usually a absorbed very close to the emission of it, usually a millimeter or less.

  This effect is the dominant effect for low energy gammas, < 0.5 MeV.

- Compton scattering: this process is similar to photoelectron effect, where the photon interacts with an electron. But, in this case is a inelastic scattering where the energy is shared by the two particles, the photon and the electron. The change of the energy of the photon follows this equation:

$$h\nu' = \frac{h\nu}{1 + \frac{h\nu}{m_0 c^2}(1 - cos\theta)} \tag{4.4}$$

  where θ is the scattering angle produced with the initial and final directions of the incident photon. The rest of the energy is transferred to the electron.

  This effect is dominant for intermediate energies.

- Pair Production: when a gamma-ray has a energy larger than twice the rest mass of an electron, 1022 keV, it is possible to produce this process. As can be seen in figure 4.2, this process become the most important in energies about a few MeVs. In pair production, the gamma ray is replaced by a pair electron and positron, where the energy above 1022 keV is shared in form of kinetic energy.

  Electron produced will deposite their energy, but when the positron is slowed to a energy similar to the electrons of the medium, it will be annihilated, with the emission of two photons that possibly will interact with the detector. But, sometimes these photons can scape producing two peaks, one for single scape (with 511 keV less energy) and other for double scape (with 1022 keV less energy).

  This effect is dominant for high energy gammas.

4.1.2 Gamma-ray energy deposited in a HPGe detector

The objetive of a gamma ray detector is to measure all the energy of the emitted photon, known like **Full Energy Peak**. For low energy events, a Photoelectric interaction will absorbe all this energy. But, when the gamma ray energy is bigger, Compton Scattering and Pair Production appears. In these cases, the energy is shared between electrons and photons. In figure 4.3 we can observe a schematic view of some gamma interactions inside a detector.

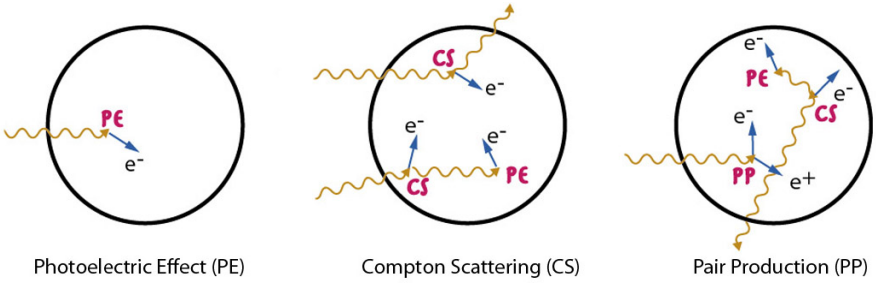

Figure 4.3: Different events that can happen in a HPGe.

For **Photoelectric Effect**, left side of figure 4.3, is easy to observe that the energy is transferred to the electron and this event will be a part of the Full Energy Peak.

These are the ideal events, where all the energy deposited goes directly to a Full Energy Peak event.

For **Compton Scattering**, the Full Energy Peak correspond the central example of the figure 4.3, in the lower part. There, after the Compton Scattering, the photon will deposite the rest of the energy via Photoelectric Effect.

If the photon escapes without depositing its energy in the detector after the interaction, the energy deposited of the electron will be lower than the Full Energy peak. The deposited energy in the HPGe follows a smile-like continuum spectrum with the maximum energy deposition is produced in the case of backscattering of the photon, $\theta = \pi$. The energy of the end of this distribution, known like Compton edge, is:

$$h\nu'|_{\theta=\pi} = \frac{h\nu}{1 + \frac{2h\nu}{m_0c^2}} \tag{4.5}$$

The gap between Full Energy Peak as a limit, obtained in the case of high energy gammas, $2h\nu >> m_0c^2$:

$$E_c \equiv h\nu_f - E_e|_{\theta=\pi} = \frac{h\nu}{1 + \frac{2h\nu}{m_0c^2}} \cong \frac{m_0c^2}{2} = 256keV \tag{4.6}$$

In the case of the HPGes employed in our work, the size of the detector makes possible to have several Compton Scattering without depositing all the energy in the detector. That process, known like Multiple Compton Scatterings and presented in figure 4.4, makes a different continuum spectrum, where it contribution can be mainly observed between Compton Edge and Full Energy Peak.

For **Pair Production**, the process is more complex, as can be seen in figure 4.3. When the pair electron-positron is created, the positron will be thermalized and annihilated, emitting two photons with opposite directions. In this case, one photon scape and the other interacts via Compton Scattering and Photoelectric effect. In this case, this event will have the energy of the Single Scape Peak.

This figure is only an example, because the annihilation photons can independently scape, interact via Compton Scattering or interact via Photoelectric Effect. Additionally, these escaping photons will deposit (via Compton Scattering) part of their energy in the detector. Then, some events with energies between Double Scape Peak and Full Energy Peak will be measured by the detector.

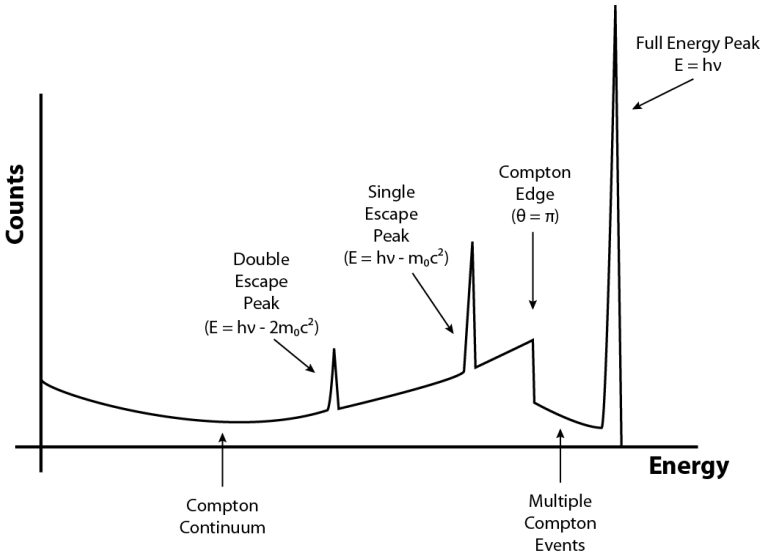

Figure 4.4: Spectrum of a High Energy Gamma source. Most remarkable parts of the spectrum are shown.

There are other second order effects that could be detected like events in the detector, produced for example when we have a very active sample and the emitted gammas interact with the shielding.

For Photoelectric Effect, rearrangement of the electrons produce some x-rays photons that can be detected like a small peak in the region of 100 keV. For

Compton Scattering, the scattered photon from the interaction with a electron from the shielding can be scape towards the detector. The interval of energies where Compton Scattering is the dominant interaction and the angle of the photons necessary to arrive to the detector (usually bigger 110 degrees) make this non- gaussian peak appears about 250 keV. And, For Pair Production, when a positron produced in the shielding and lately annihilated, it produces a pair of 511 keV photons that can be detected, producing a peak in the spectrum.

These three background sources are usually small and easy to observe and avoid, because they are not close to our experiments important peaks.

4.2 Radiopurity Services of the LSC

Canfranc Underground Laboratory (LSC, Laboratorio Subterráneo de Canfranc) is located in the Spanish side of the Pyrenees, under the Tobazo mountain. The experimental halls of the Laboratorio Subterráneo de Canfranc (LSC) have been excavated in the rock 850 m deep, approximately 2450 m.w.e. overburden that suppresses the cosmic muon flux by 5 orders of magnitude.

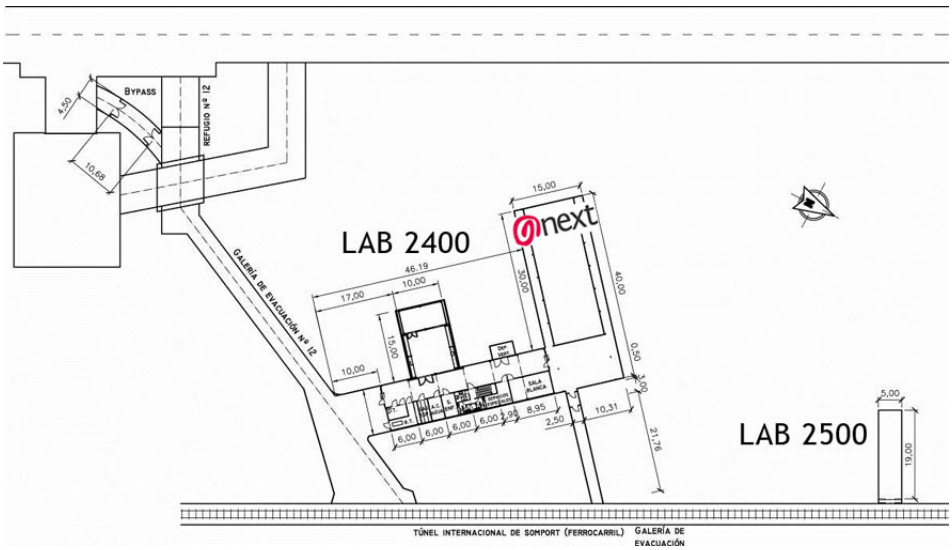

Figure 4.5: Map with the location of the two new LSC laboratories. Inside Lab2400 are placed NEXT detectors

LSC is a ICTS[1] (Infraestructuras Científicas y Técnicas Singulares) and runs by a Consortium between the Spanish Ministerio de Economía y Competitividad, the Government of Aragon and the University of Zaragoza. The underground facilities have been completed and delivered by the University of Zaragoza to the Consortium on 30 June 2010.

The LSC's total area is about $1.250m^2$ corresponding to a volume of about $10000m^3$ and it has two experimental halls ($40x15x12m^3$ and $15x10x7m^3$) in which the experiments are distributed as well as offices, a clean room a mechanical workshop and gas storage room. Outside the mountain, the LSC headquarters and administration external building has 16 offices for scientific users, 9 offices for LSC personnel and 4 specialized laboratories as well as a mechanical workshop and storage room, meeting, conference and exhibition rooms and 2 apartments.

Seven experiments have been approved (ANAIS, and ArDM on dark matter, BiPo, NEXT and SuperK-GD on neutrinos, GEODYN on geodynamics and GOLLUM on biology). The scientific users are about 254 from 19 Countries.

Figure 4.6: View of the HPGe farm at LSC

The LSC also offers a Radiopurity Service to measure ultra-low radioactivity using four high purity germanium detectors (HPGe). The HPGe detectors property of LSC are p-type close-end coaxial High Purity germanium detectors produced by Canberra France, with 100-110% relative efficiencies, that is defined

[1] http://www.idi.mineco.gob.es/portal/site/MICINN/ICTS

like the relative efficiency to a 3"x3" NaI detector at 1332 keV and for a distance of 25 cm between the source and the detector. The energy resolution at FWHM is about 2 keV at the ^{60}Co gamma line of 1332 keV.

The active volume of crystals ranges from 410 to 420 cm^3, with a cylindrical shape with similar diameter and height, about 81 cm. Cryostats are made of ultra-low background aluminum.

Figure 4.7: View of the HPGe without the shielding

Each detector has a shield consisting of 5 cm of oxygen-free copper and 20 cm of very low activity lead having <30 mBq/kg of ^{210}Pb; nitrogen gas is flushed inside a methacrylate box to avoid airborne radon intrusion.

The data acquisition system is based on Digital Signal Processing using Canberra DSA1000 modules.

The detectors used for NEXT measurements are those named GeOroel, GeTobazo, GeAnayet and GeLatuca. The name of the detectors is the same that the most important mountains around the laboratory. These detectors are in operation since 2011.

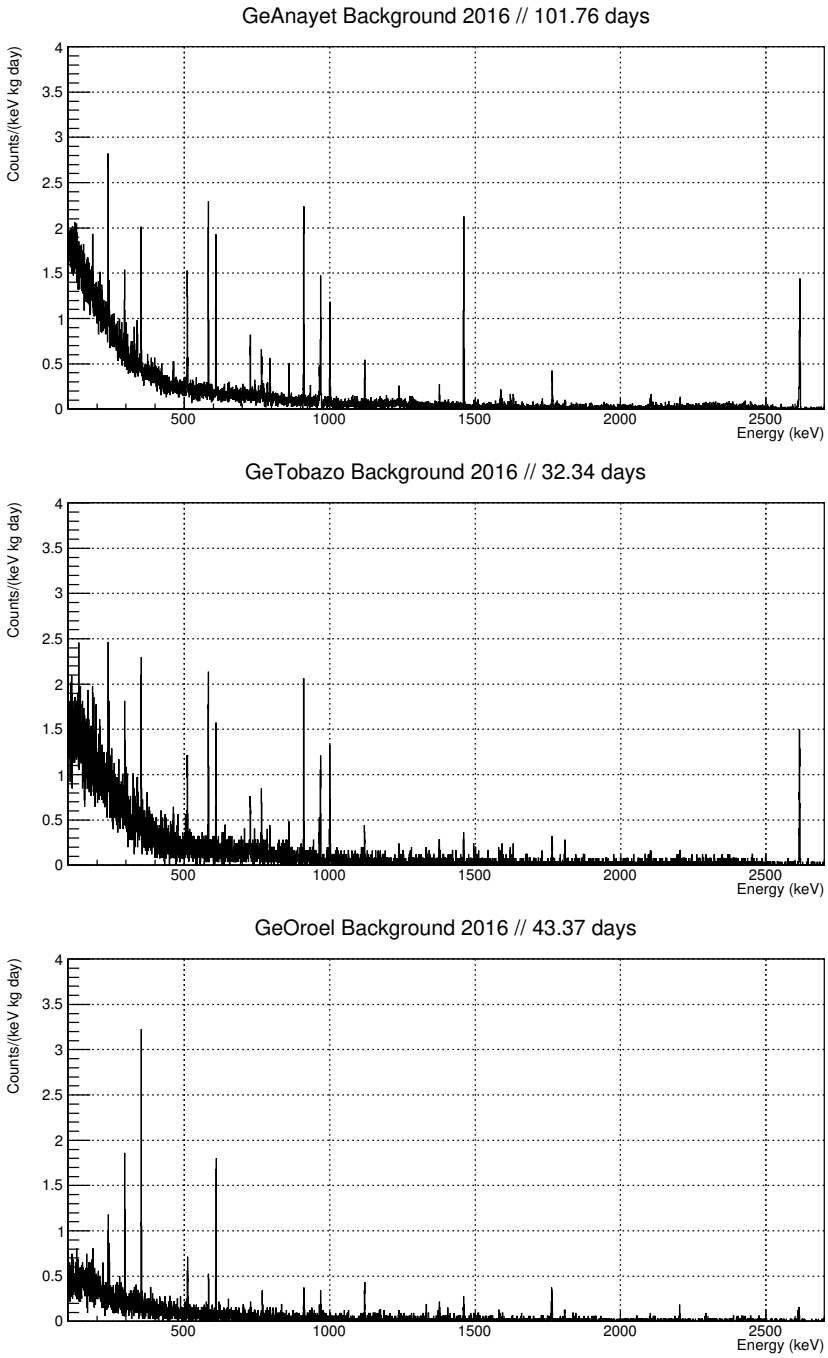

Figure 4.8: HPGe background, part 1. Detectors GeAnayet, GeTobazo and GeOroel

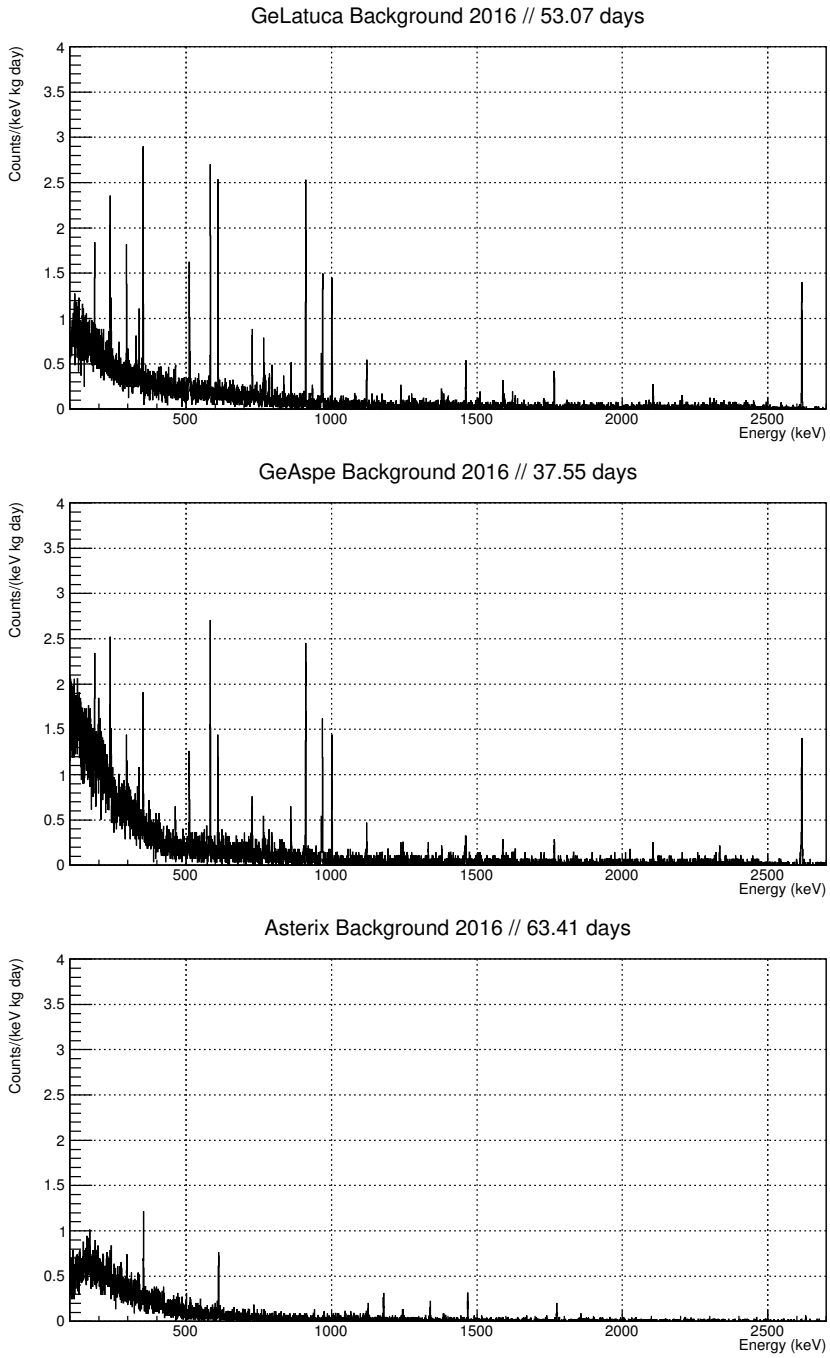

Figure 4.9: HPGe background, part 1. Detectors Gelatuca, GeAspe and Asterix

The background spectrum of one of the LSC detectors, geOroel. It amounts approximately 500 counts/day between 100-2700 keV. The relevant gamma lines of 583 keV (^{208}Tl) and 609 keV (^{214}Bi) contribute with 1 and 3 counts per day respectively.

To place the sample as close as is possible to the detector, LSC employees a **Marinelli beaker**, designed for HPGe measurements. This cylindrical container has an annular bottom part, adapted to introduce the detector and increase as much as possible the detection efficiency. This container is made by polypropylene with the cover of polyethylene. The usual sizes employed at LSC are 1 and 4 Liter.

Figure 4.10: Sample of different Marinellis beakers employed at LSC for radiopurity measurements

4.3 Typical measurement procedure

To carry out a radiopurity measurement, are involved some people from different institutions. The first step is the **sample selection**.

In NEXT, the selection of the materials depends on a joint decision from several parts of the experiments. Mechanical and electrical engineers are in charge to design the detector and usually they need to check the radiopurity of some new components to place in the detector. Different plastics, screws electronic components or metal alloys are typical options that engineers offer us for the measurements. In this point, Radiopurity Team, with some help from the

Background Model people, check in databases information from these options and choose the best options for the measurement. Sometimes, no information about these samples is found and we have to be the first to measure it. After this selection, we ask with LSC for availability of detectors to do the measurement.

In SuperK-Gd, Japanese part of collaboration are in direct contact with several companies that produce Gadolinium Sulphate. Therefore, they talk with the companies about our radiopurity requirements and send samples of about 1 to 5 kg to measure them at LSC.

Once chosen, we have to **prepare and clean** the sample. In NEXT, we have a wide variety of sample types and sizes. The sample size is limited by the marinelli size. Usually it is not necessary to use more space that marinelli offers, but sometimes we have measured bigger samples, removing the marinelli and using freely the space inside the shielding and around the detector. One example is the Copper CuA1 measurement, a 94 kg measurement that is shown in figure 5.12 and in row # 24 of the tables 5.1 and 5.2

In SuperK-Gd, the samples are powder sample that easily fits in a marinelly. The only complication is to not spill the Gadolinium Sulphate powder.

Before each measure is recommended a **calibration** run of the detector, necessary guarantee that the detector is working properly, checking possible problems like lost of detection efficiency (lower peaks) or drift in the energy of the peaks. At LSC, calibrated radioactive sources of ^{60}Co and ^{152}Eu are used during 1000 seconds for calibrations.

The first source, ^{152}Eu, is a source with a large amount of peaks, good to calibrate .For our calibrations can be used 21 different peaks in the interval of 100-1500 keV, where the most important peaks are 122 keV, 344 keV, 779 keV, 1112 keV and 1408 keV. One calibration event is shown in figure 4.11 with all the important peaks fitted.

The second source, ^{60}Co, is a well known isotope found in several radiopurity measurements. It has two strong peaks with energies of 1173 keV and 1333 keV. Additionally, we can observe the double coincidence peak, where both gamma

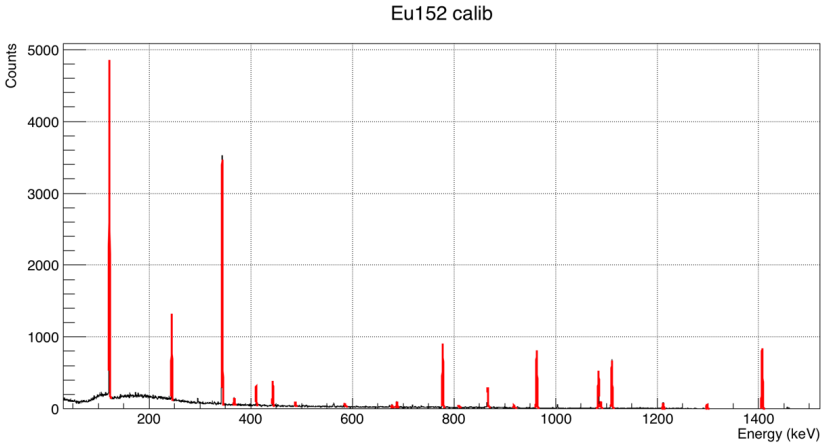

Figure 4.11: Callibration spectra with 152Eu source. The most important peaks are fitted

photons have deposited all their energy and we can observe a peak with 1173 keV + 1333 keV = 2506 keV. This peak, with a low probability in comparison with the other two, can be used for detector calibration at high energies. In our case, 1173 keV and 1333 keV peaks are about $\sim 30000 counts$ and 2506 keV peak is about $10 - 20 counts$.

After calibration, we start the **screening** of the sample and the **anaylisis** . During this process, weekly checks are done the evaluate if everything is working properly and if it necessary to extend more time the measurement. This analysis process is explained in Section 4.7. Typically, the measurement time is about 1 month.

Finally, the results are shared with the people of the collaborations and we **decide** if this sample enough radiopure for our requirements or not.

4.3.1 Sample preparation

Once the sample is selected, it must to be cleaned. Superficial contaminations from external sources can fake the radiopurities measurement and makes necessary to clean all the samples before its radiopurity measurements and also before been placed in the experiments.

The usual cleaning protocol for samples is as follows. For big samples, they will be cleaned by hand with clean room wipes and pure alcohol with ethylene or methylene, depending of the availability. If the samples are smaller, these samples will be cleaned in an ultrasonic bath and alcohol at room temperature during 30 minutes.

For the cleaning of metals, in our case Cu and Pb, is necessary to use acids for the cleaning. For copper, the process is as follows:

- External cleaning, removing the possible oxide layer in the pieces
- Soap cleaning in a bath with Elma 60 (acid soap at 5% solution) during 30 minutes at 40 degrees.
- Water bath in pure water to remove the soap.
- Acid etching at super pure nitric acid bath (4% solution at 40 degrees) during 30 minutes.
- 3 successive pure-water baths, rinsing the copper pieces to remove the acid from the surface
- passivation at citric acid bath (10% solution at 40 degrees) during 30 minutes with in water rinse
- 2 successive pure-water baths, rinsing the copper pieces to remove the acid from the surface
- Drying with clean room wipes

For Pb, the process is almost the same but without passivation step, not necessary for this material.

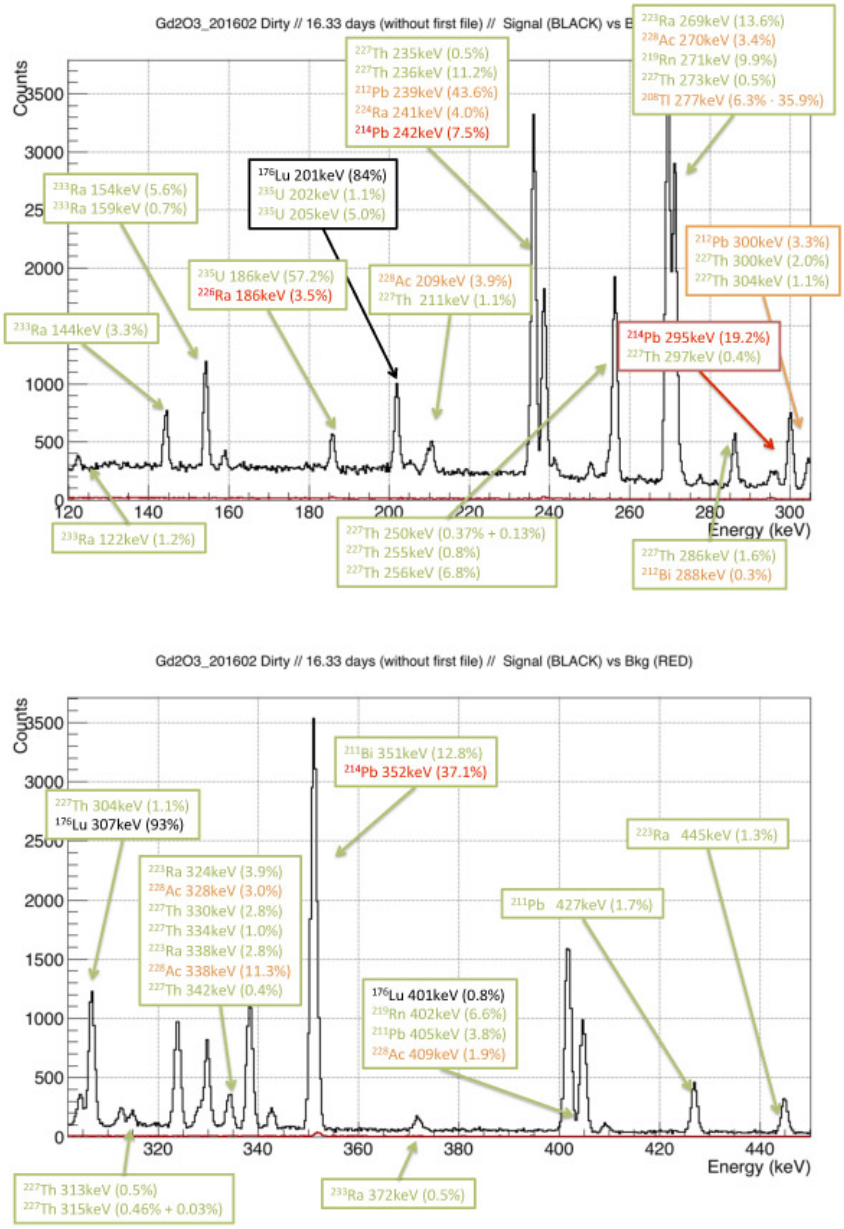

Figure 4.12: Peak identification with a very dirty sample, GOX-1602-NYC-1. First and second parts of the spectrum is shown in the figure

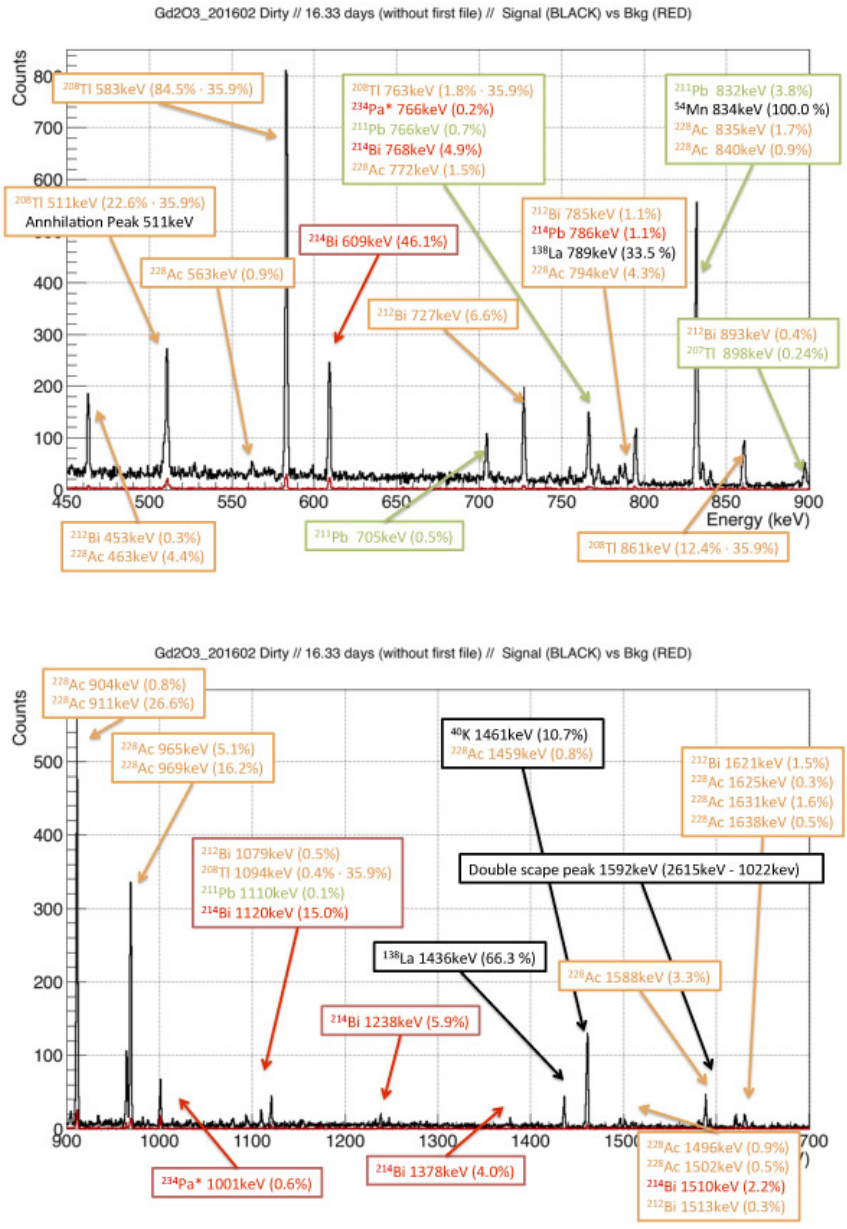

Figure 4.13: Peak identification with a very dirty sample, GOX-1602-NYC-1. Third and fourth parts of the spectrum is shown in the figure

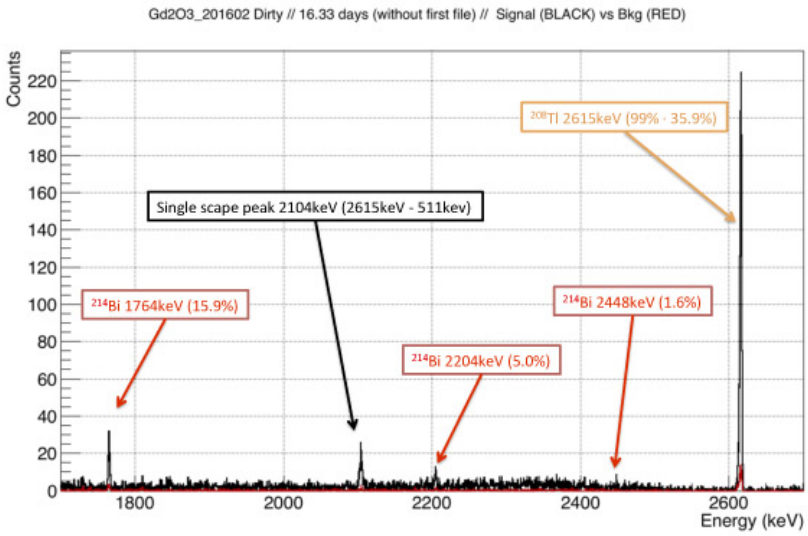

Figure 4.14: Peak identification with a very dirty sample, GOX-1602-NYC-1. Fith part of the spectrum is shown in the figure

For PMTs, the cleaning protocol is a bit different. These sensors are fragile and we have to be careful with them, mainly with the ceramic stem and with the pins. The cleaning protocol recommended by Hamamatsu consists of normal cleaning with alcohol and clean room wipes for the body and the window of the PMT and careful cleaning with special sticks for the pins and the ceramic stem.

For the metal samples prepared for germanium spectrometry, a different protocol has been used. This protocol is: diamond cut of the sample, cleaning with acetone, ultrasound bath with acid-detergent, 63% nitric acid bath, new cleaning with acetone and storing in a sealed plastic bag.

4.4 Signal Extraction

As is explained in Chapter 4.1, the signal observed in a HPGe is composed of mainly two contributions: the peak itself and the sum of the several Compton edges of the upper energies isotopes. Additionally, we have to consider the background of the detector, that we also have to extract from the measured signal.

First of all, we have to define the **Net Signal**, that is the number of counts of Full Energy Peak that correspond to the sample. To remove the background from the net signal, it is necessary to have also a background measurement that is taken during about 30 days. To compare both measurements, due to the different length of the measurements, we have to normalize the time of the background measurement to the signal measurement and compare results. In figure 4.15 we can see, fitted in black, a very large peak at 583 keV from the signal and the small contribution, fitted in red, of the background peak (normalized to the duration of the signal duration).

The background run is recommended to be taking unless one per year and check the time stability of the detector

When the net signal is very big, we can stop the measurement because the statistics is enough to get the signal with a very small error. Figure 4.15 is a good example of a measurement with enough time of measurement.

Signal and background datafiles are taken daily for, in case of any problem, discard this wrong file losing not so much measurement time.

The data obtained in each measurement give us the number of events measured per bin of the detector. With the present electronics at LSC, the number of channels is 8192 and the E_{max} is about 2700 keV (depending of the detector). Therefore, a rebinning factor of $\sim$ 0.33 keV/channel is necessary to convert channels to energy in the x axis.

Additionally, we have to remember that, despite of the nitrogen flux, the firsts days of measurement we can have atmospheric radon surrounding the sample,

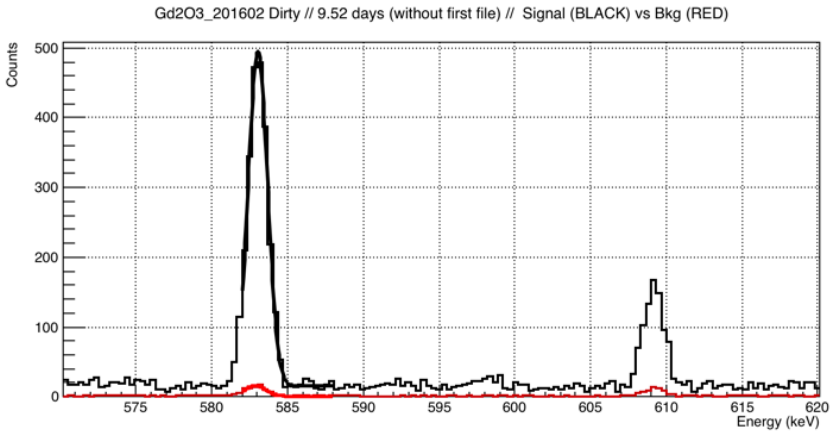

Figure 4.15: Gadolinium sample for SuperKamiokande experiment. In black is plotted the signal and in red, the background. Background duration is normalized to the duration of the signal measurement

that will fake the true value of the activity. Therefore, we have to check the 2 or 3 first datafiles and be sure that radon excess has disappeared.

For this analysis is used **ROOT**, a modified C++ software developed by René Brun and Fons Rademakers for CERN. ROOT is a powerful software designed for experimental data analysis. In my case, I have used the version 5.34/25.

We fit the signal to a gaussian plus an horizontal line (polynomial cero order). The gaussian fits to the gamma peak properly, except in the left side. The interval employed to fit the gaussian is 3 sigmas around the central position of the peak. A horizontal line is a very simple but accurate approximation to the accumulated Compton Continuum background. With the data fitted, we can calculate the area of the gaussian that is equivalent to number of events detected. This number of events will be converted to activity in 4.7.

Fitting function used by ROOT with three fitting parameters that are p0, p1 and p2, for a typical gaussian distribution equation.

$$f(x) = p0 \cdot e^{\left(-0.5\left(\frac{x-p1}{p2}\right)^2\right)} \tag{4.7}$$

The number of events are equivalent to the area of the gaussian function, but the area has been decreased with the rebin factor, necessary to convert channels to keV. Therefore, according to gaussian equations and removing the rebin factor, the area of the gaussian is:

$$Area = \sqrt{2\pi} \cdot P0 \cdot P2/rebin \tag{4.8}$$

In a very low background experiment we desire very very clean materials and sometimes we find materials where the signal is not well observed. The problem of these very good materials is that, according to our analysis methods, we cannot clearly observe a peak that can be used to quantify the activity of the sample. In these cases (where the experimental limitations cannot determine if we have a signal or not) we have to define a **lower upper-limit** (with usually $\approx$ 95% of CL) a for the activity the sample.

These lower upper limits depend on the sample (material, size, position inside the detector, Compton edge from more energetic gamma decays), the detector (background from the detector and shielding, detection efficiency) and the length of the measurement.

Therefore, we have to follow a criteria to find it with the maximum precision. We are using two different methods for this analysis: when we have a large background and Datas and Background follows gaussian behavior and when we have low background where the background doesn't follow any clear fit function or we only have Compton Continuum background.

4.4.1 Case of Large Background

In the case of Large Backgrounds, the data follows a Gaussian statistical. We can define the observed signal, like:

$$S_{net} = (S_{Peak} - S_{Compton}) - (B_{Peak} - B_{Compton}) \frac{t_{signal}}{t_{bkg}} \tag{4.9}$$

Where S_{Peak} is the area of the signal peak, $S_{Compton}$ is the area produced with Compton events. The explanation is the same for the background datas, B_{Peak}, $B_{Compton}$, both normalized to the duration of the signal measurement.

In some cases, we can measure several peaks from the same isotope that can be used each to measure the activity independently and their results can be statistically added to get a more accurate estimate. For example, in ^{228}Ac we can find three very close and intense peaks for their analysis. Individual analysis is correct but a mixed analysis gives a better result and also a lower value for the error of the measurement.

Therefore, a better estimate of this activity can be obtained from their weighted-mean. Then, the new variance is:

$$\sigma_{\kappa}^2 = \frac{1}{\sum_{i=1}^{n} 1/\sigma_{\kappa,i}^2} \tag{4.10}$$

With a mean value of:

$$\overline{\kappa} = \frac{\sum_{i=1}^{n} \overline{\kappa}_i/\sigma_{\kappa,i}^2}{\sum_{i=1}^{n} 1/\sigma_{\kappa,i}^2} \tag{4.11}$$

There two cases where we are going to obtain upper limits instead of value of the activity: first is when Net Signal has a negative value. Activity can only take positive values; negative values are always interpreted as no source being present. Second case is when the number of counts of the Net Signal is smaller than the error.

In this two cases, we will get a interval where, with a 95% of c.l., we will find the true value of the number of counts:

$$\kappa \leq \overline{\kappa} + 1.645\sigma_{\kappa} \tag{4.12}$$

How to get the activity from this number of counts, is explained in Section 4.7.

4.4.2 Case of Low Background

This is method we follow for those signal that cannot be fitted with a gaussian function. This method is widely in [Baudis et al. 2011]. It is usually used to estimate the lower upper limit of the activity, but can be used to quantify activities. The problem is that any small excess can be easily fit to a gaussian. If not, we try (if it is possible) to extend exposure of the sample until the peak could be fitted.

First of all, we define **Detection Limit** L_d like the level of a true net signal that can be detected with a probability of $\approx 95\%$.

$$L_d = 2.86 + 4.78\sqrt{S_{Compton} + B_{Peak}\frac{t_{signal}}{t_{bkg}} + 1.36} \tag{4.13}$$

According to this criteria, we can find three different cases:

- if $S_{net} < 0$ In this case, we don't observe any signal but we cannot affirm that there isn't any background source. In this case, L_d will be taken like the lower upper-limit of the number of counts we have measured.
- if $0 < S_{net} < L_d$ In this case we have a small excess from the background but we cannot affirm if it is a signal of activity from the sample or a statistical fluctuation in the background rate. In this case, the lower upper-limit is $S_{net} + L_d$.

  It is recommended to extend the measure (if it is possible) in the case of an important peak.
- if $L_d < S_{net}$ We have a signal. In this case, it must be analyze it like a normal signal.

Independently of the case, we have a number of counts (of signal or an upper limit) that has to be converted to specific activity. In Section 4.7 is clearly explained how to obtain the activity from a number of counts.

4.5 JANIS database for Nuclear decays

JANIS[2] is a free and complete database developed by OECD Nuclear Energy Agency and Aquitaine Electronique Informatique. JANIS contains information of the Nuclear Decays, of Fission yields and Interaction data, like resonance parameters, cross-sections or neutron multiplicities.

This database is developed in Java. That means that can be used under Windows, Mac OS X and Linux.

For our experiments, we have use the Decay Lines database, where we can find the energy of the photons emitted in a Nuclear Decay with intensity of photon, also with their errors. It can be also used to identify unknown peaks observed in a data spectrum, looking in the database for peaks in the interval of energies close to the peak.

A complete tutorial of JANIS can be found in [N. Soppera and Dupont 2014].

4.6 Monte Carlo simulation

This part of the radiopurity work, lead by Susana Cebrián from Universidad de Zaragoza, consist on simulations to estimate de efficiency of the detector for this sample.

Concerning the estimate of the detection efficiency, Monte Carlo simulations based on the Geant4 [Agostinelli et al. 2003] code have been performed for each sample, accounting for intrinsic efficiency, the geometric factor and self-absorption at the sample. No relevant change has been observed in the Geant4 simulation when changing version or the physical models implemented for interactions (considering the low energy extensions for electromagnetic processes based on theoretical models and on exploitation of evaluated data, G4EmLivermorePhysics class and the previous G4LowEnergy classes[3]). Validation of the simulation has been made by comparing the efficiency curve of

[2] *http : //www.oecd − nea.org/janis/*
[3] *http : //geant4.cern.ch/support/userdocuments.shtm*

the detectors measured with a ^{152}Eu reference source of known activity located at 25 cm from the detector with the simulated one.

More or less, all the detectors have similar detection efficiency, but GeOroel a bit better than the others. The higher efficiency shown by GeOroel is due to a slightly larger volume in comparison with the other detectors

To simulate the samples two characteristics of the sample must be known: the size and the composition, where that means percentage ratio of the elements of the sample. We these two parameters, we usually simulate an homogeneous and isotropic emission from the sample. In some cases, where we know (thanks to the databases or to our accumulated experience) that a heterogeneous sample has some radiopure parts and some radioactive parts, we decide to simulate the emission of the gammas only from those radioactive parts. One example of this case can be the simulation of the activity of the welding of two pieces of Stainless Steel, previously measured and with very good radiopurity results.

To quantify the detection efficiency in a measurement, we simulate the emission of 100.000 gammas with the same energy. This step is repeated in steps of 50 keV for low energy events. For energies above 500 keV, where the behavior of the efficiency is more stable, 100 keV are used.

To estimate the error associated to the MC simulation, we have consider these factors:

- Detector simulation: with several parts that are complicated to perfectly know and simulate.
- Sample simulation: with several factors that can change between samples like size, shape, composition or position.
- GEANT 4: error associated to program and the different libraries employed to estimate the efficiency of the measurement. It may change by the employed version in the simulation of the measurement.
- MC method: the error associated to the MC simulation itself. It will be reduced with a larger number os simulated events.

Considering all these factors, we estimated that the error associated to MC simulations is $\sim 10\%$.

4.6.1 Efficiency Estimation: typical examples

Now, we will show two small examples of how simulations have been made to estimate the detection efficiency of the detectors.

For NEXT, the chosen sample are the Sapphire windows for the Energy Plane. Each crystal is 6 mm high and has a diameter of 83.8 mm, with the total mass was 527 g. To avoid problems with the surface of the windows, the windows are on a teflon supporter. For the composition of the sample, we have use the simplest possible: Aluminium Oxide, Al_2O_3

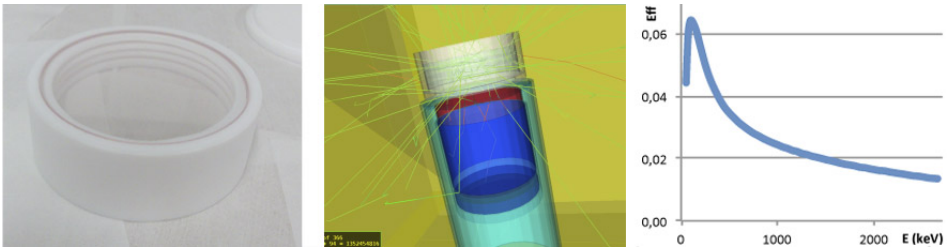

Figure 4.16: Montecarlo simulation of Sapphire windows for NEXT experiments. Left side, The sample prepared. Center, the simulated sample with the emission of some photons. Right side, the efficiency simulated

The sample chosen from **Superk-Gd** is GOX-1603-SHT-236. This sample is a Gadolinium powder sample that adapts its form to the marinelli. In this case, the sample has a cylindrical geometry with $h = 110mm$, $r_{int} = 120mm$ and $r_{ext} = 195mm$.

In figure , in the left side we can observe the emission of 100 keV photons. These low energy photons are in more of the cases self-absorbed by the gadolinium itself.

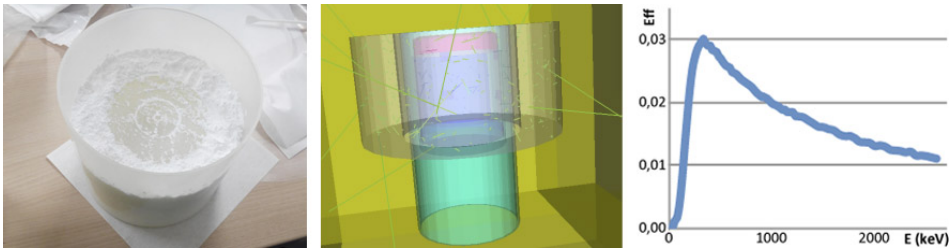

Figure 4.17: Montecarlo simulation of one sample of Gadolinium for SuperK-Gd

4.7 Quantification of the radioactive contamination of the materials

To derive the activity in a sample of an isotope producing a gamma emission of a certain energy, we need the net signal (the number of events of the peak from to the sample, explained in section 4.4) and the Full Energy Peak detection efficiency at the corresponding energy, together with the time of the measurement and the branching ratio of the emission.

Now, for determining ultra-low activities of a sample (at the level of mBq/kg and below), we have to compare the measured signal of the sample with the detector background and following a criteria depending of the level of background (large or low background). Finally we have obtained signal or an upper limit that we have to convert to specific activity.

The steps taken to convert signal to specific activity are:

- Fist step is, as I mentioned before, to obtain the Net Signal. To do this we have to extract it using the data run and the background run of the HPGe detectors. In this moment we have detected counts / measurement time.
- Second step is to divide per the duration of the measurement in seconds. Now, we have detected counts / second.
- Third step is divide per the emission intensity, according to Janis database. Now we have detected disintegration / second

- Forth step is divide be the detection efficiency of the Full Energy Peak, estimated with MC simulations. Now we have disintegrations / second, that is Bq.
- The las step is to convert this activity to specific activity, dividing by kg, number of units, length... depending of the sample screened.

4.8 Other techniques

Not only HPGe are employed to measure the amount of radioimpurities of the materials. These other techniques are not capable to directly quantify the lower parts of the chains but in some cases they are necessary for our experiments.

The two different techniques employed are Mass Spectrometry (MS) and Radon Emanation analysis.

4.8.1 GDMS and ICPMS

In these techniques, ions are extracted from the sample for mass spectrometry; the main difference between is how to obtain these ions. Mass Spectrometry techniques are fast and requires only a small sample of the material. In our case and for GDMS, the samples were prepared with a surface of $2x2cm^2$ for NEXT radiopurity measurements). For our experiments, we have used Glow Discharge Mass Spectrometry (GDMS) and Inductively coupled plasma mass spectrometry (ICPMS)

Several samples have been measured for NEXT and SuperK-Gd. This technique is more relevant for SuperK-Gd because it can quantify better the number of atoms of ^{238}U, an important source of background.

In GDMS are used solid samples to function as the cathode in a plasma or discharge gas, typically argon. Direct analysis of solid samples can be advantageously performed, without chemical sample preparation. The gas ions are accelerated toward the sample resulting in erosion and atomization of its surface, and those extracted atoms will be detected with a mass spectrometer.

This technique is recommended for metals, used in NEXT in several samples like Stainless Steel, Copper or Lead (see 5).

For our ICPMS measurements, the sample most be prepared before the measurement, converting it into a liquid. The sample is nebulized and converted in atomic ions that finally goes to a Mass Spectrometer.

We have to remark two strong disadvantages of Mass Spectrometry: first is the uniformity of the sample. We are only analyzing a small part of the sample and is the sample is not uniform, very different results can be obtained.

Second disadvantage is that this method cannot measure our most important radiopurity peaks. Measured concentrations of U, Th and K have been converted to ^{232}Th, ^{238}U and ^{40}K activities. No information on daughter nuclides in the chains and a possible disequilibrium in the lower part of the chain cannot be detected.

In any case, this technique is very useful to make a pre-selection of samples, with information of the activity in the upper part of the chain. Later, these samples must be screened with germanium detectors underground.

4.8.2 Radon emanation

As was commented in Chapter 2 radon is present in the natural decay series and is a gas that can also scape from the materials, mainly by diffusion or by nuclear recoil after an alpha decay. The most dangerous These is not a direct measure of the amount of ^{214}Bi, it measures the number of atom of radon that scape from the material that lately will undergo several decays to ^{214}Bi.

These measurements, carried out by Grzegorz Zuzel from Jagiellonian University, Cracow, Poland.

The detector consist of a vacuum chamber for the sample and a cryogenic adsorption trap to capture radon to detect the alpha decays of its daughters. The sensitivity limits are about some $\mu Bq/sample$ and the duration of these measurements are about 2 or 3 weeks.

Some positive results have been obtained from these measurements but they are still not published.

4.9 Conversions between ppb and Bq/kg

When you make a measurement with HPGe, you are counting decays, usually Bq/kg. In the other hand, using Mass Spectrometer you are getting concentration units, usually ppb.

These two techniques are very common to quantify the radioactive contamination of a sample, but it is not usual to find the conversion process between these two units. An important point is that these two magnitudes are not equivalent, specific activity and concentration don't have the same units and are related by these two equations.

$$A = \lambda N \tag{4.14}$$

$$n = \frac{N_a}{m_a} m \tag{4.15}$$

Combining these two equations and taking care with the units, we will finally get the conversion equation:

For example, for Uranium, we will get:

$$a = \frac{1Bq \quad U}{kg \quad sample} \Leftrightarrow Conc = 7.46 \cdot 10^{-11} m_a t_{1/2} ppb \quad of \quad U \tag{4.16}$$

With the half-life in years. In the case of ppb of U and activity of one isotope, for example ^{238}U

$$a = \frac{1Bq \quad U}{kg \quad sample} \Leftrightarrow Conc = 7.46 \cdot 10^{-11} \frac{m_a t_{1/2}}{n_{abun}} ppb \quad U \tag{4.17}$$

Or, in the opposite direction:

$$1ppb \quad U \Leftrightarrow a = 1.33 \cdot 10^{10} \frac{n_{abun}}{m_a t_{1/2}} Bq \quad U^{238}/kg \tag{4.18}$$

With these equations, we can find out the typical conversion factors:

$$1Bq/kg \quad {}^{238}U \Leftrightarrow 81ppb \quad U \tag{4.19}$$

$$1Bq/kg \quad {}^{232}Th \Leftrightarrow 246ppb \quad Th \tag{4.20}$$

$$1Bq/kg \quad {}^{40}K \Leftrightarrow 32.3ppb \quad K \tag{4.21}$$

5

Radioactive contamination in NEXT detector

5.1 Introduction

The study of the background of the detector is a key part of the low-background detectors. We have to understand the background effects, select the most appropriate materials, quantify their activity and estimate the impact of these radioactive background in our $2\beta0\nu$ decay search.

The most important components in our detectors are those that are in the inner parts and the PMTs. Inner components have less shielding and bigger solid angle to emit background events inside the fiducial volume. PMTs are photosensors

that can't be replaced (they are the best for our requirements), but they are handmade and is possible to have individual differences or radioimpurities, that makes necessary to screen all these units and check whether they are enough radiopure or not for our experiment.

In NEXT, we have divided the detector un four sections: Energy Plane, Tracking Plane, Vessel and Shielding and External Parts. Each part is explained in detail in individual sections.

Furthermore, we have developed NEXUS, a software based in GEANT-4, to quantify the effect of these activities in our experiment. For a more complete explanation, I recommend *The NEXT experiment for neutrinoless double beta decay searches*, [Justo Martín-Albo 2015] and *Sensitivity of NEXT-100 to neutrinoless double beta decay*, [J. Martín-Albo et al. 2016]

5.2 Energy Plane

This section is destined to study the activity of all the components, inside the detector, used to measure the energy of the events. We have to consider mainly the PMTs and their bases, the copper plate and the windows, but there are also other small components.

All this work is published in *Radiopurity assessment of the energy readout for the NEXT double beta decay experiment*, [Cebrian et al. 2017].

5.2.1 PMT base

Tha base of the PMTs, also known as divider circuit, is necessary to divide the high voltage of the PMT and also to improve the signal, in our case, to have the needed linearity. Each PMT base in the NEW set-up is composed of a total of 19 resistors of different electrical resistance, 7 capacitors (5 having a capacity of $1.5\mu F$ and 2 with $4.7\mu F$) and 18 pin receptacles fixed on a kapton substrate using epoxy, a copper cap with a mass of $\sim 50g$ and a 1-m-long cable made of kapton and copper. A paste was used for soldering. All these components used in the PMT bases have been separately screened.

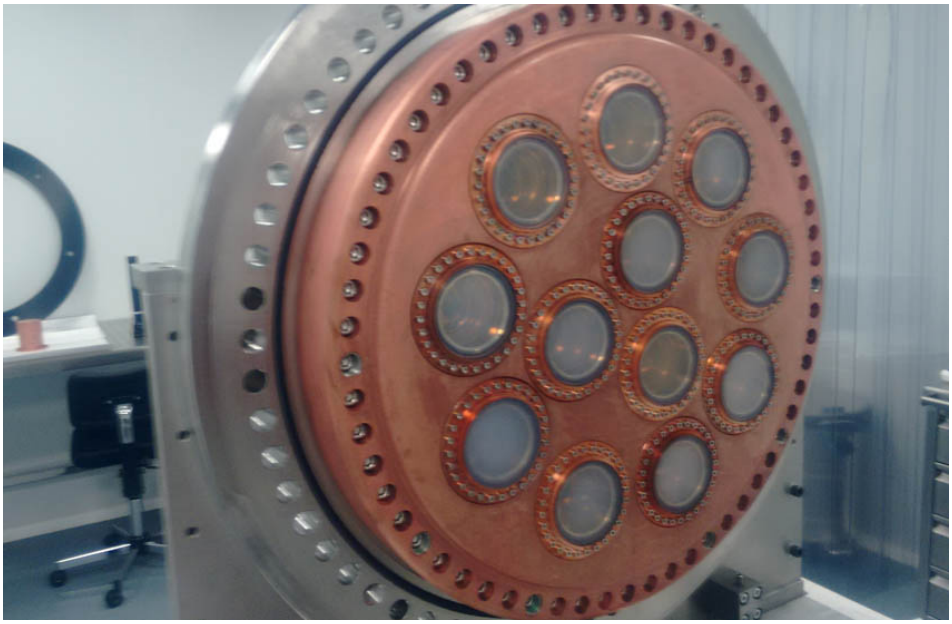

Figure 5.1: Complete view of the Energy Plane of NEW detector. We can observe the Copper Plate with 12 holes for PMTs, behind the Sapphire windows

Base capacitors are Tantalum Solid Electrolytic Chip Capacitors with Conductive Polymer Electrode, TCJ Series, supplied by AVX[1]. Two samples of units with the different capacities and different size and mass have been screened. It was possible to quantify the activities from ^{40}K, ^{232}Th and the lower part of the ^{238}U chain (rows # 1 and 2 of the tables 5.1 and 5.2). The measured activities in the larger capacitors are roughly a factor of 2 higher than in the smaller ones, which is also the ratio between the masses of each unit. The presence of ^{182}Ta (beta emitter with $Q = 1814.3keV$, $T_{1/2} = 114.6days$, produced by neutron activation on ^{181}Ta) was identified by means of several of its gamma emissions.

In addition, a sample of capacitors from Vishay[2] (Metallized Polypropylene Film Capacitors, $5\mu F$, $32x11x21mm^3$ each unit) having the dielectric made of polypropylene was screened too. All common radioisotopes were quantified

[1] http://www.avx.com
[2] http://www.vishay.com

Figure 5.2: Left side, AVX Capacitors $1.5\mu F$. Center, AVX Capacitors $4.7\mu F$. Right side, Vishay Capacitors

with activities of a few $mBq/unit$ (row # 3 of the tables 5.1 and 5.2), which are unacceptable for NEXT, and consequently the use of these polypropylene capacitors was disregarded.

The **Resistors** of the base, necessary to divide the high voltage in different stages, are Surface Mount Device (SMD). Several samples from some suppliers have been screened in order to obtain the most radiopure possible units.

First of them was SM2 resistors, supplied by the Japanese company Finechem[3] have an alumina ceramic substrate. The dimensions of each unit are $3.2x1.6x0.55mm3$. Activities have been derived for ^{40}K as well as for the ^{232}Th and ^{238}U chains (row # 4 of the tables 5.1 and 5.2). In addition, the resistors showed important activities from ^{134}Cs and ^{137}Cs isotopes, which could be related to the Fukushima accident. For ^{134}Cs (beta emitter with $Q = 2058.98keV$, $T_{1/2} = 2.06y$), activity was $32.7 \pm 1.6\mu Bq/unit$. The obtained results can be compared with the ones for SM5D Finechem resistors, showing no Cs activity, presented at [20, 30]; results are roughly consistent taking into account that the volume of SM5 resistors is four times the one of SM2 resistors.

Other sample consisted of resistors produced by KOA Speer [4] and supplied by RS (Thin Film 1206, 62Ω). Dimensions of each unit are $3.2x1.6x0.6mm^3$. No one of the common radioisotopes has been quantified and upper limits to their activities have been set (row #5 of tables 5.1 and 5.2).

[3] http://www.jfine.co.jp
[4] http://www.koaspeer.com

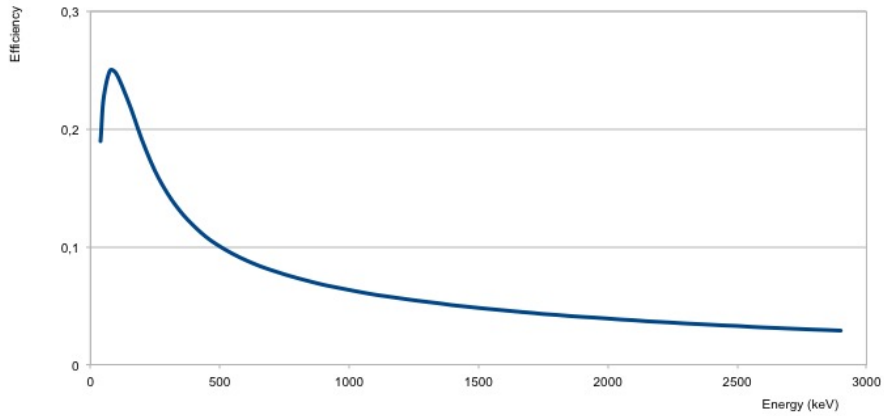

Figure 5.3: Results of the MC simulation of the detection efficiency with GeLatuca detector for Finechem resistors sample. This small sample with very small mass and placed above the detector, achieve a very large detection efficiency

Finally, resistors from Mouser[5] (62Ω) were analyzed too. In this case, activity of some isotopes has been quantified and upper limits for the other ones have been set (row # 6 of the tables 5.1 and 5.2).

Comparing the results from the three considered resistors, it can be concluded that the quantified activities or upper limits are at similar levels of a few $\mu Bq/unit$ for all of them; finally, 14 units from Finechem and 5 from RS have been selected.

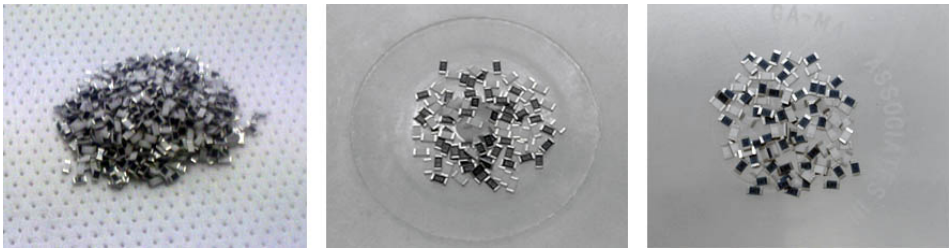

Figure 5.4: Left side, Finechem Resistors. Center, Resistors KOA RS. Right side, Resistors Mouser

[5]http://www.mouser.com

Pin receptacles from Mill Max[6] (model 0327-0-15-15-34-27-10-0) having a shell made of brass alloy 360 were screened. Activities for most of the common radioisotopes have been quantified (row #7 of the tables 5.1 and 5.2).

Figure 5.5: Left side, Pin Receptacles. Center, Thermal Epoxy. Right side, Epoxy Araldite 2011

Thermally Conductive Epoxy produced by Electrolube[7] (division of HK WENTWORTH LTD) was screened to be used at PMT bases to dissipate heat in vacuum. To prepare the sample the epoxy (EER2074A) and corresponding hardener (EER2074B) were mixed inside a clean container following specifications. A sample of the **Epoxy Araldite 2011**[8] was screened too. A mixture of Araldite2011-A (resin) and Araldite 2011-B (hardener) was prepared. As shown in rows #8-9 of the tables 5.1 and 5.2, Araldite epoxy showed a better radiopurity since only ^{40}K was quantified and upper limits for the other common radioisotopes were derived; these are more stringent than those available at [Busto et al. 2002]. Therefore, the epoxy Araldite 2011 was finally used in the PMT bases because it fulfills our heat dissipation requirements.

[6] http://www.mill-max.com
[7] http://www.electrolube.com
[8] http://www.go-araldite.com

#	Component, Supplier	Detector	Sample Size	Time
1	Capacitors 1.5μF, AVX	GeLatuca	392 units	37.8 days
2	Capacitors 4.7μF, AVX	GeAnayet	156 units	28.0 days
3	Polypropylene Capacitors, Vishay	GeAnayet	46 units	22.5 days
4	Resistors, Finechem	GeLatuca	1200 units	38.5 days
5	Resitors, KOA RS	GeTobazo	100 units	32.2 days
6	Resistors, Mouser	Obelix	100 units	54.1 days
7	Pin Receptacles, Mill Max	GeLatuca	1535 units	31.9 days
8	Thermal Epoxy, Electrolube	GeLatuca	706 g	40.4 days
9	Epoxy 2011, Araldite	GeLatuca	1712 g	29.6 days
10	Solder Paste, Multicore	GeLatuca	457 g	44.3 days
11	Kapton-Cu cable, Allectra	GeAspe	352 g	12.2 days
12	Cuflon, Polyflon	GeOroel	1876 g	24.3 days
13	Kapton Substrate, Flexible Circuit	GeAnayet	50 units	54.7 days
14	Windows, Prec. Sapphire Tech.	GeAnayet	527 g	44.9 days
15	Optical Gel, Nye Lubricants	GeAnayet	53.5 g	58.3 days
16	TPB, Sigma Aldrich	GeAnayet	4.1 g	38.3 days
17	PEDOT:PSS, Aldrich Chemistry	GeAspe	115 ml	77.1 days
18	Brazing paste	GDMS		
19	Brass bolts	GDMS		
20	SS screws	GDMS		
21	M4 screws (manual cleanning)	GeLatuca	40 units	30.3 days
22	M4 screws (Alconox cleanning)	GeLatuca	267 units	56.6 days
23	Vacuum Grease, Apiezon M	GeAspe	85.4 g	44.4 days
24	Copper CuA1, Lugand Aciers	GeAnayet	94 kg	68.6 days
25	CuA1	GDMS		
26	CuC1	GDMS		
27	CuSn braid, RS	GeAnayet	1875 g	38.2 days

Table 5.1: Description of the samples measured for the Energy Plane of NEW

#	Component	Unit	^{238}U	^{226}Ra
1	Capacitors 1.5μF AVX	$\mu Bq/unit$	< 360	72 ± 3
2	Capacitors 4.7μF AVX	$\mu Bq/unit$	< 900	123 ± 7
3	Capacitors Vishay	$mBq/unit$	10.4 ± 2.7	5.3 ± 0.3
4	Resistors Finechem	$\mu Bq/unit$	85 ± 23	4.1 ± 0.3
5	Resitors KOA RS	$\mu Bq/unit$	< 852	< 7.7
6	Resistors Mouser	$\mu Bq/unit$	< 182	< 7.0
7	Pin Receptacles	$\mu Bq/unit$	217 ± 42	< 1.1
8	Thermal Epoxy	mBq/kg	$(1.0 \pm 0.2)10^3$	169 ± 8
9	Epoxy 2011 Araldite	mBq/kg	< 182	< 1.4
10	Solder Paste	mBq/kg	< 310	< 2.7
11	Kapton-Cu cable	mBq/kg	$< 1.1 \cdot 10^3$	46.8 ± 3.3
12	Cuflon	mBq/kg	< 33	< 1.3
13	Kapton Substrate	$\mu Bq/unit$	$< 2.8 \cdot 10^3$	< 23
14	Sapphire Windows	mBq/kg	< 275	< 2.7
15	Optical Gel	mBq/kg	$< 1.7 \cdot 10^3$	< 22
16	TPB	Bq/kg	< 23	< 0.17
17	PEDOT:PSS	$\mu Bq/ml$	< 626	< 6.9
18	Brazing paste	$\mu Bq/kg$	55 ± 10	
19	Brass bolts	$\mu Bq/kg$	8.9 ± 0.7	
20	SS Screws	mBq/kg	3.25 ± 0.25	
21	M4 screws (manual cleanning)	$\mu Bq/unit$	$< 2.2 \cdot 10^3$	< 21
22	M4 screws (Alconox cleanning)	$\mu Bq/unit$	< 616	< 8.6
23	Vacuum Grease	mBq/kg	$< 1.0 \cdot 10^3$	< 10
24	CuA1	mBq/kg	< 4.1	< 0.16
25	CuA1	$\mu Bq/kg$	< 12	
26	CuC1	$\mu Bq/kg$	25 ± 5	
27	CuSn braid	mBq/kg	< 168	< 2.4

Table 5.2: Results of the samples measured for the Energy Plane of NEW

^{232}Th	^{228}Th	^{235}U	^{40}K	^{60}Co	^{137}Cs	#
49 ± 3	38 ± 2		71 ± 9	< 1	< 1	1
95 ± 7	86 ± 6		123 ± 21	< 3	< 2	2
8.5 ± 0.5	8.8 ± 0.5		5.3 ± 0.6	< 0.04	< 0.04	3
5.6 ± 0.5	4.4 ± 0.3		83.6 ± 8.7	< 0.2	104 ± 11	4
< 14	< 4.1	< 3.5	< 29	< 2.1	< 1.5	5
5.3 ± 1.5	< 8.0	3.7 ± 1.1	< 37	< 1.7	< 1.8	6
5.6 ± 0.5	4.5 ± 0.4	6.1 ± 0.5	20.5 ± 0.4	< 0.3	< 0.2	7
52 ± 4	54.4 ± 3.2		105 ± 12	< 1.1	< 1.3	8
< 3.7	< 2.5	< 0.8	15.0 ± 2.4	< 0.4	< 0.4	9
< 4.7	< 2.5	< 5.2	< 13	< 1.0	< 1.6	10
< 40	< 32		166 ± 27	< 5.2	< 4.4	11
< 1.1	< 1.1	< 0.6	4.8 ± 1.1	< 0.3	< 0.3	12
77 ± 13	43.9 ± 7.2	< 18	< 216	< 6.4	< 6.7	13
< 7.6	< 5.5	< 2.1	< 18	0.7	< 1.0	14
< 49	< 18	< 16	< 173	< 4.5	< 5.8	15
< 0.57	< 0.15	< 0.11	< 1.7	< 0.05	< 0.05	16
< 23	< 4.8	< 3.9	49 ± 11	< 1.7	< 1.8	17
49 ± 4			< 31			18
6.9 ± 0.2			< 31			19
0.57 ± 0.08			< 0.19			20
< 60	20.0 ± 4.6	< 12	< 93	14.0 ± 1.8	< 6.0	21
14.9 ± 3.4	17.4 ± 1.8	3.7 ± 1.0	< 19	13.4 ± 1.1	< 1.4	22
< 43	< 8.5	< 6.1	< 49	< 3.5	< 2.9	23
< 0.15	< 0.13	< 0.17	< 0.37	0.04 ± 0.01	< 0.04	24
< 4.1			62			25
15 ± 4			190			26
< 7.1	< 2.1	< 1.8	< 14	< 0.6	< 0.5	27

Figure 5.6: Left side, Solder Paste. Center, Kapton-Copper Cable. Right side, Cuflon

A sample of **lead-free SnAgCu solder paste** supplied by Multicore (ref. 698840) was screened and results are presented in row # 10 of the tables reftab:5-EP-1 and 5.2. $^{108*}Ag$, induced by neutron interactions and having a half-life of $T_{1/2} = 438y$, has been identified in the paste, with an activity of $(5.26 \pm 0.40)mBq/kg$, while upper limits of a few mBq/kg have been set for the common radioactive isotopes.

A roll of the **kapton-copper cable** supplied by Allectra company[9] was screened. Activities of some isotopes were quantified (row # 11 of the tables 5.1 and 5.2) and in addition, presence of $^{108*}Ag$ (decaying by electron capture with a half-life of $418y$) can be reported through the identification of its most intense gamma lines.

Concerning the **base substrate**, cuflon and kapton have been considered. Cuflon© offers low activity levels, as shown in the measurement of samples from Crane Polyflon[10] by GERDA [D. Budjas et al. 2009] and at [Nisi et al. 2009], using both ICPMS and Ge gamma spectroscopy. As presented in [Alvarez et al. 2013], a measurement of Polyflon cuflon made of a 3.18-mm-thick PTFE layer sandwiched by two $35-\mu$m-thick copper sheets was made for NEXT and results are shown in row #12 of the tables 5.1 and 5.2. Only activity of ^{40}K could be quantified. Although cuflon could have been used too, kapton was finally selected and a sample of the produced 0.5-mm-thick base substrates by Flexible Circuit[11] was screened. Upper limits were set for all common radioisotopes except for ^{232}Th (row # 13 of the tables 5.1 and 5.2).

[9] http://www.allectra.com
[10] http://www.polyflon.com
[11] http://www.flexiblecircuit.com

5.2.2 Windows, PMT enclosures and other components

Other components also used in the energy readout plane have been taken into consideration. Four **Sapphire Crystals** to be used as PMT windows were screened; each crystal is 6 mm high and has a diameter of 83.8 mm. They were measured on a teflon support for protection. No isotope was quantified (row # 14 of the tables 5.1 and 5.2). Since the upper limits obtained from germanium spectrometry are quite high, results from Neutron Activation Analysis (NAA) presented at measurement # 155 in [Leonard et al. 2008] by EXO collaboration have been considered for the moment in the development of the NEXT-100 background model.

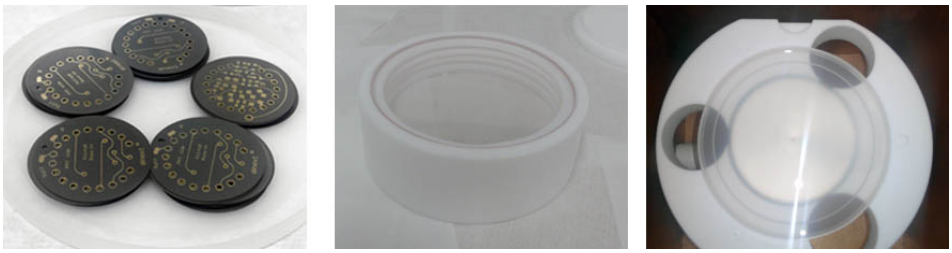

Figure 5.7: Left side, Kapton Substrate. Center, Sapphire Crystals placed in a Teflon support. Right side, Optical Gel

The **Silicone-based Optical Gel** from Nye Lubricants Inc.[12] (SmartGel NyoGel OCK-451), used for PMTs coupling, was screened. Optical fluid and thickening agent were mixed at the clean room of LSC and left there for 26 hours in order to get a solid disk. The sample was prepared on a clean container. No isotope was quantified and upper limits were set for all of them (row # 15 of the tables 5.1 and 5.2). The quantity to be used per window is estimated to be about 2 g.

A sample of the **TPB** material coating the enclosure windows, supplied by Sigma Aldrich[13], was analyzed. The powder was prepared inside a clean Petri dish. Upper limits on the specific activity were set for all the radiosotopes (row # 16 of the tables 5.1 and 5.2). Due to the small mass of our sample, better results for this material from the same supplier can be found at [Lawson and Cleveland

[12] http://www.nyelubricants.com
[13] http://www.sigmaaldrich.com

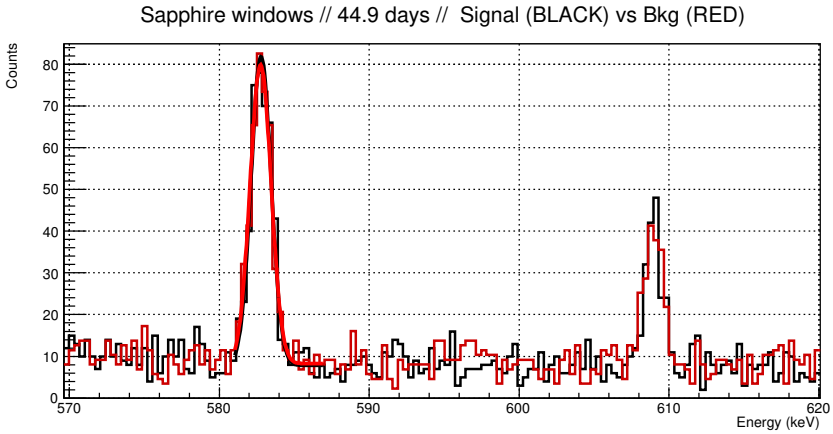

Figure 5.8: Spectrum of the Sapphire windows in the region of interest of the 208Tl and 214Bi. We can observe that both fits in 583 keV are overlapping and the only result that we can obtain is an upper limit for this value

2011] and [Vacri et al. 2015]; activities for ^{238}U and ^{232}Th at the level of tenths of mBq/kg or even lower are reported there.

A sample of **PEDOT:PSS** (1.3 wt% dispersion in water) also from Aldrich Chemistry to be used as conductive coating on sapphire windows was screened too (row # 17 of the tables 5.1 and 5.2); only activity of ^{40}K could be quantified. It is applied by spin-coating and then dried to evaporate water, resulting in a $\sim$100-nm-thick layer.

Other materials or components to be used at the PMT enclosures were analyzed by GDMS, made by Shiva Technologies (Evans Analytical Group[14]) in France. A sample of **Brazing Paste** made of 72% Ag and 28% Cu with dimensions $12x12x12mm^3$ was measured quantifying the U and Th content (row # 18 of the tables 5.1 and 5.2). **M4 vented screws** made of 316 stainless steel were screened; the mass of each 2-cm-long unit is 2.32 g. A sample of a **M4 bolt made of brass**, with length 22.65 mm and mass 3.08 g, was also analyzed. Following results at rows # 19-20 of the tables 5.1 and 5.2, and since 28 units are needed per PMT can, brass bolts were preferred instead of the vented screws from the

[14]http://www.eaglabs.com

radiopurity point of view. However, in principle, stainless steel have been used for mechanical reasons in the NEW set-up.

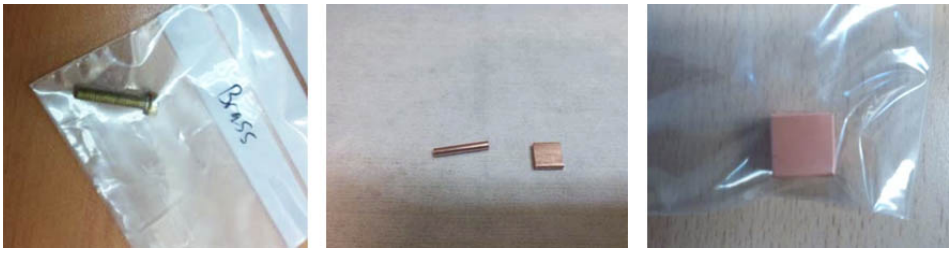

Figure 5.9: Left side, Brass Bolt for GDMS. Center, CuA1 sample for GDMS. Right side, CuC1 sample for GDMS

Samples of **M4 screws** were screened using germanium detectors. Since these screws were pre-greased, a cleaning procedure was necessary to remove the grease, which could affect the purity of the xenon gas and is expected to be non-radiopure; two options were analyzed. A manual cleaning was applied to a sample, by wiping the screws several times with alcohol by hand, cleaning them in ultrasounds bath with soap and afterwards rinsing with alcohol. For another sample of screws, cleaning was made using Alconox[15] detergent 8 (5% solution in water) in ultrasound bath. Activities from ^{60}Co, ^{235}U and for the ^{232}Th chain have been quantified (rows # 21-22 of the tables 5.1 and 5.2). Results obtained for the two samples with different cleaning procedures are compatible; upper limits derived for sample cleaned using Alconox are more stringent thanks to the larger number of screened units. Once removed the original grease of the screws, **Vacuum Grease** must be used; a sample of Apiezon[16] M grease designed for high vacuum applications was analyzed and only upper limits were set (rows # 25 of the tables 5.1 and 5.2). Due to the very relevant contribution of these M4 screws (quoted for reference in table 4) the use of the much more radiopure brass bolts is foreseen in the NEXT-100 detector.

[15] http://alconox.com
[16] http://www.apiezon.com

Figure 5.10: Left side, TPB. Center, PEDOT:PSS. Right side, M4 Screws

Two types of **Copper** supplied by Lugand Aciers company[17] were screened for use at the energy plane: CuA1[18] for PMT enclosures and base caps and CuC1[19] for both the tracking and energy readout plates. The weight of each PMT copper enclosure is 4.1 kg and that of the energy plate 475.6 kg. A large mass of CuA1 copper was accumulated to carry out a measurement using a germanium detector at LSC; a special cleaning procedure typically used for copper shielding was performed at LSC before the measurement, consisting of soap cleaning, nitric acid etching, passivation with citric acid and drying.

As shown in row # 24 of the tables 5.1 and 5.2, only ^{60}Co activity was quantified. Peaks from other cobalt isotopes also common cosmogenic products in copper induced by the exposure of the material to cosmic nucleons at sea level were identified (^{56}Co with $T_{1/2} = 77.27d$ and ^{58}Co with $T_{1/2} = 70.86d$); since their half-lives are of the order of the live time in the screening measurement, the direct quantification of their activities was not performed. GDMS analysis was additionally made for two samples, with dimensions $12x12x12mm^3$, made of CuA1 and CuC1 copper, having received the same cleaning protocol. Following results presented in rows # 25-26 of the tables 5.1 and 5.2, GDMS upper limits for CuA1 sample are much lower than the ones derived from germanium spectrometry in # 24. The good results obtained for this copper advised to use it also for the shielding against gamma radiation to be placed inside the pressure copper vessel made of 316Ti stainless steel. Results for CuA1 from Lugand

[17] http://lugand-aciers.fr

[18] This type of copper is also referred as Cu-ETP (Electrolytic Tough Pitch) or C11000. Its copper purity is 99.90% (minimum).

[19] This type of copper is also referred as Cu-OF (Oxygen-Free) or C10200. Its copper purity is 99.95%.

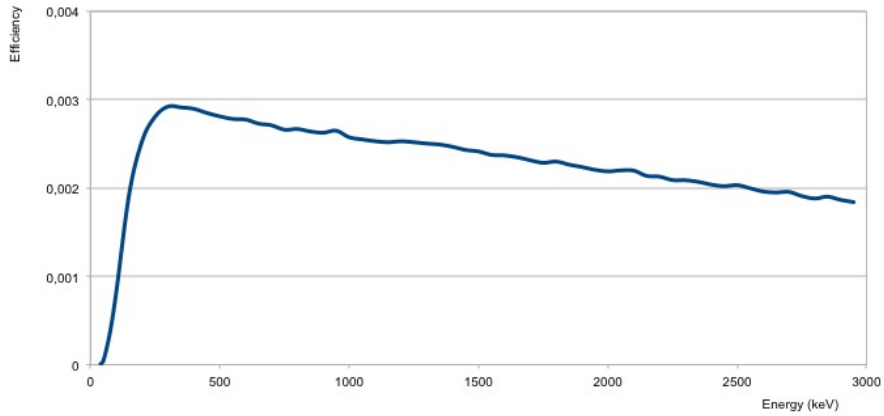

Figure 5.11: Results of the MC simulation of the detection efficiency with GeOroel detector for CuA1 sample. This large sample of 98kg, has a very low efficiency because of the strong shielding capacity of the copper

Aciers, at the level of a few $\mu Bq/kg$ for ^{238}U and ^{232}Th, are equivalent to those obtained for C10100 copper supplied by the Luvata company [Alvarez et al. 2013] and similar to those for the Norddeutsche Affinerie[20] copper [Laubenstein et al. 2004]. Results at or even below tenths of $\mu Bq/kg$ have been presented for electroformed and also commercial copper analyzed by ICPMS for the Majorana experiment [LaFerriere et al. 2015] [Abgrall et al. 2016].

A sample of the **CuSn braid** used to dissipate heat at the PMT cans was measured using a germanium detector. It is soft tinned copper wire braid 2536P provided by RS. The total length of the sample was 19.4 m. Upper limits were set for all the common radioisotopes (row # 27 of the tables 5.1 and 5.2).

Finally, the expected contribution to the background level in the region of interest of NEXT- 100, assuming a NEW-like design having 60 PMT modules, from the activities of all the relevant components of the energy plane has been evaluated by Monte Carlo simulation (see details at [J. Martín-Albo et al. 2016]) and is reported in table 4.REVISAR

[20] Re-branded as Aurubis, http://www.aurubis.com

Figure 5.12: Left side, Vacumm Grease. Center, part of the CuA1 sample for HPGe. Right side, CuSn Braid

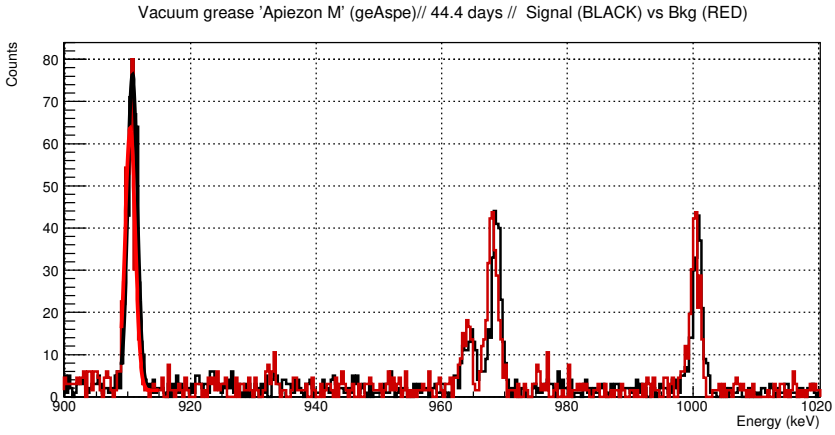

Figure 5.13: Spectrum of the Vacuum Grease in the region of interest of the 228Ac and 234*Pa. We can observe that both fits in 911 keV are overlapping and the only result that we can obtain is an upper limit for this value

5.2.3 PMTs: PMT campaign

The photomultiplier tubes are the basic element of the energy readout plane of NEXT. The 55 available units of the selected model, Hamamatsu[21] R11410-10, to be used at NEW and NEXT-100 detectors have been screened. The number of required PMTs is 12 for NEW and 60 for NEXT-100.

When the campaign started, no information about the radiopurity of these PMTs was published. The first condition for the experiment was to define like bad PMT those with a radioactivity $> 10 mBq/unit$ and to define like

[21] http://www.hamamatsu.com

dangerous PMTs those with a radioactivity $> 5mBq/unit$. Bad PMTs are unacceptable for our requirements and the number of dangerous PMTs must be controlled. Additionally, all the PMTs should be measured, because of the manual production process of these photosensors.

Figure 5.14: Left side, horizontal configuration of the PMTs, with the unit above the detector. Right side, 3 PMTs configuration, with them around the detector.

Two position configuration was chosen for this measurements (see figure 5.14): first was a PMT alone, horizontal and above the detector. Second was 3 vertical PMTs around the detector. For both cases, was designed and builded a teflon support to hold the PMTs. For the background runs of the detectors, this support was still inside the shielding, giving a small contribution of ^{40}K to the background. The simulation of the efficiency, done with Geant 4.9.5 and shown in the figure 5.15, concluded that the efficiency is better with horizontal mode. But, using the 3PMTs configuration the efficiency is slightly worst but enough for our requirements and, also, we need less time to finish this campaign.

The detector chosen for this campaign was GeAnayet because it is a detector with a very low level of background and because it was a detector that was available for carry out these measurements during two years. GeAnayet was used for this campaign at LSC along 2013, 2014 and 2015.

The final decision was to measure 3 PMTs simultaneously, a good compromise between time of the measurement and capability to detect radioactive PMTs. A first estimation of the upper limits (in case of non-detectable activity) was made for GeAnayet. This estimation, dependent of the background of the detector, the efficiency of the configuration and the duration of the measurement.

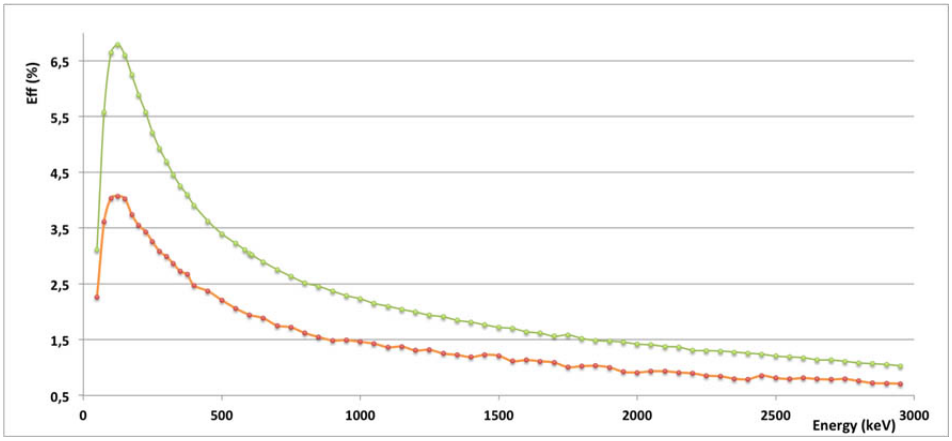

Figure 5.15: In green, the MC efficiency with the horizontal configuration. In orange, with the 3PMTs configuration

According to figure 5.16, two weeks enough time to detect a PMT too dirty for our requirements.

In the case of a very dirty PMT, a second measurement can be done to find out it

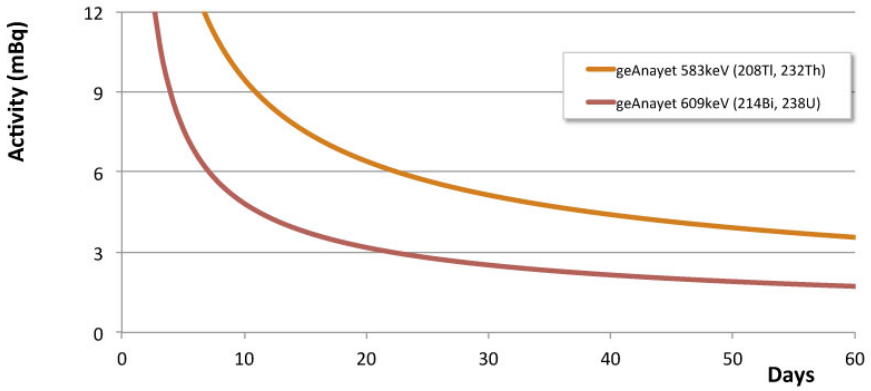

Figure 5.16: Time evolution for the two most dangerous radiosotopes for our experiment.

First, a single photomultiplier was analyzed (row # 1 of of table 5.3) and then eighteen runs of measurements with three units altogether placed around the detector on a teflon support were carried out; data taking at each run ranged

from 18.3 to 41.0 days per run and several reference backgrounds were measured in between. For the detection efficiency simulation, emissions are assumed to be uniformly generated in the kovar PMT enclosure.

Figure 5.17: Montecarlo simulation of PMTs

Activities for the three PMTs at each independent measurement were deduced and are summarized in table 3. The results obtained from different runs are roughly compatible; ^{60}Co activity has been always quantified, those of ^{40}K and ^{54}Mn only in the most sensitive runs while upper limits have been obtained in general for all the other common isotopes, more or less stringent according to the different sensitivity of each measurement.

Run	Serial numbers	Start	Duration	^{228}Ac	^{228}Th
PMT-hor1	KA 0126	24-01-2013	33.7 days	<5.4	<3.4
PMT01	KA 0029, KA 0036, KA 0134	04-03-2013	30.6 days	<7.8	<6.1
PMT02	KA 0086, KA 0093, KA 0064	09-04-2013	20.2 days	<9.1	<7.9
PMT03	KA 0065, KA 0087, KA 0074	02-05-2013	22.0 days	<10	<7.3
PMT04	KA 0104, KA 0123, KA 0078	30-05-2013	18.3 days	<9.5	<9.6
PMT05	KA 0085, KA 0094, KA 0050	19-06-2013	41.0 days	<6.6	<7.2
PMT06	KA 0076, KA 0059, KA 0057	01-08-2013	39.8 days	<9.3	<6.2
PMT07	KA 0075, KA 0119, K A0055	31-10-2013	23.0 days	<9.1	<6.5
PMT08	KA 0122, KA 0124, KA 0131	26-11-2013	38.7 days	<9.3	<5.9
PMT09	KA 0100, KA 0097, KA 0088	07-01-2014	19.5 days	<9.2	<10
PMT10	KA 0090, KA 0095, KA 0058	28-01-2014	27.8 days	<9.4	<6.3
PMT11	KA 0073, KA 0099, KA 0107	10-04-2013	30.4 days	<11	< 6.8
PMT12	KA 0106, KA 0136, KA 0077	12-05-2014	33.5 days	<6.9	<6.5
PMT13	KA 0080, KA 0098, KA 0083	17-06-2014	23.6 days	<8.3	<8.7
PMT14	KA 0011, KA 0092, KA 0084	14-07-2014	38.6 days	<8.9	<6.9
PMT15	KA 0082, KA 0081, KA 0089	10-09-2014	24.2 days	<8.6	<6.2
PMT15-2	KA 0082, KA 0081, KA 0089	20-05-2015	25.3 days	<11	<8.5
PMT16	KA 0103, KA 0125, KA 0110	07-10-2014	24.1 days	<11	<7.9
PMT17	KA 0079, KA 0102, KA 0120	05-03-2015	19.3 days	<10	<8.6
PMT18	KA 0054, KA 0109, KA 0101	27-03-2015	23.6 days	<8.8	<9.0

Table 5.3: Results of the PMT Campaign, carried out during two years. Results are presented in mBq/sample and each sample consist of 3 PMTs

^{238}U	^{226}Ra	^{235}U	^{40}K	^{60}Co	^{137}Cs	^{54}Mn	Run
<187	<1.8	<1.6	<29	2.8 ± 0.3	<0.6		PMT-hor1
<266	<2.7	<3.4	30.4 ± 8.1	12.2 ± 1.0	<1.0	1.1 ± 0.3	PMT01
<340	<3.3	<3.4	<60	11.1 ± 0.9	<1.3	<1.7	PMT02
<320	<3.3	<4.4	39.5 ± 9.4	10.4 ± 0.9	<1.2	<1.3	PMT03
<351	<4.3	<3.8	41 ± 10	11.5 ± 1.0	<1.4	1.1 ± 0.3	PMT04
<229	<2.5	<3.1	32.3 ± 7.7	10.8 ± 0.8	<0.8	1.1 ± 0.2	PMT05
<232	<2.7	<3.1	30.0 ± 7.5	10.4 ± 0.8	<0.8	1.0 ± 0.3	PMT06
<317	<4.3	<2.6	34.2 ± 8.9	10.9 ± 0.9	<1.1	<1.4	PMT07
<234	<3.0	<3.2	35.5 ± 7.9	12.3 ± 1.0	<0.8	<1.2	PMT08
<330	<3.4	<4.3	34.8 ± 9.5	11.3 ± 0.9	<1.2	<1.8	PMT09
<293	<3.9	<4.4	36.9 ± 8.6	12.0 ± 0.9	<1.0	<1.4	PMT10
<286	2.7 ± 0.8	<2.2	38.0 ± 8.7	11.1 ± 0.9	<1.3	<1.4	PMT11
<405	<3.2	<3.8	28.3 ± 7.9	11.0 ± 0.9	<0.8	0.9 ± 0.3	PMT12
<361	<5.2	2.5 ± 0.7	50 ± 10	11.4 ± 0.9	<1.1	1.2 ± 0.3	PMT13
<337	<3.7	<3.0	30.7 ± 7.8	11.7 ± 0.9	<0.8	0.9 ± 0.2	PMT14
<470	3.0 ± 0.9	<4.3	34.5 ± 9.0	10.3 ± 0.8	<1.2	<1.4	PMT15
<341	<3.4	<2.7	42.5 ± 9.1	9.9 ± 0.8	<1.1	<1.1	PMT15-2
<418	<4.5	<4.1	41.6 ± 9.4	12.2 ± 1.0	<1.1	0.8 ± 0.2	PMT16
<443	<4.9	<3.5	<61	12.1 ± 1.0	<1.2	<1.7	PMT17
<448	<5.6	<2.6	45.3 ± 9.3	12.5 ± 1.0	<1.0	<1.1	PMT18

After the analysis of 3PMT15, we observed a unexpected excess of ^{214}Bi that was supposed to be from radon intrusion. This measurement was repeated at the end of the campaign with normal values.

Since, following these results, it seemed that the activity levels of all the screened PMTs was similar, a joint analysis of the available data was done to increase the sensitivity. The idea is to combine the information of the eighteen independent runs performed with three PMTs, assuming that we have repeat the same measure 18 times. This result has been obtained following the criteria for large background, presented in Chapter 4.

Isotope	Activity (mBq/unit)
^{228}Ac	< 0.66
^{228}Th	0.50 ± 0.31
^{238}U	< 32
^{226}Ra	0.36 ± 0.15
^{40}K	11.46 ± 1.86
^{60}Co	3.70 ± 0.06
^{137}Cs	
^{54}Mn	0.27 ± 0.03

Table 5.4: Results of the global fit with all the data of the PMT Campaign

The obtained results are shown in the table 5.4 and may be interpreted as an statistical analysis of the activity of the PMTs. Since it was assumed that all the PMTs were equivalent, activity values per PMT were estimated just considering one third of the net signal measured; these results are shown in table 5.3. In this joint analysis, activity of 235U has been properly evaluated; although there is also a clear net signal from ^{54}Mn, since its half-life (312.3 days) is comparable to the time span of the measurements, a direct quantification of the activity has not been performed. Concerning the lower parts of the ^{232}Th and ^{238}U chains, several lines show an excess of events above background statistically significant thanks to the accumulation of data; therefore, it has been possible to quantify

the activity of some of their isotopes and a quite safe estimate of the average activity per PMT of ^{226}Ra and ^{228}Th has been achieved.

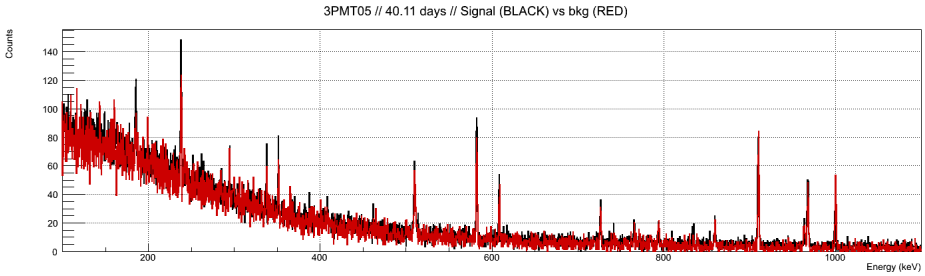

Figure 5.18: First part of the Spectrum of 3PMT5. It can be observe that that, in this part of the spectrum, the number of counts measured is similar.

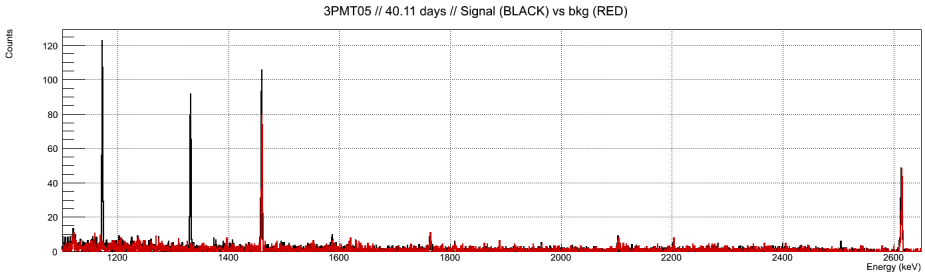

Figure 5.19: First part of the Spectrum of 3PMT5. In this case, we can observe 1173 keV and 1333 keV peaks, corresponding to 60Co.

The same model of PMT has been screened for other experiments too [Aprile et al. 2011], [D. S. Akerib et al. 2013], [Wang et al. 2016] and our results are in very good agreement with those found by XENON; in particular, ^{60}CO and ^{40}K activities are virtually the same. The XENON1t collaboration has carried out a deep study of the radioactivity of the new PMT version Hamamatsu R11410-21 [Barrow et al. 2016], based on the analysis by GDMS and germanium spectrometry of individual components and units [Aprile et al. 2015]. The main differences with respect to the version R11410-10 are the use of Co-free kovar body and high purity (instead of standard purity) Al seal. Comparing results for the two versions, it can be concluded that ^{40}K and ^{235}U activities are compatible, ^{60}Co has been reduced about a factor 5 in the new version and for the lower parts of the natural chains of ^{232}Th and ^{238}U, activity is at the same level, about

a half mBq/PMT. Results for the version R11410-20 have been presented by LUX-ZEPLIN collaboration [D. S. Akerib et al. 2015].

5.3 Tracking plane

In the other side of the detector, we will find the Tracking Plane, designed to precisely observe the track of the measured events. In terms of radiopurity, the most complicated part are SiPMs, because they are very small, but we will use thousands of them. Then we have to know very precisely the specific activity this component.

Almost all the information of this section can be found in *Radiopurity assessment of the tracking readout for the NEXT double beta decay experiment*, [Cebrián et al. 2015]

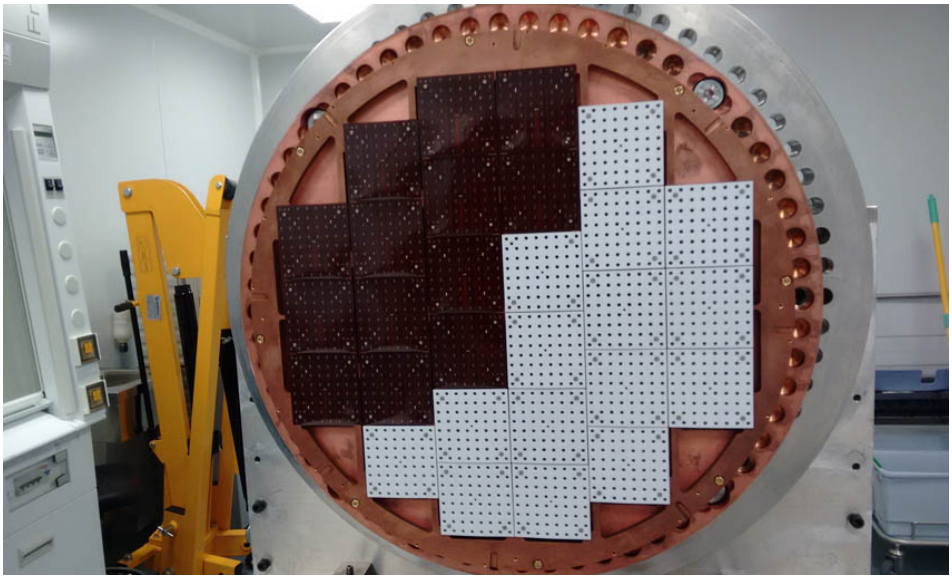

Figure 5.20: Tracking plane with some teflon masks covering the DICE-Boards

5.3.1 Printed Circuit Boards and cables

Printed Circuit Boards (PCBs) are commonly made of different materials and a large number of radiopurity measurements can be found in ILIAS database[22]. Therefore, several options have been taken into consideration for the substrate of SiPMs arrays. FR4 was disregarded because of both an unacceptable high rate of outgassing and bad radiopurity; glass fiber-reinforced materials at base plates of circuit boards are generally recognized as a source of radioactive contamination Heusser 1995.

Cuflon© offers low activity levels, as shown in the measurement of samples from Crane Polyflon[23] by GERDA [D. Budjas et al. 2009] and at [Nisi et al. 2009], using both ICPMS and HPGe gamma spectroscopy. As presented in [Alvarez et al. 2013], a measurement of Polyflon cuflon made of a 3.18-mm-thick PTFE layer sandwiched by two 35-μm-thick copper sheets was made for NEXT and results are shown in row #12 of the tables 5.1 and 5.2.

Adhesive films to glue cuflon sheets are used to prepare multilayer PCBs; a sample of bonding films made of a polyolefin co-polymer and supplied also by Crane Polyflon were screened and results are presented in row # 1 of the tables 5.5 and 5.6. Four cuflon DB produced by Pyrecap company using these Polyflon materials were screened.

Each DB, with a surface of $79x79mm^2$ and a mass of 35 g, was made of three cuflon sheets glued with two bonding films; results are shown in row # 2 of the tables 5.5 and 5.6, being fully consistent with the individual measurements of components. Total activity from each cuflon DB was too high for NEXT requirements, since they could produce a background of $2.1x10^{-4} counts keV^{-1} kg^{-1} y^{-1}$ in the region of interest; consequently, other option was searched for.

Components made of just kapton (like cirlex) and copper offer very good radiopurity, as shown in the measurement of kapton-copper foils in [Aznar et al. 2013] and [Cebrian et al. 2011]. Therefore, new DB produced by Flexible-circuit

[22] http://radiopurity.in2p3.fr
[23] http://www.polyflon.com

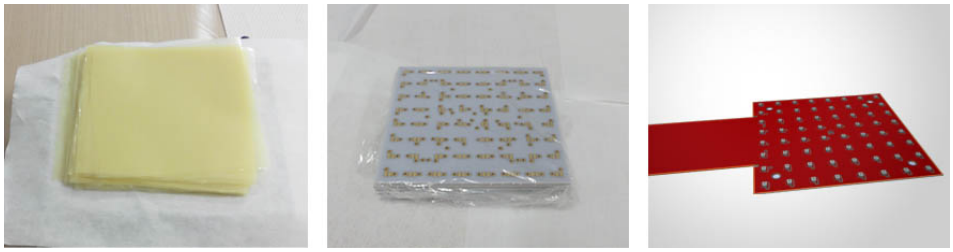

Figure 5.21: Left side, Bolding Film. Center, Cuflon DBs. Right side, Kapton-Cu DBs

using only kapton, metallized copper and adhesive were analyzed. A two layer adhesiveless base substrate with plyimide coverlay on both sides, wich only requires a little amount of adhesive, was chosen for the boards manufacturing. As shown in figure 3, each DB consists of a square part with 8 cm side, where SiPMs are fixed; and with a long flexible tail which allows to locate connectors behind the inner copper shielding ICS. The mass of each kapton DB is 16.7 g. A total of 12 units, together with residual pieces from production to increase the mass sample, were screened.

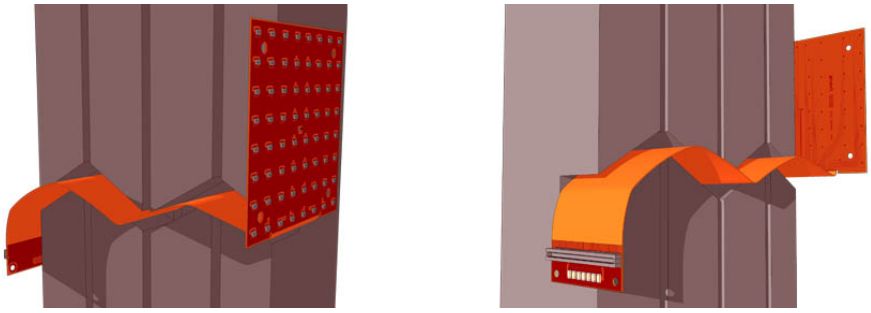

Figure 5.22: View of the Kapton-Cu DBs placed in the detector. Inner Copper Shielding will partially shield the tail of the DBs

Results normalized to the DB part actually exposed to the detector are presented in # 3 of the tables 5.5 and 5.6. Although a higher content of ^{40}K (of relevance for the study of the double beta decay mode with neutrinos) has been observed. Activities for the isotopes in the lower parts of ^{238}U and ^{232}Th chains are almost one order of magnitude lower than cuflon DB. As shown in table 4, the quantified activity of ^{208}Tl and ^{214}Bi gives a rate of $2.8x10^{-5} counts keV^{-1} kg^{-1} y^{-1}$

and consequently Kapton-DBs have been chosen as the final option for the tracking readout substrate.

5.3.2 Connectors

Information on the radiopurity of different types of connectors is available at ILIAS database, [Arpesella et al. 2002], [Lawson and Cleveland 2011]. Different kinds of board-to-cable connectors were measured [Alvarez et al. 2013] and results are reported in rows # 4-6 of the tables 5.5 and 5.6. In particular, FFC/FCP (Flexible Printed Circuit & Flexible Flat Cable) connectors supplied by Hirose[24] and similar P5K connectors from Panasonic[25] were considered, finding activities of at least a few mBq/pc for isotopes in ^{232}Th and the lower part of ^{238}U chains and for ^{40}K. Thermoplastic connectors 503066-8011 from Molex[26] were also screened, giving values slightly smaller but of the same order.

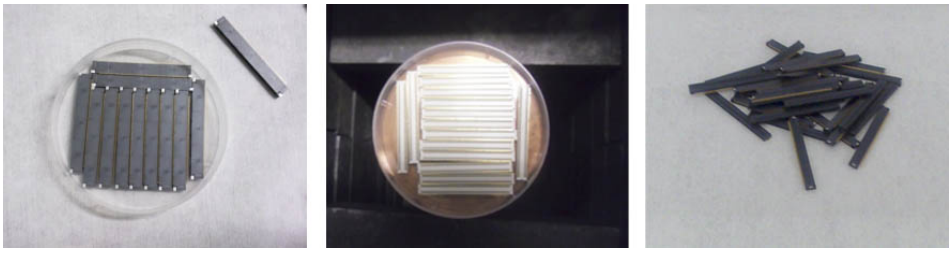

Figure 5.23: Left side, FFC Connectors. Center, P5K Connectors. Right side, Thermoplastic Connectors

Since all these connectors contain Liquid Crystal Polymer (LCP), it seems that the activity measured is related to this material. As the activity of connectors would give an unacceptable high rate in the region of interest (see table 4 REVISAR for the Hirose connectors), a direct bonding of the cables to the cuflon DBs was originally foreseen; however, in the final design using the all-in-one kapton DBs, connectors are easily placed behind the inner copper shield.

[24] http://www.hirose.com
[25] http://www.panasonic-electric-works.com
[26] http://www.molex.com

5.3.3 Soldering materials

Different materials intended to be used to solder electronic components on boards have been analyzed [Alvarez et al. 2013]. A sample of lead-free **SnAgCu Solder Paste** supplied by Multicore (Ref. 698840) was screened and results are presented in row # 10 of the tables 5.1 and 5.2. As we commented in the previous section, $^{108*}Ag$, induced by neutron interactions and having a half-life of $T_{1/2} = 438y$, has been identified in the paste, with an activity of $(5.26 \pm 0.40) mBq/kg$, while upper limits of a few mBq/kg have been set for the common radioactive isotopes. Consequently, some tens of grams of the solder paste could be used without concern.

Solder Wire with similar composition from Multicore (Ref. 442578) was also screened (see row #7 of the tables 5.5 and 5.6), finding in this case a high activity of the lower part of the ^{238}U chain. An activity of ^{210}Pb of $(1.2 \pm 0.4) x10^3 Bq/kg$ was deduced using the bremsstrahlung emission from its daughter nuclide ^{210}Bi [Nachab and Hubert 2012].

Figure 5.24: Left side, Solder Wire. Center, Silver Epoxy. Right side, NTC Sensors

A sample of Circuit Works **Conductive Epoxy CW2400** mainly made of silver was measured. It was prepared at LSC just before screening by mixing epoxy and hardener following specifications. Results are presented in row # 8 of the tables 5.5 and 5.6. Activity of $^{108*}Ag$ has been measured in this sample too at a level of $(24.6 \pm 1.6) mBq/kg$. Even though the use of this type of silver epoxies was finally disregarded for electronic boards, it could be used for the field cage components.

#	Component, Supplier	Detector	Sample Size	Time
1	Bonding Film, Polyflon	GeAnayet	288 g	30.8 days
2	Cuflon DBs, Pyrecap	GeOroel	140 g	45.1 days
3	Kapton-Cu DBs, Flexiblecircuits	GeOroel	647 g	26.6 days
4	FFC Connectors, Hirose	Paquito	19 units	6.8 days
5	P5K Connectors, Panasonic	Paquito	15 units	7.6 days
6	Thermopl. Connect., Molex	GeLatuca	29 units	17.2 days
7	Solder Wire, Multicore	Paquito	91 g	7.7 days
8	Silver Epoxy, Multicore	GeLatuca	125 g	55.1 days
9	SiPMs 1x1 mm, SensL	GeAspe	102 units	41.4 days
10	SiPMs 6x6 mm, SensL	GeAspe	99 units	59.6 days
11	SiPMs TSV 3x3 mm, SensL	Obelix	20 units	38.2 days
12	SiPMs 1x1 mm, Hamamatsu	GeTobazo	53 units	30.45 days
13	NTC sensors, Murata	GeLatuca	1000 units	28.3 days
14	LED, Osram	GeLatuca	989 units	32.4 days
15	Plexiglas (PMMA), Evonik	GeLatuca	1669 g	48.9 days
16	Ta Capacitors, Vishay Sprague	GeAnayet	227 units	20.0 days

Table 5.5: Description of the samples measured for the Tracking Plane of NEW

#	Component	Unit	^{238}U	^{226}Ra
1	Bonding Film	mBq/kg	1140 ± 300	487 ± 23
2	Cuflon DBs	$mBq/unit$	< 7.6	0.28 ± 0.08
3	Kapton-Cu DBs	$mBq/unit$	< 1.3	0.031 ± 0.004
4	FFC Connectors	$mBq/unit$	< 50	4.6 ± 0.7
5	P5K Connectors	$mBq/unit$	< 42	6.0 ± 0.9
6	Thermopl. Connect.	$mBq/unit$	< 7.3	1.77 ± 0.08
7	Solder Wire	mBq/kg	< 4900	$(7.7 \pm 1.2) \cdot 10^2$
8	Silver Epoxy	mBq/kg	$< 1.0 \cdot 10^3$	13.6 ± 2.8
9	SiPMs SensL 1x1 mm	$\mu Bq/unit$	< 320	< 2.7
10	SiPMs SensL 6x6 mm	$\mu Bq/unit$	< 410	< 3.2
11	SiPMs TSV 3x3 mm	$\mu Bq/unit$	< 400	< 21
12	SiPMs Hamamatsu 1x1 mm	$\mu Bq/unit$	< 1300	33 ± 3
13	NTC sensors	$\mu Bq/unit$	< 96	< 0.8
14	LED	$\mu Bq/unit$	< 90	1.4 ± 0.2
15	Plexiglas (PMMA)	mBq/kg	< 208	< 1.3
16	Ta Capacitors	$mBq/unit$	< 0.8	0.043 ± 0.004

Table 5.6: Results of the samples measured for the Tracking Plane of NEW

^{232}Th	^{228}Th	^{235}U	^{40}K	^{60}Co	^{137}Cs	#
79.8 ± 6.6	66.0 ± 4.8		832 ± 87	< 4.4	< 3.8	1
< 0.28	< 0.16	< 0.13	< 1.2	< 0.07	< 0.06	2
0.027 ± 0.008	0.042 ± 0.004		12.1 ± 1.2	< 0.01	< 0.01	3
6.5 ± 1.2	6.4 ± 1.0	< 0.75	3.9 ± 1.4	< 0.2	< 0.5	4
9.5 ± 1.7	9.4 ± 1.4	< 0.95	4.1 ± 1.5	< 0.2	< 0.8	5
3.01 ± 0.19	2.82 ± 0.15	< 0.31	2.12 ± 0.25	< 0.022	0.27 ± 0.03	6
< 147	< 14		< 257	< 30	< 36	7
< 18	< 16	< 4.5	< 52	< 1.9	< 2.2	8
< 6.9	< 2.0	< 1.0	< 16	< 0.8	< 2.0	9
< 12	< 2.8	< 2.5	< 25	< 1.2	< 1.3	10
< 11	10 ± 6	< 9	1092 ± 91	3 ± 2	< 10	11
65 ± 7	46 ± 5	< 9	< 80	< 3	< 6	12
< 0.9	< 0.3	< 0.3	< 2.9	< 0.2	< 0.2	12
3.5 ± 0.4	3.0 ± 0.3	< 0.6	< 4.0	< 0.2	< 0.3	13
< 2.2	< 1.0	< 1.1	< 8.1	< 0.4	< 0.6	14
0.034 ± 0.004	0.032 ± 0.003	< 0.01		< 0.002	< 0.003	15

5.3.4 The SiPM case

Although silicon is, as germanium, a very radiopure material with typical intrinsic activities of ^{238}U and ^{232}Th at the level of few $\mu Bq/kg$ [Heusser 1995]. Very low specific activities have been recently obtained by Neutron Activation Analysis for bare devices from FBK manufacturer [Ostrovskiy et al. 2015], but materials used in the substrate or package of the chip can be radioactive.

The first sample that we evaluated were **Hamamatsu SiPMs, model S10362-11-050P/NG**. The sample consisted of 53 units with $1x1mm^2$ of active area. We did measure several radioimpurities, (as can be seen in row # 12 of the tables 5.5 and 5.6) that were estimated to be too large for the experiment. Therefore, we had to evaluate other commercial options.

Two samples of non-functional **SiPMs** from **SensL**[27], reported as MLP (Moulded Lead-frame Package) plastic SMT (Surface-Mount Technology) elements, were screened. One consisted of 102 units with an active area of $1x1mm^2$ each, and the other of 99 units with $6x6mm^2$ of active area (rows # 9 and 10 of the tables 5.5 and 5.6). In these cases, no activity was quantified for any isotope and upper limits were derived. Limits per unit are very similar for both samples, but since the production process is the same and the proportion of components scales with area, results from the large $6x6mm^2$ units allow to set limits on activities per surface much more stringent.

Another different sample of SensL was also screened. This sample consisted of 20 units of SensL SiPMs, type TSV (Through Silicon Via), with $3x3mm^2$ of active area and made of different materials. A slightly worse radiopurity was observed.

Finally, the last measurements are included in a **R&D program with Hamamatsu**. The program consist of the screening of several components to choose the most appropriate and build a radiopure SiPM. Nowadays, these units are still in prototype versions, but the results are very promising.

[27] http://sensl.com

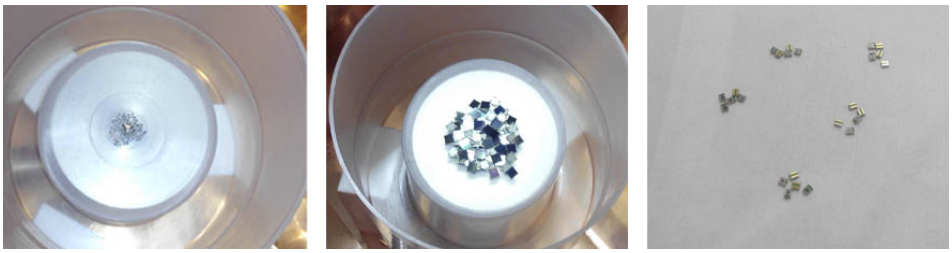

Figure 5.25: Left side, SiPMs SensL 1x1mm. Center, SiPMs SensL 6x6mm. Right side, Hamamatsu SiPMs 1x1mm

With all of this information, we finally decided to use for NEW detector the 1x1 SensL SiPMs.

5.3.5 Other components

NTC thermistors chip type from Murata Manufacturing Co. Ltd[28], to be used as temperature sensors at DB, were screened. Each unit is 1.6 mm long and 0.8 mm wide. As shown in row # 13 of the tables 5.5 and 5.6, upper limits of a few μBq/pc have been set for the common radioisotopes.

Chip **LEDs** 0603 supplied by Osram[29], with blue emission at 470 nm (LBQ39E) and made with InGaN technology, were measured. Each unit has a volume of $1.6x0.8x0.3mm^3$. Results are presented in row # 14 of the tables 5.5 and 5.6; high specific activities for 40K, 232Th and 238U chains have been quantified, despite the very small mass of the sample, which correspond to levels of a few $\mu Bq/pc$. NUMERO DE LEDS y NTC to minimize the impact on radiopurity due to this sensors.

SiPMs have high photon detection efficiency in the blue region. For this reason, they need to be coated with a wavelength shifter (TPB), to shift the UV light of the scintillation of xenon to blue, as the windows of the PMTs at the energy readout plane. Instead of directly coating the DBs, an envisaged solution was to place quartz or **PolyMethyl Methacrylate** (PMMA) thin windows coated with TPB in front of DBs. A sample made of 134 PMMA sheets ($79x79x1.5mm^3$ and a

[28] http://www.murata.com
[29] http://www.osram.com

mass of 12.46 g each one) was screened. Material is reported as Plexiglas GS/XT from Evonik Industries AG[30]. Results are shown in row # 15 of the tables 5.5 and 5.6, setting upper limits to the analyzed radioisotopes. Although these results are not bad, the final option is to use a quartz anode, having this material also an acceptable radiopurity [Leonard et al. 2008].

Figure 5.26: Left side, LEDs . Center, PMMA. Right side, Ta Capacitors

In a first design of the cuflon DBs, **Capacitors** were needed. According to ILIAS Database, Ceramic capacitors were disregarded for being radioactive. Tantalum capacitors (Vishay Sprague 597D[31]) were screened at LSC and results are presented in row # 16 of the tables 5.5 and 5.6; activity levels are lower than for other tantalum capacitors [20]. In addition to activities shown in table 3, the presence of ^{182}Ta, beta emitter with Q = 1814.3 keV and $T_{1/2} = (114.74 \pm 0.12) days$, produced by neutron activation on ^{181}Ta, was identified. In any case,in the final design of kapton-DBs no capacitor is used.

As mentioned in the previously, Section 5.2), the Copper used for this Copper Plate was the same of the Energy Plane, CuC1 from Lugand Aciers Company.

5.4 Vessel and External parts

We have talk about the two planes of the detector, but now is time to talk about the other parts of it. It is important to remark that some of these components are the most massive components of the detector. In the case of only an upper limit of the measurement, it is necessary to reduce this specific activity limit as

[30] http://www.evonik.com
[31] http://www.vishay.com

much as possible because it will be produce a large uncertainty in the activity of massive components.

The main part of this work can be found in *Radiopurity control in the NEXT-100 double beta decay experiment: procedures and initial measurements*, [Alvarez et al. 2013].

5.4.1 Vessel

The pressure vessel of NEXT must be able to hold 15 bar of xenon. It consists of a cylindrical center section (barrel) with two identical torispherical heads on each end [Alvarez et al. 2012]. The vessel orientation is horizontal, so as to minimize the overall height. Although it will be ultimately made of stainless steel, the first considered option was titanium, so several samples of both materials have been screened. Inconel (nickel-chromium alloy) will be used to bolt the end-caps to the main body due to its excellent strength properties and therefore its radiopurity has been analyzed too.

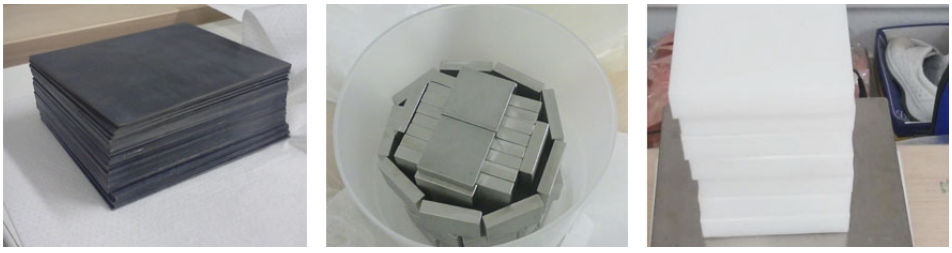

Figure 5.27: Left side, Lead sample . Center, 316Ti Stainless Steel. Right side, Polyethilene

Grade 2 Titanium was initially proposed to be used for the main components of the vessel. Two samples were screened at LSC, one from a Spanish supplier, Titanio SMP[32] and the other from Titanium Metal Supply[33]. Information of this measurement is shown in rows # 11-13 of of the tables 5.7 and 5.8. The Ti SMP sample was screened using two different germanium detectors, GeOroel (row # 11) and GeTobazo (row # 12) as a cross-check exercise; the small differences found can be well understood taking into account the differences

[32] http://www.titaniosmp.com
[33] http://www.titaniummetalsupply.com

in the background rates of the detectors in several energy ranges. Thanks to the much larger mass available in the sample, upper limits on activities derived for the Ti Metal Supply sample are much lower than for the Ti SMP sample and it has been possible to quantify the activity of the lower part of the ^{232}Th chain. Production of ^{46}Sc, beta emitter with Q=2366.7 keV and $T_{1/2} = 83.8 days$, has been also observed for this sample; it must have been generated by (n,p) reactions on ^{46}Ti induced by fast neutrons. The LUX collaboration has carried out an exhaustive analysis of Ti samples [D. Akerib et al. 2012], obtaining different levels of radiopurity for them; the presence of ^{46}Sc is usually identified.

A great deal of activity measurements for different types of **Stainless Steel** (SS) can be found in the literature (see for example refs. [Arpesella et al. 2002], [Lawson and Cleveland 2011], UKDMC Radioactivity Data[34] and ILIAS Database) showing a wide range of values. One sample of type 304L (a vacuum system piece from Pfeiffer[35]) was screened using the Paquito detector (see results in row # 14 of the tables 5.7 and 5.8), obtaining the usual quite high levels of activity from natural chains. Material referenced as austenitic 1.4571 (also 316L) has been extensively studied by XENON [Aprile et al. 2011] and GERDA [Maneschg et al. 2008] experiments, finding materials supplied by the Nironit[36] company with activity levels (values or upper limits) of even tenths of mBq/kg for isotopes from the natural chains in the best cases. Three samples of 316Ti stainless steel supplied by Nironit were screened at LSC and results are presented at rows # 15-17 of the table 5.8; they have different thickness since they are intended to be used in different parts of the NEXT pressure vessel (10 mm for body, 15 mm for end-caps and 50 mm for flanges). Activities from ^{60}Co and ^{54}Mn, commonly present in steel, have been quantified for the three samples. Results for cosmogenic ^{54}Mn, not quoted in table 3 REVISAR, are 0.29 ± 0.05, 0.5 ± 0.07 and 0.97 ± 0.14 mBq/kg for increasing thickness of sample. For the 10- and 15-mm-thick samples, upper bounds for all the other emitters investigated have been derived; for the 50-mm-thick sample, the activity of the isotopes of the ^{232}Th chain has been quantified, pointing to secular equilibrium. It is worth noting that the sensitivity for the thickest sample was worse than for

[34] http://hepwww.rl.ac.uk/UKDMC/Radioactivity/
[35] http://www.pfeiffer-vacuum.com
[36] http://www.nironit.de

the other two, because of the lower mass available in the sample (see table of the tables 5.7) and the lower efficiency detection due to self-absorption. The activity values obtained for Nironit 316Ti stainless steel are of the order or below NEXT requirements; therefore, the booked batches from where the samples were taken will be used for pressure vessel construction.

Samples of **Inconel 718** and **Inconel 625** from the Spanish company Mecanizados Kanter[37] were screened at LSC and results are shown in rows # 18-19 of table 5.8. No previous results on radiopurity of this material have been found; upper limits on activities of the lower parts of the ^{238}U and ^{232}Th chains have been set at some mBq/kg for both types of inconel. Presence of ^{58}Co was identified for Inconel 625.

Inside the vessel, we will find the **Inner Copper Shielding**, ICS, the last shielding of the experiment. It consist of 12-cm-thick inner layer of copper to attenuate the radiation originated in the vessel material [Alvarez et al. 2012]. Copper is expected to shield in-vessel electronics components if necessary and for the photomultipliers enclosures too.

Three **Copper** samples having different origins were also screened by GDMS for this shielding. Other copper measurements are explained in detail in 5.2. One of this GDMS samples is Electrolytic Tough Pitch (ETP) copper supplied by the Spanish company Sanmetal[38] while the other two were made of C10100 copper from the Luvata[39] company, having different production mechanism (hot versus cold rolling). The Luvata copper samples were screened together using the Paquito detector as well. All results on copper are shown in rows # 7-10 of table 5.8. The upper bounds on activities derived from the germanium spectrometry measurement were much less stringent than those from GDMS due to its limited sensitivity; hence a new measurement, with much more mass and time and using a bigger germanium detector is foreseen. The cleanest copper we are aware of is that supplied by Norddeutsche Affinerie (Germany)[40]; very low upper limits for its activity were set in measurements at the Gran Sasso

[37] http://www.mecanizados-kanter.es
[38] http://www.sanmetal.es
[39] http://www.luvata.com
[40] Now re-branded as Aurubis, http://www.aurubis.com

Underground Laboratory [Laubenstein et al. 2004] and by the EXO Collaboration [Leonard et al. 2008] and even activity from the natural chains and ^{40}K was quantified by the XENON experiment [Aprile et al. 2011], at levels of a few tens of $\mu Bq/kg$.

Although the GDMS measurement of Luvata copper has given information only on U and Th concentration, the upper limits derived are at the same level or even better than the results for the Norddeutsche Affinerie copper, and Luvata copper has therefore been chosen as the first option for the NEXT shield.

5.4.2 High Voltage and electroluminescence components

The main body of the field cage to be placed inside the vessel will be made of high density polyethylene, with attached copper strips connected to resistors [Alvarez et al. 2012]; PEEK was also considered as an alternative. Wire meshes separating the different field regions of the detector, including the electroluminescence volume, will be made of stainless steel. To improve the light collection efficiency of the detector, reflector panels coated with a wavelength shifter will cover the inner part of the field cage. This light tube will be made of Tetratex© fixed over a 3M substrate, coated with tetraphenyl butadiene (TPB) [Alvarez et al. 2012]. The ArDM experiment has screened specifically polytetrafluoroethylene (PTFE) Tetratex from Donaldson Membranes[41] by Inductively Coupled Plasma Mass Spectrometry (ICPMS) [Boccone et al. 2009] and TPB from two different manufacturers were measured at SNOlab [Lawson and Cleveland 2011]. A sample of PEEK from Sanmetal Spanish company was screened using the Paquito detector; values obtained are shown in row # 20 of table 5.8, pointing to a non-negligible activity. Only upper bounds on activity of PEEK were presented in [Lawson and Cleveland 2011].

Polyethylene from IN2 Plastics company[42] has a very good radiopurity according to XENON results [Aprile et al. 2011] and a sample of High Molecular Weight polyethylene (type PE500) was therefore chosen for screening at LSC. First results, shown in row # 21 of table 5.8, have produced only upper limits

[41] http://www.donaldson.com
[42] http://www.in2plastics.com

for common radioisotopes. Semitron© ES225 plastic produced by Quadrant Engineering Plastic Products[43] has been also measured and the results on its radiopurity are presented in row # 22 of table 5.8; in this case, a quite high activity of ^{40}K has been registered.

For the Field Cage, are necessary to use high resistance **resistors**. Our provisional option chosen to be screened is Ohmcraft resistors HVC-G3512-FDD with $10G\Omega$. Results of this measurement are shown in row # 21 of table 5.8. We can observe a strong contribution of ^{214}Bi that makes them unacceptable for a low background experiment. Other options are now under study.

Light Tube, a surface to be coated with a WLS, is a inner barrel of **Teflon**. AIMPLAS is the supplier of Teflon powder that will be melted and converted in the barrel. A sample of the **Teflon powder** (grain diameter 0.5-1 mm) with a mass of 1.058 kg was screened. Results of this measurement are shown in row # 24 of table 5.8. Results are very promising but is tentative to repite the measurement with a larger mass sample to reduce the upper limits of this material.

Figure 5.28: Left side, 10GOhm Ohmcraft Resistors. Center, Teflon Powder. Right side, Getter pills

5.4.3 External components of the detector

The external castle is designed to stop the radiation coming from the mountain and the laboratory. This external passive shielding for NEXT-100 is made of lead bricks forming a 20-cm-thick lead castle and there will placed in a steel structure.

[43] http://www.quadrantplastics.com

Lead samples from different suppliers (Mifer[44], using two different raw materials, and Tecnibusa[45] from Spain and COMETA[46] from Italy) were screened by GDMS. Results are shown in rows # 1-4 of table 5.8; it must be noted that the quantified U and Th concentrations were reported to be at the ultimate limit of detection. The results obtained for COMETA lead are in agreement with the specifications given by the company. Since a large amount of the lead bricks will be ultimately provided by Tecnibusa, two different half-brick samples ($10x10x5cm^3$ each) from this company were measured at LSC; results are presented in rows # 5-6 of table 5.8. This lead has a low activity of ^{210}Pb at the level of some tens of Bq/kg. U and Th contamination in lead are normally not very important [Heusser 1995], since radioactive contaminants are effectively removed from lead together with silver [Alessandrello et al. 1991]. For instance, for Dow Run lead produced by JL Goslar[47], activities of tens of $\mu Bq/kg$ were measured in [Laubenstein et al. 2004] and even lower values have been presented by EXO [Leonard et al. 2008] and GERDA [B. Budjas et al. 2008] experiments as upper limits.

[44] http://www.mifer.com
[45] http://www.tecnibusa.com
[46] http://www fonderiaroma.com
[47] http://www.doerun.com, http://www.jlgoslar.de

#	Component, Supplier	Detector	Sample Size	Time
1	Pb, Cometa	GDMS		
2	Pb, Mifer	GDMS		
3	Pb, Mifer	GDMS		
4	Pb, Tecnibusa	GDMS		
5	Pb, Tecnibusa	GeAnayet	5585 g	19.4 days
6	Pb, Tecnibusa	GeAnayet	5585 g	36.0 days
7	Cu (ETP), SanMetal	GDMS		
8	Cu (C10100), Luvata (hot rolled)	GDMS		
9	Cu (C10100), Luvata (cold rolled)	GDMS		
10	Cu (C10100) Luvata (hot+cold rolled)	Paquito	681 g	39.2 days
11	Ti, SMP	GeOroel	121 g	38.5 days
12	Ti, SMP	GeTobazo	121 g	43.1 days
13	Ti, Ti Metal Supply	GeOroel	1804 g	47.2 days
14	304L Stainless Steel, Pfeiffer	Paquito	347 g	19.6 days
15	316Ti Stainless Steel, 10 mm, Nironit	GeTobazo	7684 g	33.0 days
16	316Ti Stainless Steel, 15 mm, Nironit	GeTobazo	10205 g	35.6 days
17	316Ti Stainless Steel, 50 mm, Nironit	GeAanyet	4816 g	34.7 days
18	Inconel 625, Mecanizados Kanter	GeTobazo	1004 g	28.0 days
19	Inconel 718, Mecanizados Kanter	GeOroel	611 g	27.9 days
20	Peek, SanMetal	Paquito	459 g	24.3 g
21	Polyethylene, IN2 Plastics	GeAnayet	1315 g	36.8 days
22	Semitron ES225, Quadrant EPP	GeOroel	1618 g	35.1 days
23	Field Cage Resistors, Ohmcraft	GeAspe	409 units	12.78 days
24	Teflon Powder, AIMPLAS	GeLatuca	1058 g	36.7 days
25	Getters Pills Lot F0458102574, SAES	GeTobazo	102.7 g	32.3 days
26	Getters Pills Lot F0458102593, SAES	GeLatuca	99.6 g	30.49 days
27	Getters Pills Lot F0458102597, SAES	GeAspe	99.8 g	53.7 days

Table 5.7: Description of the samples measured for the Vessel and the External Parts of NEW

#	Component	Unit	^{238}U	^{226}Ra
1	Pb	mBq/kg	0.37	
2	Pb	mBq/kg	< 1.2	
3	Pb	mBq/kg	0.33	
4	Pb	mBq/kg	0.37	
5	Pb	mBq/kg	< 94	< 2.0
6	Pb	mBq/kg	< 57	< 1.9
7	Cu (ETP)	mBq/kg	0.062	
8	Cu (C10100)	mBq/kg	< 0.012	
9	Cu (C10100)	mBq/kg	< 0.012	
10	Cu (C10100)	mBq/kg		< 7.4
11	Ti	mBq/kg	< 233	< 5.7
12	Ti	mBq/kg	< 361	< 6.6
13	Ti	mBq/kg	< 14	< 0.22
14	304L SS	mBq/kg		14.3 ± 2.8
15	316Ti SS	mBq/kg	< 21	< 0.57
16	316Ti SS	mBq/kg	< 25	< 0.46
17	316Ti SS	mBq/kg	67 ± 22	< 1.7
18	Inconel 625	mBq/kg	< 120	< 1.9
19	Inconel 718	mBq/kg	309 ± 78	< 3.4
20	Peek	mBq/kg		36.3 ± 4.3
21	Polyethylene	mBq/kg	< 140	< 1.9
22	Semitron ES225	mBq/kg	< 101	< 2.3
23	Field Cage Resistors	$\mu Bq/unit$	$(0.56 \pm 0.15) \cdot 10^3$	217 ± 10
24	Teflon Powder	mBq/kg	< 281	< 1.8
25	Getters Lot F0458102574	mBq/kg	$(5.2 \pm 1.0) \cdot 10^3$	< 15
26	Getters Lot F0458102593	mBq/kg	$(6.7 \pm 1.2) \cdot 10^3$	< 13
27	Getters Lot F0458102597	mBq/kg	$(6.2 \pm 0.5) \cdot 10^3$	< 8

Table 5.8: Results of the samples measured for the Vessel and the External Parts of NEW

^{232}Th	^{228}Th	^{235}U	^{40}K	^{60}Co	^{137}Cs	#
0.073			< 0.31			1
< 0.41			0.31			2
0.10			1.2			3
0.14			0.91			4
< 3.8	< 4.4	< 30	< 2.8	< 0.2	< 0.8	5
< 1.7	< 2.8	< 22	< 1.7	< 0.1	< 0.5	6
< 0.020						7
< 0.0041			0.061			8
< 0.0041			0.091			8
< 0.8	< 4.3		< 18	< 0.8	< 1.2	10
< 8.8	< 9.5	3.4 ± 1.1	< 22	< 3.3	< 5.2	11
< 11	< 10	< 8.0	< 15	< 1.0	< 1.8	12
< 0.5	3.6 ± 0.2	0.43 ± 0.08	< 0.6	< 0.07	< 0.07	13
9.7 ± 2.3	16.2 ± 3.9	3.2 ± 1.1	< 17	11.3 ± 2.7	< 1.6	14
< 0.59	< 0.54	< 0.74	< 0.96	2.8 ± 0.2	< 0.12	15
< 0.69	< 0.88	< 0.75	< 1.0	$< 4.4 \pm 0.3$	< 0.17	16
2.1 ± 0.4	2.0 ± 0.7	2.4 ± 0.6	< 2.5	4.2 ± 0.3	< 0.6	17
< 3.4	< 3.2	< 4.6	< 3.9	< 0.4	< 0.6	18
< 5.1	< 4.4	15.0 ± 1.9	< 13	< 1.4	< 1.3	19
14.9 ± 5.3	$< 11.0 \pm 2.4$	< 7.8	8.3 ± 3.0	< 3.3	< 2.6	20
< 3.8	< 2.7	< 1.0	< 8.9	< 0.5	< 0.5	21
< 3.8	< 2.7	< 1.0	< 8.9	< 0.5	< 0.5	22
44 ± 4	32 ± 5	< 0.20	95 ± 13	< 2	< 2	23
< 4.5	< 3.3	< 1.0	< 6.8	< 0.5	< 0.6	24
< 37	< 18	165 ± 15	< 40	< 3.2	< 4.2	25
< 27	< 27	222 ± 19	< 42	< 2.7	< 3.1	26
< 27	< 14	192 ± 5	< 26	< 1.1	< 2.1	27

5.4.4 Gas System

The **gas system** is the responsible to produce vacuum, fill the detector with xenon, circulate the gas and clean the gas removing impurities. Mainly, all the gas system is outside the castle and it is not a priority to measure these components. But, to purify the gas we need to use getters to remove the impurities. Unfortunately, the getters can be a strong source of background because of the radon emanated from the active materials of the getters.

The option chosen for NEW is a **hot Getter SAES GT707, model MC4500-902FV**, from SAES Advanced Technologies[48]. Three different samples of active material, small cylindrical pills with 4-mm diameter and 2-mm height were screened. The composition of the pills is 70% Zirconium, 24.6% Vanadium and 5.4% Iron.They become active only at a temperature well above 200 degrees. The samples are from 3 different production batches.

At room temperature the samples are passive components (i.e. do not interact with the medium), thus no special preparation was needed for the radiopurity measurement. A Petri dish was used to place them on the detector.

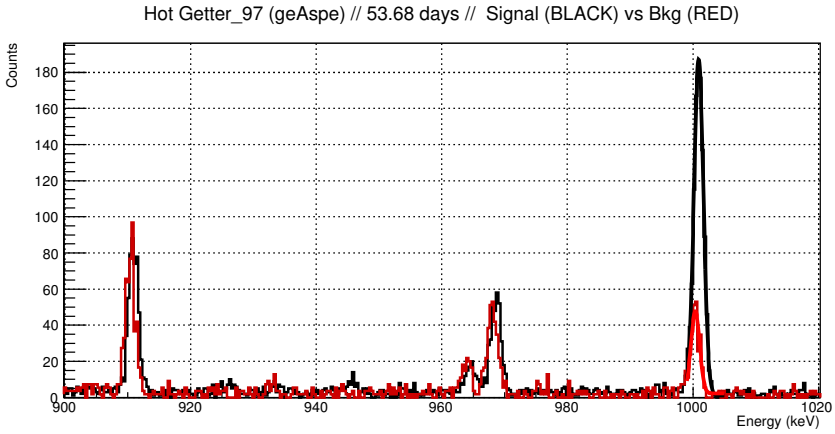

Figure 5.29: Spectrum of the selected getter for the Gas System of NEW. In this case, we can observe the big activity in 1001 keV peak, 234*Pa

[48]https://www.saesgetters.com

Activities of these three sample are in row # 25, 26 and 27 of table 5.8. None of the most dangerous isotopes, ^{208}Tl and ^{214}Bi have been observed and only upper limits are set. These two isotopes are in equilibrium with the activity of the radon of their chains. That means that, in the moment of the measurement, the number of radon atoms is very small. However, strong non-equilibrium activities for the whole ^{235}U chain and also from the upper part of ^{238}U series have been measured.

We can observe in figure 2.10 that ^{238}U will decay in ^{222}Rn, the longest half-lived isotope of radon and a dangerous source of background because it can emanate from the getters and mix with the xenon that is passing through the purification system.

A study of the possible presence of radon in this pills is necessary, following the equation 2.27 presented in Chapter 2. We are only going to consider the four red coloured (with larger half-lifes) isotopes,^{238}U, ^{234}U, ^{230}Th and ^{226}Ra; that is in equilibrium with ^{222}Rn. ^{234}Th and $^{234*}Pa$ are not considered because their half lifes are very small in comparison with the others.

To simplify this equation, we have consider that ^{234}U, ^{230}Th and ^{226}Ra initial number of atoms is $\cong 0$. Therefore, the time evolution of the number of atoms of a chain with 4 elements follows this equation:

$$S = \lambda_1\lambda_2\lambda_3 P_0\left(\frac{e^{-\lambda_1 t}}{(\lambda_2-\lambda_1)(\lambda_3-\lambda_1)(\lambda_4-\lambda_1)} + \frac{e^{-\lambda_2 t}}{(\lambda_1-\lambda_2)(\lambda_3-\lambda_2)(\lambda_4-\lambda_2)}\right.$$

$$\left. + \frac{e^{-\lambda_3 t}}{(\lambda_1-\lambda_3)(\lambda_2-\lambda_3)(\lambda_4-\lambda_3)} + \frac{e^{-\lambda_4 t}}{(\lambda_1-\lambda_4)(\lambda_2-\lambda_4)(\lambda_3-\lambda_4)}\right) \tag{5.1}$$

Where P_0, P and λ_1 are the initial number of atoms, the final number of atoms and the decay constant of ^{238}U. Where λ_2 is the decay constant of ^{234}U. Where λ_3 is the decay constant of ^{230}Th. Where λ_4 is the decay constant of ^{226}Ra.

After this study, we have conclude that **no significative presence of radon** will be produced in the xenon caused by the radon emanation of the getters.

In addition, presence of naturally occurring isotope ^{138}La has been identified and assessed too $T_{1/2} = 1011y$.

5.5 Impact of the Radioimpurities on the Physics of NEXT

This section is destined to estimate how these activities measured can affect to the background of the detector. With all the information of the measurements and using the Background Model, we can estimate the contribution of these activities to the total background of the detector. As explained in Subsection 3.1.3, simulations have estimated a Rejection Factor that shows the capability of the detector to detect these events as background. This factor is bigger than 10^6 for all the studied components of the detector.

For a more complete explanation of this work, please read *Sensitivity of NEXT-100 to neutrinoless double beta decay*, NEXT collaboration (J. Martín-Albo et al.), [J. Martín-Albo et al. 2016]

Detector SubSystem	^{208}Tl	^{214}Bi	TOTAL
Pressure vessel	< 0.14	< 0.14	< 0.28
Energy Plane	< 0.37	< 0.61	< 0.98
Tracking Plane	< 0.08	< 0.48	< 0.56
Electric-Field Cage	< 0.16	< 1.00	< 1.16
Inner Shield	< 0.18	< 0.73	< 0.91
Outer Shield	0.015(3)	0.130(30)	0.140(30)
TOTAL	< 0.94	< 3.09	< 4.03

Table 5.9: Estimated contributions for detector NEXT-100 in $10^{-4}keV^{-1}kg^{-1}yr^{-1}$

We can observe in Table 5.9 the estimated contribution of several parts and the Total contribution of the future detector NEXT-100. Finally, we obtain the estimated overall background rate for NEXT-100:

$$< 4 \cdot 10^{-4} counts/(keV \cdot kg \cdot year) \tag{5.2}$$

In figure 5.30, are shown the most significant contributions of some elements of the detector. These is a very good reference to decide where to improve the radiopurity measurements or what elements must to be replace.

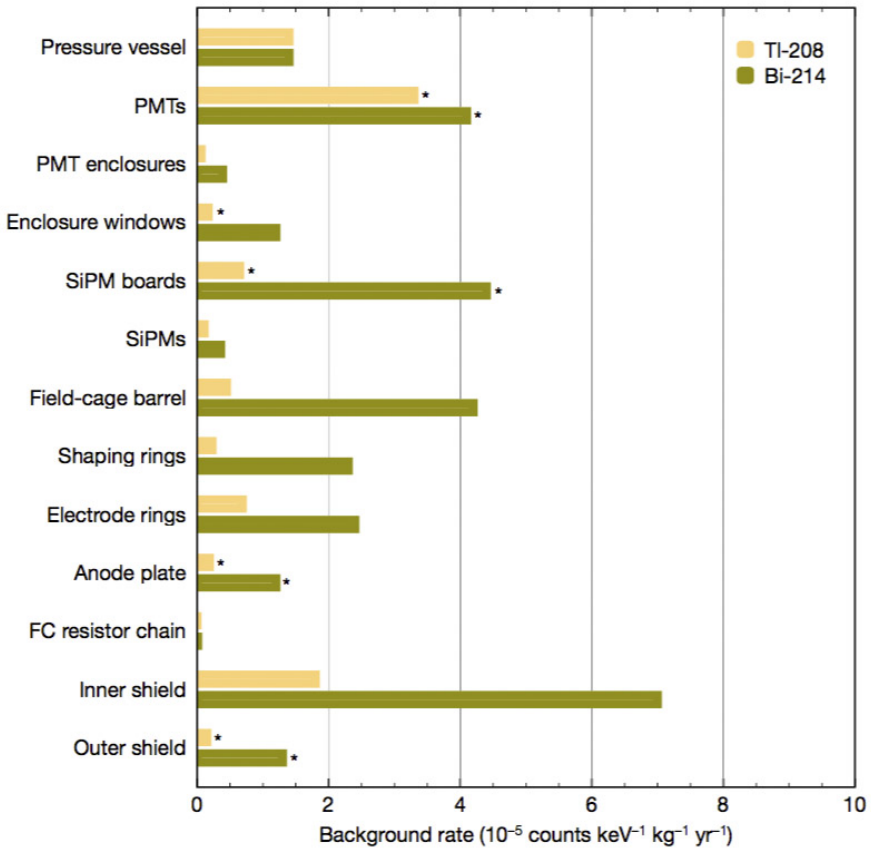

Figure 5.30: Estimated contribution to the Background of NEXT-100. Asterix (*) contributions indicates a measure; in the other cases there are only an upper limit.

6

Radioactive Contamination in SuperK-Gd

6.1 Introduction

SuperK-Gd will be an improved version of the Super-Kamiokande detector. In this new version, a salt of gadolinium, $Gd_2(SO_4)_3$, will be solved in the ultrapure water tank, making this salt the larger possible source of radioimpurities.

A complete program of Market-survey of Gd is a key point to reduce the background and achieve the detector goals.

6.2 Measurements and results

SuperK-Gd, as a low background experiment, needs to carry out a radiopurity campaign to evaluate as much as possible the contribution of the background to the sensibility of the detector. Two underground laboratories have been involved in this radiopurity campaign: the Kamioka Observatory and the Canfranc Underground Laboratory. In the last years, also the Boulby Underground Laboratory (U. Sheffield) has joined efforts.

The usual samples to measure were $Gd_2(SO_4)_3$, the salt to be solved in the water of the detector tank. But, to study the purification process, we also measured Gd_2O_3, that was mixed with H_2SO_4 to get $Gd_2(SO_4)_3$. The study of both Gadolinium samples can show us some very important information about the purification process and how to improve it.

These works all together with a thorough market-survey to find the best samples has been very fruitful: the evolution of the radiopurity in time with new samples is clearly observable.

Tha naming convention for the Gd samples is material-date-company-lot where each item is as follows:

- Material: type of salt, using GSF for Gadolinium Sulphate and GOX for Gadolinium Oxide.
- Production date: writing first the two last numbers of the year and later the two numbers of the month.
- Company: we nickname them as shown in the table
- Lot number or number of the sample: it is the last parameter to differentiate samples. In cases of no information, 1 is the default value employed.

Supplier Name	Sample name
Beijing Jinghonganxin	BEJ
Changshu Huanyo Intl.	CHS
Kojundo Ch. Lab. Co. Ltd.	KJD
Kanto Chemical	KNT
Molycorp Inc.	MLC
Nippon Yttrium Company	NYC
Stanford Materials Co.	SFM
Shinetsu Chemical Co., Ltd.	SHT
HK Tai Kun Intl.	TAI

6.2.1 Sample Preparation for Gd measurements

Sample preparation was clearly explained in Chapter 4, but we want to remark that Gadolinium Sulphate has moderate health hazards: can irritate eyes and mucous membranes. Security procedures have been followed in sample preparation using goggles and working with ventilation to avoid eye contact or inhalation of the powder.

To measure this powder sample, the marinelli is always closed to avoid any contamination to the detector. That means that some radon can be trapped inside the marinelli, making some of the first datafiles contaminated in the lower part of the ^{238}U with an excess of activity from atmospherical radon.

6.2.2 Measurements of Gd samples with HPGe

These are the mains part of the Radiopurity Campaign for SuperK-Gd. 26 different samples (including Gadolinium Sulphate and Gadolinium Oxide) were screened during almost the seven years of this Campaign.

Typical radioisotopes found in Gd samples

The samples have the three usual chains, showed in figures 2.9, 2.10 and 2.11. But, not usual strong contributions of the ^{235}U has been observed, especially in the lower part of chain. Figure 6.1 is a good example of this strong activity.

There are also 4 radiosiotopes observed mainly in these samples: the two first of them are well understood and the other two are under study:

- ^{176}Lu, is a rare earth that undergo beta decay emitting two gamma photons with 201.8 keV (with 77.97% of probability) and 306.8 keV (with 93.6% of probability)
- ^{138}La is also a rare earth undergo β^- (with 34.4% of probability) emitting one gamma photon with 788.7 keV; but also can undergo β^+ (with 65.6% of probability) emitting one gamma photon with 1435.8 keV.
- ^{7}Be is a cosmogenic radioisotope produced by spallation several elements, por example ^{14}C. This isotope has a gamma photon with an energy of 477.6 keV, where we are also observing a peak.
- $^{148*}Pm$ The two peaks are clearly observed in several measurements with energies of 550.3 keV and 630.0 kev that can correspond to $^{148*}Pm$. The main problem is that is Pm is a very uncommon element and only can be produced in trace quantities after a spontaneous fission of ^{238}U, a spontaneous fission of ^{235}U or an alpha decay of ^{151}Eu. These 3 isotopes were present in Gd samples. Finally, $^{148*}Pm$ can be produced by (n, γ) in ^{147}Pm [Eldridge and Lyon 1961].

#	Name	Detector	Sample Size	Time
1	GSF-0904-SFM-1	GeOroel	5.00 kg	24.08 days
2	GSF-1008-SFM-100723	GeAnayet	1.00 kg	47.15 days
3	GSF-1208-BEJ-1	GeAnayet	0.87 kg	15.76 days
4	GSF-1302-CHS-1	GeOroel	2.00 kg	12.02 days
5	GSF-1303-BEJ-1	GeOroel	2.01 kg	22.28 days
5-2	GSF-1303-BEJ-1	GeLatuca	2.01 kg	18.30 days
6	GSF-1308-SFM-1	GeOroel	1.00 kg	17.38 days
6-2	GSF-1308-SFM-1	GeOroel	1.00 kg	18.50 days
7	GSF-1307-TAI-1	GeAsterix	1.00 kg	11.38 days
8	GSF-1307-TAI-2	GeOroel	1.00 kg	15.68 days
9	GSF-1412-SFM-1	GeAspe	2.96 kg	11.32 days
10	GSF-1508-KJD-1	GeOroel	2.00 kg	25.19 days
11	GOX-1510-MLC-1	GeAspe	2.18 kg	11.59 days
12	GSF-1512-NYC-1	GeOroel	0.60 kg	26.11 days
13	GOX-1512-NYC-1	GeAspe	0.60 kg	28.61 days
14	GOX-1602-NYC-1	GeAspe	1.44 kg	29.59 days
15	GOX-1603-SHT-237	GeAspe	2.22 kg	32.79 days
16	GOX-1603-SHT-239	GeLatuca	2.24 kg	29.90 days
17	GOX-1603-SHT-236	GeOroel	2.23 kg	17.26 days
18	GSF-1604-NYC-160303	Asterix	2.23 kg	30.50 days
19	GSF-1604-NYC-160311	GeTobazo	1.90 kg	33.26 days
20	GOX-1604-NYC-160353	Asterix	1.98 kg	31.25 days
21	GSF-1604-SHT-1	GeLatuca	2.23 kg	26.48 days
21-2	GSF-1604-SHT-1	Obelix	2.23 kg	26.52 days
22	GSF-1611-SHT-003	Asterix	2.50 kg	77.89 days
23	GSF-1701-MLC-003	Asterix	5.00 kg	17.45 days
24	GSF-1703-SHT-(RGD-OSF-005)	Asterix	3.00 kg	70.32 days
25	GSF-1703-KNT-702142	Obelix	3.00 kg	46.18 days
26	GSF-1705-MLC-001	Obelix	5.00 kg	18.34 days

Table 6.1: Description of the samples of Gadolinium for SuperK-Gd experiment

#	Component	^{238}U	^{226}Ra	^{232}Th
1	GSF-0904-SFM-1	51 ± 21	8 ± 1	11 ± 2
2	GSF-1008-SFM-100723	< 33	2.8 ± 0.6	270 ± 16
3	GSF-1208-BEJ-1	292 ± 67	74 ± 2	1099 ± 12
4	GSF-1302-CHS-1	74 ± 28	13 ± 1	205 ± 6
5	GSF-1303-BEJ-1	334 ± 76	9 ± 1	20 ± 2
5-2	GSF-1303-BEJ-1	< 108	< 6	187 ± 4
6	GSF-1308-SFM-1	< 56	1.2 ± 0.6	4 ± 1
6-2	GSF-1308-SFM-1	14 ± 7	1.0 ± 0.4	12.0 ± 1.0
7	GSF-1307-TAI-1	< 105	< 2	11.4 ± 2
8	GSF-1307-TAI-2	< 98	4 ± 1	3 ± 1
9	GSF-1412-SFM-1	< 76	< 1.4	2 ± 1
10	GSF-1508-KJD-1	< 34	< 0.8	< 1.1
11	GOX-1510-MLC-1	1606 ± 109	4.1 ± 1.2	245.3 ± 3.9
12	GSF-1512-NYC-1	< 139	< 2.1	2.8 ± 1.9
13	GOX-1512-NYC-1	< 280	< 4	< 10
14	GOX-1602-NYC-1	1221 ± 112	29 ± 2	274 ± 5
15	GOX-1603-SHT-237	< 63	< 0.8	< 2.7
16	GOX-1603-SHT-239	< 113	< 0.9	< 2.1
17	GOX-1603-SHT-236	< 38	< 0.7	< 1.4
18	GSF-1604-NYC-160303	< 20	< 0.64	< 0.67
19	GSF-1604-NYC-160311	< 59	< 0.7	3.2 ± 1.0
20	GOX-1604-NYC-160353	< 21	< 1.0	8.2 ± 0.7
21	GSF-1604-SHT-1	< 160	< 1.2	< 2.9
21-2	GSF-1604-SHT-1	< 25	< 0.6	< 0.7
22	GSF-1611-SHT-003	< 10	< 0.2	< 0.2
23	GSF-1701-MLC-003	< 45	0.4 ± 0.2	28.5 ± 1.1
24	GSF-1703-SHT-(RGD-OSF-005)	< 7.0	< 0.24	< 0.20
25	GSF-1703-KNT-702142	< 7.0	< 0.7	< 0.22
26	GSF-1705-MLC-001	< 11	2.5 ± 0.4	12.2 ± 1.0

Table 6.2: Results of the samples of Gd for SuperK-Gd experiment. Units are in mBq/kg. MC errors ($\sim 10\%$) are not included

^{228}Th	^{235}U	^{227}Th	^{40}K	^{138}La	^{176}Lu	#
29 ± 3	< 32	214 ± 10	29 ± 5	8 ± 1	80 ± 8	1
86 ± 5	< 32	1700 ± 20	12 ± 3		21 ± 2	2
504 ± 6	< 112	2956 ± 30	101 ± 10	683 ± 15	566 ± 6	3
127 ± 3	< 25		< 60	3 ± 1	11 ± 1	4
360 ± 4	< 12		< 12	43 ± 3	6 ± 2	5
211 ± 2	3 ± 1	< 11	< 13	44 ± 1	7 ± 1	5-2
117 ± 2	< 3	231 ± 6	< 10	3.5 ± 0.5	25 ± 1	6
62 ± 2	< 2.5	196 ± 5	< 4.4	3.2 ± 0.3	24 ± 1	6-2
8 ± 2	< 3	< 11	4 ± 3	< 3	1.4 ± 0.4	7
411 ± 5	< 28	< 16	< 22	< 2	< 1.2	8
29 ± 2	< 1.8	190 ± 6	< 5	23 ± 1	2.5 ± 0.6	9
2.0 ± 0.5	< 0.6	11 ± 4	< 3	< 0.6	2.9 ± 0.2	10
116 ± 2	28.7 ± 1.5	< 33	21 ± 6	< 3.2	7.4 ± 1.2	11
1.8 ± 0.9	< 2.4	< 10	< 14	< 1.9	< 1.6	12
< 9	< 7	< 11	< 11	< 1.7	2.6	13
233 ± 4	50 ± 4	1813 ± 14	219 ± 11	10 ± 1	78 ± 2	14
< 1.7	< 1.3	< 3.5	< 3.0	< 0.5	< 0.7	15
< 1.3	< 0.8		< 3.1	< 0.6	< 0.6	16
< 0.8	< 1.0	< 0.9	< 4.1	< 0.6	< 0.5	17
0.5 ± 0.2	< 0.7	< 2.3	< 1.6	< 0.3	< 0.4	18
< 1.4	< 1.2	< 4.1	< 2.7	< 0.2	< 0.7	19
1.5 ± 0.5	1.0	< 3.4	< 5.3	0.4 ± 0.1	9.1 ± 0.5	20
< 2.5	< 0.9	< 3.6	< 3.3	< 0.5	1.3 ± 0.3	21
0.9 ± 0.3	< 3	< 6	< 2	< 0.5	0.4 ± 0.2	21-2
< 0.3	< 0.5	< 1.2	< 1.8	< 0.15	0.4 ± 0.2	22
6.3 ± 0.5	< 1.5	< 5.5	< 1.0	< 0.25	26.5 ± 0.8	23
< 0.35	< 0.4	< 1.3	< 1.2	< 0.21	0.23 ± 0.09	24
1.6 ± 0.3	< 0.8	< 4.7	< 1.8	< 0.2	2.6 ± 0.2	25
4.6 ± 0.7	< 1.0	3.4 ± 1.4	< 1.8	< 0.4	6.0 ± 0.4	26

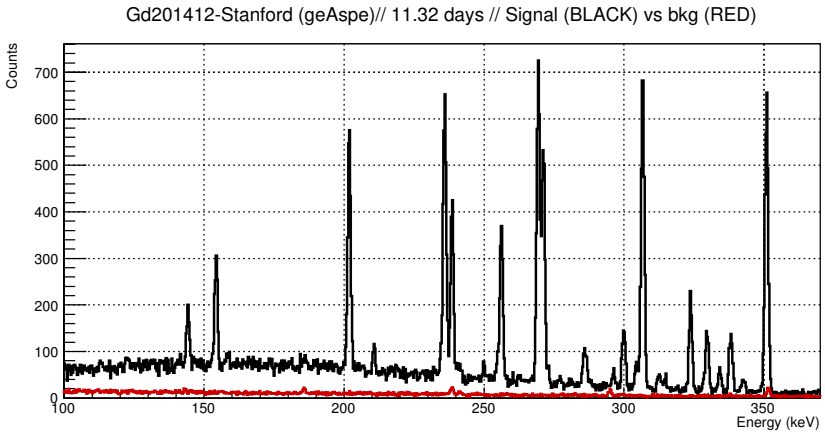

Figure 6.1: Spectrum of the gadolinium sulphate sample GSF-1412-SFM-1. We can observe the strong contribution in the lower part of the spectrum of the 235U chain. Also, we can observe the shift of the background Compton around the peaks, produced by the strong activity of this sample.

First and one of the most remarkable difference between with NEXT measurements is that is usual to find gamma lines from other rare earth radioisotopes. An important topic about rare earth is that they have a very similar chemical behavior and is harder to isolate one element from the others. In our case, we observe two cosmogenic radionuclides, ^{176}Lu and ^{138}La. The two last columns of the tables are used to quantify the activities of these two isotopes.

An important point for the radiopurity measurements for SuperK-Gd it to quantify the activity of ^{238}U. This isotope, that is observed with the gamma line emitted from $^{234*}Pa$ (γ emission at 1001.03 keV) is in equilibrium with the activity of ^{238}U. But, the very low intensity of this gamma line makes very complicated to achieve low quantifications of this isotope. Only very detectors with very low backgrounds in this energy are recommended for these measurements. For this reason, the most recommended detectors for SuperK-Gd measurements are GeOroel, Asterix and Obelix.

First measurements, done by L. Labarga before the start of my PhD period, were the first contact with Gd samples. **GSF-0904-SFM-1** and **GSF-1008-SFM-100723**.

Strong contributions were found in almost all the isotopes studied, see rows # 1 and 2 of the tables 6.1 and 6.2. GSF-0904-SFM-1 was the first sample and necessary to understand the typical radioisotopes we can find in these samples. In these sample was the first where we observed ^{138}La and ^{176}Lu. GSF-1008-SFM-100723 was also used in early stages of EAGDS, in a non-instrumented version of it.

GSF-1208-BEJ-1, a small test sample ($\sim$ 0.9 kg) from Beijing Jinghonganxin was measured, with the largest activities observed in this campaign (row # 3 of the tables 6.1 and 6.2). This is the first case were very careful with the ^{40}K peak, because the strong activity of ^{228}Ac can mimic this peak. We have calculate how many counts can come from ^{228}Ac and the number is similar to the number of measured counts. Then, we finally only can put an upper limit on this activity.

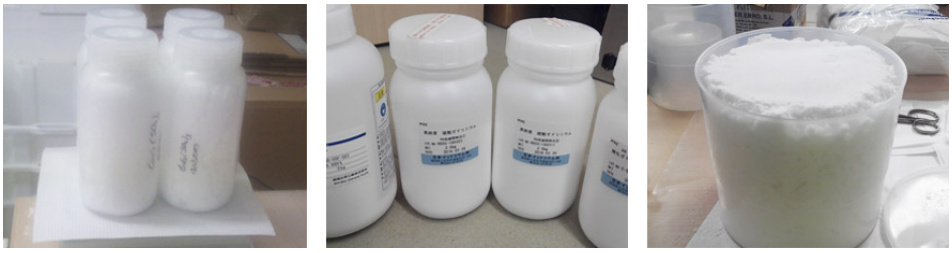

Figure 6.2: Different packaging of the some Gadolinium samples. Left side, GSF-1308-SFM-1 sample. Center, GSF-1604-SHT-1, GSF-1604-NYC-160303, GSF-1604-NYC-160311 and GSF-1604-NYC-160353. Right side, GSF-1701-MLC-1

The only sample from Changshu Huanyo Intl., **GSF-1302-CHS-1**, $\sim$ 2 kg of $Gd_2(SO_4)_3$ is one of the dirtier samples measured, specially in the lower part of ^{235}U (row # 4 of the tables 6.1 and 6.2). But no time evolution were observed and that means that one long half-life isotope is still present in the chain.

GSF-1303-BEJ-1 and **GSF-1308-SFM-1** ($\sim$ 2.6 kg of $Gd_2(SO_4)_3$ from the 500 Kg batch from the American supplier Stanford Materials Co.) where two samples used in the instrumented period of EGADS. The activities for relevant isotopes for both samples are large. Additionally, these two samples where measured two times to observe the time evolution of the decay chains. GSF-1303-BEJ-1 is one of the most complete and important samples of all the campaign of Gd measurements. Results are in rows # 5, 5-2, 6 and 6-2 of the tables 6.1 and 6.2.

Several long half-lifes isotopes have been removed and can be observed the evolution of the chains clearly, during the time of the measurement and also a in the second measurement. In GSF-1303-BEJ-1 we can observe the two different cases of time evolution studied: short and long time evolution of the activity

GSF-1308-SFM-1 is also a example of long time evolution of the decay chains (see subsection 6.4).

Two samples of $Gd_2(SO_4)_3$, **GSF-1307-TAI-1** and **GSF-1307-TAI-2**, $\sim$ 1 kg each, from a new supplier from China, HK Tai Kun International. Unfortunately, first measurements of both samples measurement were very short, a few days time each. The reason for this was the limited availability of LSC detectors. Later, these two samples were screened again with duration of about two weeks, showed in rows # 7 and 8 of the tables 6.1 and 6.2

Even though the shortness of the last 2 measurements, their results are of large interest and importance. Namely, there is no significant radioactivity from the ^{235}U chain downstream. These samples were a step in the right direction, with activities and limits that would imply a reduction of the radioactivity induced neutrons within the Super-Kamiokande water by at least one order of magnitude.

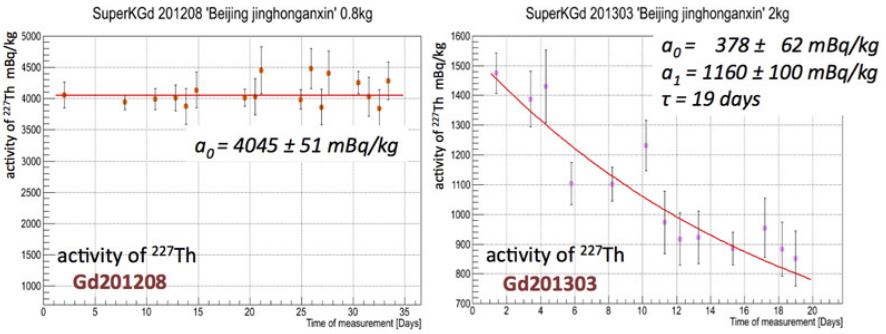

Figure 6.3: Figures with the daily activity of ^{227}Th in two samples of Gd GSF-1208-BEJ-1 and GSF-1303-BEJ-1. Left side, GSF-1208-BEJ-1 with non-observable time evolution. Right side, GSF-1303-BEJ-1 with a clear evolution of the daily activity.

GSF-1412-SFM-1 is the fourth sample from Stanford Materials Co., with $\sim$ 3 kg (row # 9 of the tables 6.1 and 6.2). Despite its activities aren't still good enough, we can observe an improvement in the purification process of the samples, for example in ^{226}Ra and ^{176}Lu activities.

GSF-1508-KJD-1 was in the measurement moment the cleanest $Gd_2(SO_4)_3$ sample, showed in row # 10 of the tables 6.1 and 6.2. But, unfortunately, we do see significant amounts of ^{134}Cs and ^{137}Ca in this sample. These isotopes make are suppose that this Gd was related to a Nuclear Fission process.

GOX-1510-MLC-1 was the first sample of Gadolilium Oxide. This sample consisted of $\sim$ 2.2 kg from Molycorp Inc. It was extremely dirty, remarking the isotope, ^{238}U, one of the most dangerous sources of background. This step was necessary to understand properly the purification process. Results are in row # 11 of the tables 6.1 and 6.2

Following the campaign, three samples from a new provider, NIPPON YTTRIUM CO., LTD, were measured. These samples are considered a first contact with it. One is **GSF-1512-NYC-1**, measured with the detector geOroel, the other is **GOX-1512-NYC-1** measured with geAspe. Both are very small samples, 0.6kg. Even though the statistics is limited, the two samples are found rather clean (rows # 12 and 13 of the tables 6.1 and 6.2)

The third sample, 1.44 Kg of Gd_2O_3, **GOX-1602-NYC-1**, measured with geAspe. This sample is of the same batch as GOX-1512-NYC-1 above, but before any cleaning procedure. It is found extremely dirty, with ^{238}U chain in an amazingly large non-equilibrium and the presence of a large amount of in the lower part of ^{235}U (see rows # 14 of the tables 6.1 and 6.2).

Three Gd_2O_3 samples from SHINETSU of $\sim$ 2.2 kg Chemicals were measured: **GOX-1603-SHT-237** measured at detector geAspe, **GOX-1603-SHT-239** at geLatuca, and **GOX-1603-SHT-236** at geOroel. Results of these three measurements are presented in rows # 15, 16 and 17 of the tables 6.1 and 6.2.

They are very clean, probably the cleanest ones measured by SuperK-GD. With their very clean background was possible to observe (for the first time) the small

peaks of 550 keV and 630 keV, supposed to be from $^{148*}Pm$ and also a peak of 478 keV (only present in GOX-1603-SHT-239), supposed to be from ^{7}Be.

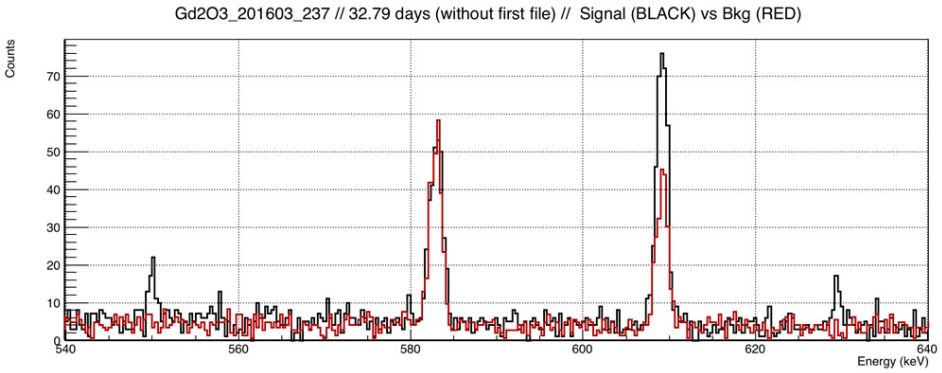

Figure 6.4: Peaks of 550 keV and 630 keV in GOX-1603-SHT-237. $^{148*}Pm$ is the main candidate to emit these photons

The following samples are again from NIPPON YTTRIUM CO., LTD (see rows # 18, 19 and 20 of the tables 6.1 and 6.2). One sample of $Gd_2(SO_4)_3$, **GSF-1604-NYC-160303** (2.23 kg), in the detector Obelix. It was processed from the same Gd_2O_3 batch from where the sample **GOX-1604-NYC-160353** (1.90 kg) that is measured afterwards, was taken. This sample was again the cleanest $Gd_2(SO_4)_3$ sample measured for SuperK-Gd at LSC.

Another sample of $Gd_2(SO_4)_3$ from NYC, **GSF-1604-NYC-160311** (1.98 kg). This comes from the same raw material as GOX-1604-NYC-160353 and GSF-1604-NYC- 160303; but has undergone a different production process than the latter.

The sample of 2.23 kg $Gd_2(SO_4)_3$ from Shinetsu Chemicals **GSF-1604-SHT-001** was measured first with the geLatuca detector. This sample was produced from a Gd2O3 from the same batch as the sample GOX-1603-SHT-236 previously measured. The batch of GSF-1604-SHT-001 was the final product of a process for which high purity was expected. As the precision obtained was not enough, the measurement was repeated in the Obelix detector. Only upper limits were observed, expect for the lower part of ^{232}Th. Both measurements are presented in rows # 21 and 21-2 of the tables 6.1 and 6.2.

One sample of 2.5 kg of $Gd_2(SO_4)_3$ from a new production batch by Shinetsu Chemicals **GSF-1611-SHT-003** was measured with the detector Asterix (row # 22 of the tables 6.1 and 6.2). This batch features the use of a more radio pure H_2SO_4 at the last stage of production in an attempt to further reduce the impurities currently achieved in GSF-1604-SHT-001.

A large sample of 5 kg of $Gd_2(SO_4)_3$ from a new production iteration by Molycorp Inc. **GSF- 1701-MLC-003** with the detector Asterix. There is a dramatic improvement in radioimpurities cleanness with respect to the first sample provided by the Company time ago. See rows # 23 of the tables 6.1 and 6.2)

A sample of 3 kg of a new 'ultrapure-production' batch by Shinetsu Chemicals **GSF-1703-SHT-(RGD-OSF-005)** was measured with the detector Asterix. The results are excellent (rows # 24 of the tables 6.1 and 6.2), of similar quality as the GSF-1611-SHT-003. Because of its incredible cleanness, we decided to extend this measurement as long as we could.

One sample of $Gd_2(SO_4)_3$ of 3 kg from Kanto Chemicals **GSF-1703-KNT-702142** with the detector Obelix. Up to now, all the samples provided by Kanto were small and produced at the Company's laboratories, and all the radioimpurities information about them was provided by the Company itself from ICP-MS measurements. They featured excellent cleanness of isotopes ^{238}U and ^{232}Th.

This is the first Kanto sample produced at Factory (regular production process) and, also, it is the first sample measured by Ge detectors, thus accessing to the whole radioactive chains and also to other isotopes with intermediate life-times. In fact our measurements confirm the lack of ^{238}U and ^{232}Th isotopes but they show instead small but significant contaminations from the lower parts of the chains (rows # 25 of the tables 6.1 and 6.2). This is relevant information that will be transmitted to Kanto Chemicals for any possible correction.

The last sample of this campaign was **GSF-1705-MLC-001**, 5 kg of $Gd_2(SO_4)_3$. (rows # 26 of the tables 6.1 and 6.2)

6.2.3 Measurements of Gd samples with ICP-MS

Mass Spectrometry has a strong point for Gd samples: it is powerful to measure very long half-lifes isotopes, like the initial radioisotopes of the chains. That means that can quantify precisely the concentration of ^{238}U. These measurements are very fast and are very useful to choose those Gd samples that seem to be radiopure. Some companies also gave us this confidential information of the ICP-MS analysis about their samples to show us the quality of their Gd samples.

We considered necessary to complement our HPGe measurements with ICP-MS. The measurements presented in this subsection were carried out at 'Servicio Interdepartamental de Investigación' (SIdI) of UAM.

The first measurement was the **concentration** of different isotopes in three selected samples: GSF-1208-BEJ-1 and GSF-1307-TAI-2.

Element	GSF-1208-BEJ-1	GSF-1307-TAI-2
K	0.000	0.000
La	650.685	0.251
Th	0.000	0.000
Tl	0.005	0.00
U	0.000	0.000
Bi	0.011	0.00

In these analysis, Lu is not considered because of the possible interference with Gd, producing an overestimation in this measurement. It is necessary to repeat this measurement with a MS with high resolution to validate this concentration.

To validate both measurement methods, HPGe and ICP-MS, we have compared both measurements. We have convert concentration of La to activity of ^{138}La, following the procedure presented at the end of Chapter 4.

ICP-MS measurement:

$$650ppm \quad La \Leftrightarrow 527mBq/kg \quad ^{138}La \tag{6.1}$$

HPGe measurement:

$$685 \pm 15 mBq/kg \tag{6.2}$$

If we add a 10% of error coming from the MC, we can affirm that both measurements are slightly compatible.

The second interesting analysis were the **Isotopic Composition** of each Gadolinium isotope. MS can precisely estimate the isotope concentration of one element. This analysis have be done for several samples:

Gd Isot.	N. Abund.	GSF-1208-BEJ-1	GSF-1307-TAI-2
152	0.20	0.20 ± 0.01	0.20 ± 0.01
154	2.18	2.17 ± 0.02	2.13 ± 0.01
155	14.80	14.84 ± 0.04	14.84 ± 0.04
156	20.47	20.50 ± 0.08	20.57 ± 0.08
157	15.65	15.64 ± 0.02	15.63 ± 0.04
158	24.84	24.80 ± 0.01	24.76 ± 0.01
160	21.86	21.86 ± 0.06	21.87 ± 0.05

Table 6.3: Isotopic Composition of GSF-1208-BEJ-1 and GSF-1307-TAI-2 samples. In this case, the samples have an Isotopic Composition compatible with Natural Abundance

Gd Isot.	N. Abund.	GSF-1008-SFM-100723	GSF-1308-SFM-1	GSF-1307-TAI-1
152	0.20	0.20 ± 0.01	0.20 ± 0.01	0.20 ± 0.01
154	2.18	2.18 ± 0.01	2.16 ± 0.02	2.16 ± 0.01
155	14.80	14.77 ± 0.10	14.62 ± 0.10	14.61 ± 0.06
156	20.47	20.78 ± 0.15	20.91 ± 0.09	20.93 ± 0.06
157	15.65	14.70 ± 0.04	14.54 ± 0.09	14.45 ± 0.05
158	24.84	25.22 ± 0.01	25.36 ± 0.01	25.35 ± 0.01
160	21.86	22.15 ± 0.06	22.22 ± 0.05	22.31 ± 0.09

Table 6.4: Isotopic composition of GSF-1008-SFM-100723, GSF-1308-SFM-1 and GSF-1307-TAI-1. Significant differences can be observed in the Natural Abundance

We can clearly observe lower values of odd Gadolinium isotopes and larger values of odd+1 Gadolinium isotopes. It is important to remark than odd Gadolinium isotopes have a Thermal Neutron Capture Cross Section orders of magnitude larger than the others isotopes. A strong neutron flux can explain these effect in the different natural abundance of the Gadolinium samples studied.

6.2.4 Other Measurements for SuperK-Gd

Not only Gd samples were studied, other 3 different samples from the water tank were evaluated for SuperK-Gd, see figure **??**.

Figure 6.5: Three samples of the water tank of SuperK. Left side, FRP (Fibre-reinforced plastic) sample. Center, Stainless Steel from the water tank. Right side, SiO_2 candidate to seal a small leak in the water tank

After the chain implosions of a hundreds of PMTs in the water tank, all the PMTs were covered with a **FRP** (Fibre-reinforced plastic) case to prevent chain reaction implosions. As the typical PCBs samples, these sample has a large activity, in the order of 20-40 mBq/kg in the chains of ^{238}U, ^{232}Th and also in ^{40}K

We also measured the **Stainless Steel** of the Water Tank, where the results were very similar to samples of normal Stainless Steel. Activities of 6.4 ± 2.4 mBq/kg for ^{228}Ac, 1.6 ± 1.3 mBq/kg for ^{208}Tl, 3.0 ± 1.1 mBq/kg for ^{214}Bi and 10.5 ± 0.6 mBq/kg for ^{60}Co were quantified.

The last measurement consisted of 2 kg of High Purity SiO_2 **powder**, a good option to glue a water leak. The sample was provided by Kojundo Ch. Lab. Co. Ltd. The activity observed was very large, with activities about $\sim$0.5 mBq/kg in ^{238}U chain, $\sim$40 in ^{232}Th chain and 0.9 Bq/kg in ^{40}K.

6.3 Study of natural abundance: the ^{235}U case

Uranium has mainly 3 different isotopes: ^{238}U with a natural abundance of 99.274%, ^{235}U with a natural abundance of 0.720% and ^{234}U with a natural abundance of 0.005%. Therefore, if we observe in a spectrum a strong contribution of ^{238}U chain, we also will expect some peaks from the ^{235}U chain. Therefore, in very contaminated samples with Uranium, we can estimate the ratio between ^{238}U and ^{235}U. If one sample doesn't have this equilibrium, the most simple explanation we found was that the sample was in contact with enriched uranium.

It is recommended to use 205.3 keV peak of ^{235}U because in 185.7 keV, is very close the peak of ^{226}Ra and can make us overestimate the peak.

Using this equation to convert natural abundance to activity:

$$A = \lambda N \tag{6.3}$$

We conclude that a factor $\sim$ 20 must relate both activities. In our case, GOX-1510-MLC-1 (row # 11 of the tables 6.1 and 6.2) shows a good agreement with this ratio if we consider the 10% of MC error.

The agreement in GOX-1602-NYC-1 (row and 14 of the tables 6.1 and 6.2) is not so good, but gives us slightly compatible result for this study.

6.4 The non-equilibrium of the decay chains

The time evolution of the chains have been observed in several samples of Gd. It is necessary to have previously a large contamination in the sample and, after the production process, a strong removal of a long half-life isotope. Depending of the half-life of the observed isotopes, we can observe this evolution in during the measurement or we have to repeat ir several years later.

6.4.1 Short time evolution of the activity

We have observe this evolution in samples where the equilibrium was broken and one isotope with a long half-life have been removed from the sample and its daughters have half-lifes in the order of the days. In this case, the activity is reduced with the time and can also been observed during the measurement; in our case, thanks to the daily data taken.

The most significant sample of short time evolution is **GSF-1303-BEJ-1** in the lower part of ^{235}U chain. This chain is showed in figure 2.11.

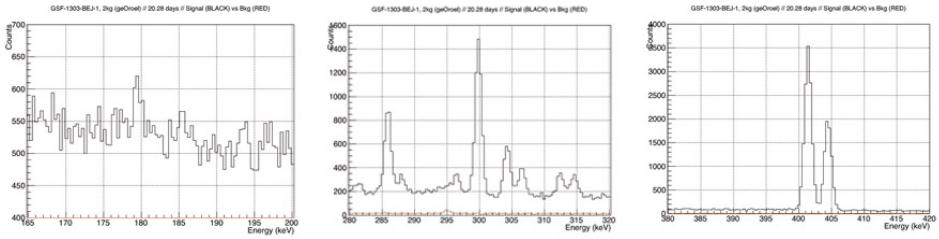

Figure 6.6: Figures with some peaks of GSF-1303-BEJ-1 of the chain 235U. These three figures show that the chain is not in equilibrium. Left side, peak of ^{235}U with 185.7 keV. Center, peak of ^{231}Pa with 302.7 keV. Right side, of ^{219}Rn with 401.7 keV

^{235}U is the first isotope of the chain and has the longest half-life of the chain, with a half-life of $7 \cdot 10^8$ years. ^{235}U has several photons to quantify its activity. The most important is 185.7 keV with an intensity of 57.2%. This peak has very close a peak from ^{226}Ra (186.1keV, with 3.5%). Despite this overlap, we can use the technique presented in Subsection 2.2.2 and estimate that the activity is small, lower than a few of mBq/kg

^{231}Th is the second isotope of the chain. Painted in green color in figure 2.11, that means that is a short half-life isotope and its activity will be almost the same that ^{235}U.

^{231}Pa is the third isotope of the chain, with a long half-life of $3 \cdot 10^4$ years. It has one peak that can be used quantify its activity, 302.7 keV with an intensity of 2.5%. This peak is in a very clean region surrounded by these peaks:^{227}Th (299.9 keV, with 2.0%), ^{231}Pa (300.0 keV, with 2.4%), ^{212}Pb (300.1 keV, with 3.3%) and

^{227}Th (304.4 keV 1.1%). In this case, again is not possible to observe a peak, only upper limits were found.

^{227}Ac is the fourth isotope of the chain, with a half-life of 22 years. The intensity and the energy of the emitted gamma is small and direct quantification of ^{227}Ac is very complicated. But in case of equilibrium it can be quantified with the several gamma photons emitted by its daughters.

^{227}Th and ^{223}Ra are the fifth and sixth isotopes of the chain, painted in yellow (intermediate half-life) in figure 2.11 with a half-life of 19 days and 11 days, respectively. In these two isotopes we started to observe evolution on the daily activity measured.

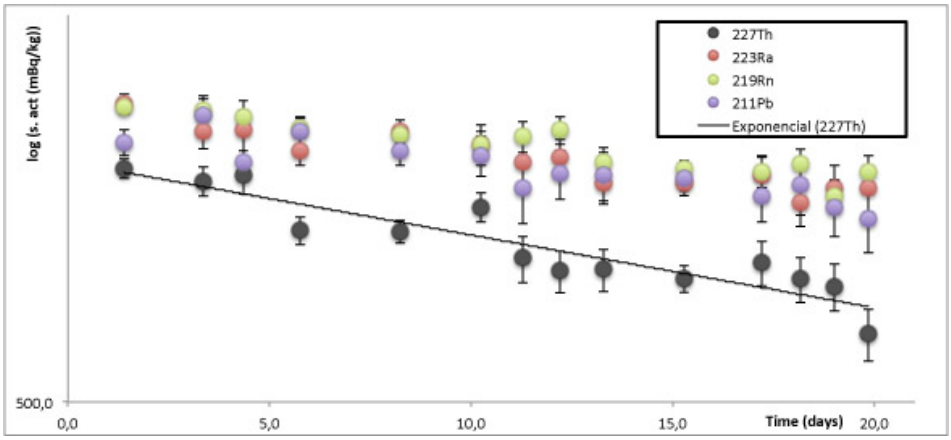

Figure 6.7: Time evolution of four different isotopes are plotted.

The rest of the chain is very fast to decay, with half-lifes in the order of the minutes or lower. We will always observe this part in equilibrium. The most recommended peak for this part of the chain is one from ^{219}Rn, 401.7 keV, with 6.6%, without any peak in the interval ± 2 keV.

^{227}Ac was removed by some kind of purification process within a time interval not longer than few weeks before receiving it in Canfranc. The strong disequilibrium of the parts of the chain with absence of the long half-life isotopes makes possible to observe this process. Plotting the specific activity obtained per

datafile versus the day when it was taken, we can observe clearly the exponential law.

We also have measured this sample again almost three years later to observe the state of the time evolution and we observed that almost all the low part has disappear. That probes that the presence of long half-lifes isotopes is very small in this sample.

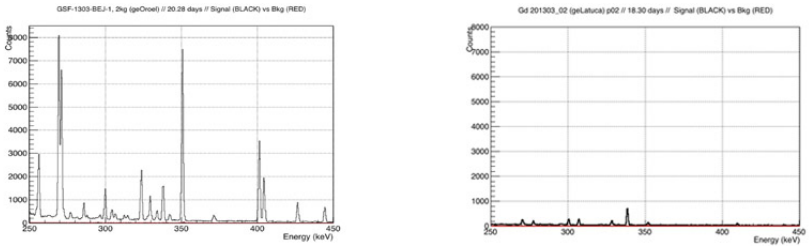

Figure 6.8: Status of the sample in two different measurements. Left side, April 2013. Right, January 2016. Both figures have the same scale

6.4.2 Long time evolution of the activity

In these cases, we have measure the sample a second time to observe clearly the evolution. Because of the two different measurements we have to use some isotopes as a reference, to be sure that the measurements conditions are the same. For this purpose, we have use the two cosmogenical isotopes we have in Gd samples, ^{138}La and ^{176}Lu.

The expected results are strong activity changes in isotopes with a half-life in the order of days and some evolutions in isotopes with half-lifes in the orders of years. Two samples are used to observe it: GSF-1303-BEJ-1 and GSF-1308-SFM-1.

In GSF-1303-BEJ-1 we can observe a large reduction of the activity of ^{238}U, that only can be explained with the partial removal of U and the progressive reduction of the number of atoms of ^{234}Th that finally will produce the 1001 keV peak.

Also, we can observe a increase of ^{232}Th in the upper part its the chain. It can be explained with the partial removal of Ra in the sample and the contribution of ^{232}Th with higher activity.

Estimation of concentration of ^{232}Th

In GSF-1308-SFM-1 the time difference between both measurements were 1.874 years. In this case, we are going to estimate the activity of ^{232}Th, the initial part of its chain that doesn't have any measurable gamma line. The Bateman equations for only two elements:

$$P = P_0 e^{-\lambda_1 t} \tag{6.4}$$

$$Q = \frac{\lambda_1 P_0}{\lambda_2 - \lambda_1} e^{-\lambda_1 t} + (\frac{\lambda_1 P_0}{\lambda_1 - \lambda_2} + Q_0) e^{-\lambda_2 t} \tag{6.5}$$

Looking the second equation, we can rewrite this equation as follows:

$$P_0 = \frac{Q - Q_0 e^{-\lambda_2 t}}{\frac{\lambda_1}{\lambda_2 - \lambda_1} e^{-\lambda_1 t} + \frac{\lambda_1}{\lambda_1 - \lambda_2} e^{-\lambda_2 t}} \tag{6.6}$$

With the information of these measurements (rows # 6 and 6-2 of the tables 6.1 and 6.2), we can define all the parameters of the second Bateman equation: $Q_0 = (12.0 \pm 1.0 mBq/kg)/\lambda_2$, $Q = (4.0 \pm 0.7 mBq/kg)/\lambda_2$, $\lambda_1 = 4.78 \cdot 10^{-11} y^{-1}$, $\lambda_2 = 0.121 y^{-1}$ and $t = 1.874 y$.

Finally, we get the activity of ^{232}Th, 41 ± 5 mBq/kg

6.5 Current status and expectations

As May 2017, we have several samples ready to be measured: one by Molycorp Inc. already shipped to Spain and two new samples by NYC produced by a new optimized (and cheaper) production process. All the experience accumulated by the companies makes us believe that these samples will be very radiopure.

Now, we are in an advanced phase of the project characterized by the presence of several major companies interested in our project; remarkably are the Japanese Nippon Yttrium Co., Ltd., Shinetsu Chemicals and Kanto Chemicals, and the American Molycorp Inc. This interest has produced the opening of those companies to their production and purification processes showing us their interest in our Project and improving their knowledge about how to produce radio-pure Gd salts. The progress is indeed very good. We have very good candidates for the final Gadolinium sample for our experiment.

Once selected the final Gadolinium sample, we start a progressive loading of the Gadolinium in the water tank in several stages. The final state of the detector will have 100 Tons of $Gd_2(SO_4)_3$, load to 0.2%.

We must measure at least one sample of every batch of the full production. One of the companies has confirmed that 1 production batch corresponds to 500 kg approximately. Therefore, in the most probable scenario with a first phase of 10 ton loading, 20 measurements have to be done and 180 for the remaining 90 ton.

They will be carried out in a pass/no-pass screening campaign (15-20 days measurement time per sample), measuring $\sim$20 samples/year/Ge-detector. In any instance, the final strategy will be getting conformed along the relevant informations about mass production become available.

7

Summary and Conclusions

Neutrino Experimental Physics is still a cave filled of treasures to discover. This elusive particle has many open questions to answer: a precise measure of the mixing parameters, exact masses of the neutrinos and their hierarachy and leptonic CP violation are of most importance. And there is overall the fundamental question of the nature of the neutrino particle: Majorana or Fermi, i.e. wether the neutrino is its own antiparticle or not. To find these answers, several neutrinos detectors are working or under construction. The kind of signal that we want to see is very tiny: rare events physics. Low background detectors are a must to maximaze the visibility of the events.

Radiopurity is the part of these experiments destined to study, understand and quantify the different sources of radioactive background that can mimic the expected signal. The main source of radioactivity are the three natural decay

chains: ^{238}U, ^{232}Th and ^{235}U. Using High Purity Germanium (HPGe) and Mass Spectrometry, the activity of the samples can be precisely estimated.

My work during my PhD period was in two radiopurity groups for two Collaborations: NEXT and Super-Kamioande. Right now, both Radiopurity Campaigns (still in progress) are in the right direction: almost all the requeriments and goals are being fulfilled.

NEXT (Neutrino Experiment with a Xenon TPC) is a Majorana neutrino detector, a TPC filled with almost 100 kg of enriched ^{136}Xe isotope capable to track the $2\beta0\nu$ events and also to measure the energy with a resolution $< 1\%$ at $Q_{\beta\beta}$.

For the NEXT experiment, a team composed by members of Universidad de Zaragoza (UNIZAR), Laboratorio Subterráneo de Canfranc (LSC) and our Universidad Autónoma de Madrid (UAM) has carried out this Campaign, also with the help of Background Model people and the engineers of the project. About 200 measurements were carried out in this radiopurity campaign, most of them at the LSC with HPGe's. The results are rather satisfactory indicating a rather correct selection of the materials conforming the NEXT project. Some of the measured components showed relatively high activities, this discarding their use in NEXT. In these cases replacements were searched for, measured their radioactivity contamination, and used if acceptable.

The NEXT photomultiplier tubes (PMT) were are a very complicated part of the campaign. The selected model was R11410-10 from Hamamatsu. They were produced manually with no information of their radiopurity. The 55 available units were screened during the three years of the Campaign. The positive results obtained were excellent and in good agreement with those reported on previous units by other experiments.

SuperK-Gd is the upgrade of the sucessfull experiment Super-Kamiokande. This upgrade consist on dissolving 100 Tons of Gadolinium Sulphate on its water to make the detector capable to tag neutrons. They will be captured by the Gadolinium, the element with the highest thermal neutrino capture cross section. A $\sim$ 8 MeV gamma cascade is emitted at the capture which can be detected by SK. With SuperK-Gd, it will be possible to observe for the first time

the Supernova Relic Neutrino (SRN) and improve dramatically other key and fundamental measurements by SK.

In the SuperK-Gd project, the campaign had two main parts. The first one was a some-sort of Market-survey of possible providers of Gadolinium. The initial samples were very dirty, with activities orders of magnitude larger that we could accept

In this Campaign, 26 Gadolinium samples have been measured at the LSC with HPGe. Nowadays, GSF-1703-SHT-(RGD-OSF-005) is the most promising, with no signal observed in the dangerous isotopes; only upper limits could be estimated. Some of these upper limits fulfill our very stringent backgrounds requeriments but it is not enough.

After the approval of SuperK-Gd by the Super-Kamiokande Collaboration in June 2015 and, also, the 2015 Nobel Price in Physics awarded to T. Kajita, several major Japanese Rare Earth companies, Shinetsu Chemicals, Kanto Chemicals and Nippon Yttrium Co., got interested and fully involved in our project. Since then, the radioactive contaminations of the produced samples have been decreased dramatically.

This generation of Neutrino Physics Experiments cannot be understood without a strong Radiopurity Group in their Collaborations. The work of these two radiopurity groups have helped both experiments to walk in the right direction, to clear up the eyes of the detectors. Amazing results are awaiting...

La Física Experimental de Neutrinos es una cueva llena de tesoros por descubrir. Esta esquiva partícula tiene muchas preguntas por responder: una medida precisa de sus parámetros de mezcla, el valor exacto de su masa y su jerarquía y a violación CP de tipo leptónica son las más importante. Además, hay una pregunta por encima de todas ellas: si los neutrinos son de Majorana o de Dirac, es decir, si son su propia antipartícula o no. Para hallar estas respuestas, varios experimentos están ahora mismo en construcción. El tipo de señal que esperamos ver es muy pequeña: estamos en física de eventos raros. Para poder maximizar estas senales, es necesario trabajar con detectores de muy bajo fondo.

La **Radiopureza** es la parte de estos experimentos en los que se estudia, entiende y cuantifican las diferentes fuentes de fondo radioactivo que pueden imitar a la señal esperada. La principal fuente de radioactividad son las 3 cadenas naturales: ^{238}U, ^{232}Th y ^{235}U. Usando High Purity Germanium (HPGe) y Mass Spectrometry, la actividad de las muestras puede ser precisamente cuantificada.

Mi trabajo durante mi periodo doctoral ha sido dentro de dos grupos de radiopureza de dos colaboraciones: NEXT y Super-Kamiokande. Ahora mismo, con ambas campañas aún a medias, estamos en la dirección adecuada: casi todos los requisitos han sido cumplidos.

NEXT (Neutrino Experiment with a Xenon TPC) es un detector de neutrinos de Majorana, una TPC llena con casi 100 kg de isótopo ^{136}Xe, capaz de reproducir las trazas de eventos $2\beta0\nu$ y además medir su energía con una resolución $< 1\%$ at $Q_{\beta\beta}$.

Para el experimento NEXT, un grupo compuesto por gente de la Universidad de Zaragoza (UNIZAR), el Laboratorio Subterráneo de Canfranc (LSC) y nuestra Universidad Autónoma de Madrid (UAM) han llevado a cabo esta campaña; también con la ayuda de la gente del grupo de Background Model y los ingenieros de la colaboración. Unas 200 medidas se han hecho dentro de esta campaña, la gran mayoría en los HPGe's del LSC. Los reultados son bastante satisfactorios y una muy adecuada selección de los materiales ha sido llevada a cabo. A pesar de todo, algunos materiales han sido reemplazados debido a sus elevados niveles de actividad rdioactiva.

Los tubos fotomultiplciadores de NEXT (PMT) han sido una parte complicada de la campaña. El modelo seleccionado, R11410-10 de Hamamatsu era de fabricación manual y no existía ninguna información previa sobre su radiopureza. El estudio de las 55 unidades disponibles durante los 3 años de la campana nos ha servido para obtener resultados muy positivos y en sintonía con los obtenidos en otras experimentos previamente.

SuperK-Gd es una mejor del existoso detector Super-Kamiokande. La mejora consiste en la disolución de 100 toneladas de sulfato de gadolinio en el agua para poder detectar la captura de neutrones; la cual producirá posteriormente una cascada de fotones con una energía de $\sim 8MeV$. Con SuperK-Gd será posible observar por primera vez los Supernova Relic Neutrino (SRN) y mejorar dramáticamente otras medidas fundamentales del experimento.

En la campana de SuperK-Gd hay fundamentalmente 2 partes. La primera es un estudio de mercado de los proveedores de Gadolinio. En las primeras muestras, la actividad era muy elevada, ordenes de magnitud superior a lo que podemos aceptar.

Durante la campaña, se han medido 26 muestras de Gadolinio. Ahora mismo, tenemos una muestra, GSF-1703-SHT-(RGD-OSF-005), de la que solo se han cuantificado límites superiores pero no señales de los picos más peligrosos. Pero esas cotas no llegan aún a cubrir todos los requisitos experimentales.

Después de la aprobación de SuperK-Gd por la Super-Kamiokande Collaboration en junio de 2015 y el Premio Nobel de T. Kajita en ese mismo año, varios proveedores (Shinetsu Chemicals, Kanto Chemicals y Nippon Yttrium Co) han aumentado su interés en producir muestras más limpias y sus niveles de contaminación disminuido dramáticamente.

Este generación de Física Experimental de Neutrinos no puede ser explicada sin un grupo fuerte de Radiopureza en sus colaboraciones. El trabajo de estos dos grupos ha servido en ambos experimentos a trabajar en la dirección adecuada, a aclarar los ojos del detector. Increíbles resultados nos están esperando...

References

Abgrall, N. et al. (2016). "The Majorana Demonstrator Radioassay Program." In: *Nucl. Instrum. Meth.* 828, pp. 22–36 (cit. on p. 121).

Agostinelli, S. et al. (2003). "GEANT4 - A Simulation Toolkit." In: *Nucl. Instrum. Meth. A* 506, p. 250 (cit. on p. 98).

Ahmad, Q. R et al. (2002). "Direct Evidence for neutrino flavor transformation from neutral-current interactions in the Sudbury Neutrino Observatory." In: *Physical Review Letters* 89.011301 (cit. on p. 4).

Akerib, D. et al. (2012). "Radio-assay of Titanium samples for the LUX Experiment." In: *arXiv:1112.1376 [INSPIRE]* (cit. on p. 142).

Akerib, D. S. et al. (2013). "An Ultra-Low Background PMT for Liquid Xenon Detectors." In: *Nucl. Instrum. Meth. A* 703.1-6 (cit. on p. 129).

Akerib, D. S. et al. (2015). "LUX-ZEPLIN Conceptual Design Report." In: *arXiv:1509.02910v2 [physics.ins-det]* (cit. on p. 130).

Alessandrello, A. et al. (1991). "Measurements on radioactivity of ancient roman lead to be used as shieldin searches for rare events." In: *Nucl. Instrum. Meth. B* 61, p. 106 (cit. on p. 146).

Alvarez, V. et al. (2012). "NEXT-100 Technical Design Report (TDR): Executive Summary." In: *JINST* 7, T06001. DOI: 10.1088/1748-0221/7/06/T06001. arXiv: 1202.0721 [physics.ins-det] (cit. on pp. 141, 143, 144).

Alvarez, V. et al. (2013). "Radiopurity control in the NEXT-100 double beta decay experiment: procedures and initial measurements." In: *JINST* 8, T01002. DOI: 10.1088/1748-0221/8/01/T01002. arXiv: 1211.3961 [physics.ins-det] (cit. on pp. 116, 121, 131, 133, 134, 141).

Aprile, E. et al. (2015). "Lowering the radioactivity of the photomultiplier tubes for the XENON1T dark matter experiment," in: *Eur. Phys. J* 75, p. 546 (cit. on p. 129).

Aprile, E. et al. (2011). "Material screening and selection for XENON100." In: *Astroparticle Physics* 35.2, pp. 43–49 (cit. on pp. 129, 142, 144).

Arpesella, C. et al. (2002). "Measurements of extremely low radioactivity levels in BOREXINO." In: *Astroparticle Physics* 18, pp. 1–25 (cit. on pp. 133, 142).

Aznar, F. et al. (2013). "Assssment of material radiopurity for Rare Event experiments using Micromegas." In: *JINST* 8, p. C11012 (cit. on p. 131).

Bahcall, J. N., J. Davis, and L. Wolfenstein (1988). "Solar Neutrinos: a Field in Transition." In: *Nature* 344, pp. 487–493 (cit. on p. 4).

Barrow, P. et al. (2016). "Qualification Tests of the R11410-21 Photomultiplier Tubes for the XENON1T Detector." In: *arXiv:1609.01654v1 [astro-ph.IM]* (cit. on p. 129).

Bateman, Harry (1910). "Solution of a System of Differential Equations Occurring in the Theory of Radio-active Transformations." In: *Proceedings of the Cambridge Philosophical Society, Mathematical and physical sciences.* 423, pp. 423–427 (cit. on p. 50).

Baudis, L et al. (2011). "Gator: a low-background counting facility at the Gran Sasso Underground Laboratory." In: *Journal of Instrumentation* 6.08, P08010 (cit. on p. 97).

Baudis, L. et al. (2015). "Cosmogenic activiation of xenon and copper." In: *The European Physical Journal C* 75.485 (cit. on p. 20).

Boccone, V. et al. (2009). "Development of wavelength shifter coated reflectors for the ArDM argon dark matter detector." In: *JINST* 4, P06001 (cit. on p. 144).

Budjas, B. et al. (2008). "Highly sensitive gamma-spectrometers of GERDA for material screening. Part I." In: *arXiv:0812.0723 [INSPIRE]* (cit. on p. 146).

Budjas, D. et al. (2009). "Gamma-ray spectrometry of ultra low levels of radioactivity within the material screening program for the GERDA experiment." In: *Applied Radiation and Isotopes* 67, p. 755 (cit. on pp. 116, 131).

Busto, J. et al. (2002). "Radioactivity measurements of a large number of adhesive." In: *Nucl. Instrum. Meth. A* 492, pp. 35–42 (cit. on p. 112).

Cebrian, S. et al. (2011). "Radiopurity of micromegas readout planes." In: *Astroparticle Physics* 34, pp. 354–359 (cit. on p. 131).

Cebrian, S. et al. (2017). "Radiopurity assessment of the energy readout for the NEXT double beta decay experiment." In: *https://arxiv.org/abs/1706.06012v1* (cit. on p. 108).

Cebrián, S. et al. (2015). "Radiopurity assessment of the tracking readout for the NEXT double beta decay experiment." In: *JINST* P05006 (cit. on p. 130).

Cherenkov, P. (1937). "Visible radiation produced by electrons moving in a medium with velocities exceeding that of light." In: *Physical Review* 52.4, p. 378 (cit. on p. 16).

Cottingham, W. N. and D. A. Greenwood (2001). *An Introduction to Nuclear Physics*. Cambridge University Press (cit. on p. 28).

Cowan, P. M. and R. C. Barber (2010). "Q value for the double-beta decay of Xe-136." In: *Physical Review C* 82, p. 024603 (cit. on p. 62).

Eldridge, J. S. and W.S. Lyon (1961). "Promethium 148." In: *Nuclear Physics* 23, pp. 131–138 (cit. on p. 158).

Fermi, Enrico (1974). *Nuclear Physics: A Course Given by Enrico Fermi at the University of Chicago*. The University of Chicago Press (cit. on p. 34).

Fernández, Pablo (2016). "Neutrino Physics in Present and Future Kamioka Water-Cherenkov Detectors with Neutron Tagging." PhD thesis. Universidad Autónoma de Madrid (cit. on p. 65).

Gamow, George (1928). "Zur Quantentheorie des Atomkernes." In: *Zeitschrift für Physik* 51.3, pp. 204–212 (cit. on p. 30).

Geiger, H. and J.M. Nuttall (1911). "The ranges of the alpha particles from various radioactive substances and a relation between range and period of transformation." In: *Philosophical Magazine Series 6* 22.120, pp. 613–621 (cit. on p. 30).

Goeppert-Mayer, M. (1935). "Double Beta-Disintegration." In: *Physical Review* 48, pp. 512–516 (cit. on p. 7).

Gonzalez-Garcia, M. C., M. Maltoni, and T. Schwetz (2014). "Updated fit to three neutrino mixing: status of leptonic CP violation." In: *arXiv:1409.5439* (cit. on p. 6).

Hahn, Otto and Fritz Strassmann (1939). "Nachweis der Entstehung aktiver Bariumisotope aus Uran und Thorium durch Neutronenbestrahlung; Nachweis weiterer aktiver Bruchstücke bei der Uranspaltung." In: *Naturwiss* 27.89, p. 163 (cit. on p. 36).

Heaviside, O. (2008). *Electromagnetic Theory*. Vol. 3. Cosimo Inc. (cit. on p. 16).

Heusser, G. (1995). "Low-Radioactivity Background Techniques." In: *Annual Review of Nuclear and Particle Sciencie* 45, pp. 543–590 (cit. on pp. 18, 75, 131, 138, 146).

Hirata, K. S. et al. (1990). "Constraints on neutrino oscillation parameters from Kamiokande II solar neutrino data." In: *Physical Review Letters* 65, pp. 1301–1304 (cit. on p. 4).

Knoll, Glenn F. (2000). *Radiation Detection and Measurement*. John Wiley and sons, Inc (cit. on p. 28).

Krane, Kenneth S. (1987). *Introductory Nuclear Physics*. John Wiley and sons, Inc (cit. on p. 28).

LaFerriere, B. D. et al. (2015). "A novel assay method for the trace determination of Th and U in copper and lead using inductively coupled plasma mass spectrometry." In: *Nucl. Instrum. Meth. A* 775, pp. 93–98 (cit. on p. 121).

Laubenstein, M. et al. (2004). "Underground measurements of radioactivity." In: *Applied Radiation and Isotopes* 61, pp. 167–172 (cit. on pp. 121, 144, 146).

Lawson, I. and B. Cleveland (2011). "Low Background Counting At SNOLAB." In: *AIP Conf. Proc.* 1338, pp. 68–77 (cit. on pp. 117, 133, 142, 144).

Leo, W.R. (2012). *Techniques for Nuclear and Particle Physics Experiments: A How-to Approach*. Springer Berlin Heidelberg. ISBN: 9783642579202. URL: https://books.google.es/books?id=yc4qBAAAQBAJ (cit. on p. 28).

Leonard, S. et al. (2008). "Systematic study of trace radioactive impurities in candidate construction materials for EXO-200." In: *Nucl. Instrum. Meth. A* 591, p. 490 (cit. on pp. 117, 140, 144, 146).

Lopez-March, N. (2016). "Sensitivity of the NEXT-100 detector to neutrinoless double beta decay." In: *NEUTRINO 2016* (cit. on p. 63).

M. Redshaw E. Wingfield, J. McDaniel and E. G. Myers (2007). "Mass and double-beta decay Q value of Xe-136." In: *Physical Review Letters* 98, p. 053003 (cit. on p. 62).

Magill, Joseph and Jean Galy (2005). *Radioactivity Radionuclides Radiation*. Springer (cit. on p. 28).

Majorana, E. (1937). "Theory of the Symmetry of Electrons and Positrons." In: *Nuovo Cimento* 14, pp. 171–184 (cit. on p. 7).

Maneschg, W. et al. (2008). "Measurements of extremely low radioactivity levels in stainless steel for {GERDA}." In: *Nucl. Instrum. Meth. A* 593.3, pp. 448–453 (cit. on p. 142).

Martín-Albo, J. et al. (2016). "Sensitivity of NEXT-100 to neutrinoless double beta decay." In: *JHEP* 05, p. 159. DOI: 10.1007/JHEP05(2016)159. arXiv: 1511.09246 [physics.ins-det] (cit. on pp. 63, 108, 121, 152).

Martín-Albo, Justo (2015). "The NEXT experiment for neutrinoless double beta decay searches." PhD thesis. Valencia U., IFIC. URL: http://roderic.uv.es/handle/10550/41728 (cit. on pp. 63, 108).

N. Soppera, M. Bossant and E. Dupont (2014). "An Improved Version of the NEA Java-based Nuclear Data Information System." In: *Nuclear Data Sheets* 120, pp. 294–296 (cit. on p. 98).

Nachab, A. and Ph. Hubert (2012). "210Pb activity by detection of bremsstrahlung in 210Bi beta-decay." In: *Nucl. Instrum. Meth. B* 274, pp. 188–190 (cit. on p. 134).

Nebot-Guinot, M. (2016). "The NEW detector: construction, commissioning and first results." In: *NEUTRINO 2016* (cit. on p. 58).

Nisi, S. et al. (2009). "Comparison of inductively coupled mass spectrimetry and ultra low-level gamma-ray spectroscopy for ultra low background material selection." In: *Applied Radiation and Isotopes* 67, p. 828 (cit. on pp. 116, 131).

Ostrovskiy, I. et al. (2015). "CharacterizationofSiliconPhotomultipliersfornEXO." In: *arXiv:1502.07837 [physics.ins-det]* (cit. on p. 138).

Petrzhak, K. A. and G. N. Flerov (1940). "Spontaneous Fission of Uranium." In: *Physical Review Letters* 58.89 (cit. on p. 36).

Petrzhak, K. A. and G. N. Flerov (1941). "Spontaneous Fission of Uranium." In: *Uspekhi Fizicheskikh Nauk* 25.2, pp. 171–178 (cit. on p. 36).

Racah, G. (1937). "On the symmetry of particle and antiparticle." In: *Nuovo Cimento* 14, pp. 512–516 (cit. on p. 7).

Reines, F. and C. L. Cowan (1956). "The Neutrino." In: *Nature* 178, pp. 446–449 (cit. on pp. 2, 3).

Relly, Doug et al. (1991). *Passive Nondestructive Assay of Nuclear Materials*. United States - Nuclear Regulatory Commission (cit. on p. 36).

Sobel, H. W. et al. (1973). "High-Energy Gamma Rays from Spontaneous Fission of 238U." In: *Physical Review C* 7.4, pp. 1564–1579 (cit. on p. 38).

Spiering, C. (2012). "Towards High-Energy Neutrino Astronomy." In: *The European Physical Journal H* 37, pp. 515–565 (cit. on p. 8).

Turkevich, L. (1991). "Double-beta decay of 238U." In: *Physical Review Letters* 67.3211 (cit. on p. 40).

Vacri, M. L. di et al. (2015). "ICP MS selection of radiopure materials for the GERDA experiment." In: *AIP Conf. Proc.* 1672.15001 (cit. on p. 118).

Valentine, T. E. (2001). "Evaluation of prompt fission gamma rays for use in simulating nuclear safeguard measurements." In: *Annals of Nuclear Energy* 28, pp. 191–201 (cit. on p. 38).

Wang, X. et al. (2016). "Material Screening with HPGe Counting Station for PandaX Experiment." In: *JINST* 11.T12002 (cit. on p. 129).